Louisiana State University
LSU Digital Commons

LSU Doctoral Dissertations | Graduate School

2007

The spectral and photophysical characterization of water solubilizing metal phthalocyanines for highly sensitive detection in biological studies

Vera Tamisha Verdree
Louisiana State University and Agricultural and Mechanical College, vverdr1@lsu.edu

Follow this and additional works at: https://digitalcommons.lsu.edu/gradschool_dissertations

 Part of the Chemistry Commons

Recommended Citation
Verdree, Vera Tamisha, "The spectral and photophysical characterization of water solubilizing metal phthalocyanines for highly sensitive detection in biological studies" (2007). *LSU Doctoral Dissertations*. 1370.
https://digitalcommons.lsu.edu/gradschool_dissertations/1370

This Dissertation is brought to you for free and open access by the Graduate School at LSU Digital Commons. It has been accepted for inclusion in LSU Doctoral Dissertations by an authorized graduate school editor of LSU Digital Commons. For more information, please contactgradetd@lsu.edu.

THE SPECTRAL AND PHOTOPHYSICAL CHARACTERIZATION OF WATER SOLUBILIZING METAL PHTHALOCYANINES FOR HIGHLY SENSITIVE DETECTION IN BIOLOGICAL STUDIES

A Dissertation

Submitted to the Graduate Faculty of the
Louisiana State University and
Agricultural and Mechanical College
in partial fulfillment of the
requirements for the degree of
Doctor of Philosophy

in

The Department of Chemistry

by
Vera TamishaVerdree
B.S., Columbus State University, 2000
August 2007

Dedication

Education is the passport to the future, for tomorrow belongs to those who prepare for it today.
– Malcolm X

With God, all things are possible - Matthew 19:26. This work is dedicated to my Mother and Father, Marilyn and Fernando Verdree, my Grandmother and Grandfather, Minnie and Lorenzo Bryant, my Grandmother and Great-grandmother Mary Verdree and Lula Mae Roberson, my Uncles, Marvin and Lorenzo Bryant, Kelvin and Stanley Verdree, my Aunts Stephanie and Margaret, and my cousins Cynthia and Omar. I would also like to dedicate this to my very dear friends, Dionysos Williams, Melanie Hinkson, Tomiko Jones, Dr. Ginger Powe, and Miss Lakia Champagne. A special dedication goes to my Uncle Jeffrey Bryant. Your remarkable strength and drive is an inspiration to all. This work would not have been possible without your love and support. I am blessed to be loved by all of you.

Acknowledgments

There are number of professors that have contributed to the completion of my doctoral degree. I would like to thank those members of my committee and others:

- Dr. Steven A. Soper, for believing in my ability and giving me an opportunity to work in his lab; and for challenging me to achieve my highest potential.
- Dr. Robert Hammer, for your support and expertise in this research area;
- Dr. Steven Watkins, for your continued support and guidance;
- Dr. Andy Maverick, for the insightly discussions that help me in better understanding my research; and
- Dr. Floyd R. Jackson, whose mentorship inspired me to pursue this degree

I would also like to acknowledge:

- My extended family Steven and Vera Watkins; Your support and guidance have helped me to become the young woman I am today.
- Dr. Irena Nesterova, Dr. Michael Allen, Dr. Guifa Su, and Dr. Serhii Pakhomov for all your help and support with this research project. Thank you.

Table of Contents

Dedication ..... **ii**

Acknowledgements ..... **iii**

List of Tables ..... **vii**

List of Figures ..... **viii**

Abstract ..... **xiv**

Chapter 1 Theory of Fluorescence Spectroscopy and Near-IR Detection **1**
1.1 Theory of Fluorescence Spectroscopy 1
1.1.1 Quantum Efficiency 3
1.1.2 Fluorescence Lifetimes 4
1.1.3 Radiative Lifetimes 5
1.1.4 Steady-State and Time-Resolved Fluorescence 6
1.2. Fluorescence Measurements and Instrumentation 7
1.2.1 Steady-State Fluorescence 7
1.2.2 Time-Correlated Single Photon Counting (TCSPC) 10
1.2.2.1 Components for TCSPC Instrumentation 11
1.2.2.2 Data Analysis Methods for TCSPC Measurements 12
1.3 Factors Affecting Fluorescence 13
1.3.1 Intramolecular Effects 13
1.3.2 Environmental Effects 14
1.4 Characteristics of Ideal Probes 15
1.4.1 Visible Fluorescent Probes (400-650) 16
1.4.2 Near-Infrared (NIR) Probes (650-1000 nm) 17
1.4.3 Metal Phthalocyanines (MPc's) as Near-IR Fluorescent Probes 18
1.5 References 19

Chapter 2 Water Soluble Metal Phthalocyanines: The Role of the Functional Groups on the Spectral and Photophysical Properties **23**
2.1 Introduction 23
2.2 Materials and Methods 25
2.2.1 Reagents and Samples 25
2.2.2 Synthesis of Metal and Metal-Free Phthalocyanines (MPc's 26
2.2.3 Spectral and Fluorescence Measurements of Metal-Free and MPc's 31
2.3 Results 34
2.3.1 Synthesis of Metal and Metal-Free Phthalocyanines 34
2.3.2 Spectral Properties 37
2.3.3 Photophysics of MPc's 41
2.4 Discussion 45
2.5 Conclusions 49
2.6 References 49

Chapter 3 Labeling Peptides, Proteins and Oligonucleotides with Metal Phthalocyanines for Highly Sensitive Fluorescence Detection Application 54
3.1 Introduction to Fluorescence Labeling Techniques.....54
3.1.1 Fundamental Aspects of Carbodiimide Coupling.....56
3.2 Materials and Methods.....58
3.2.1 Instrumentation 60
3.3 Results and Discussion 62
3.3.1 ^{13}C NMR Analysis of Derivatized Zn4CPc 62
3.3.2 Spectral Properties of Labeled BSA, Insulin Chain B and Oligonucleotide 64
3.3.3 Fluorescence Lifetime of Labeled Streptavidin.....68
3.3.4 Separation of Labeled Conjugates Using Reverse Phase Chromatography 70
3.3.5 Influence of Amino Linker Chain Length on the Conjugation of Amine Modified Oligonucleotides 72
3.4 Conclusions.....74
3.5 References.....75

Chapter 4 Fluorescence Microplate-Based Assays for High Throughput Optimization of Protein Labeling Using Functionalized Zinc Phthalocyanine 78
4.1 Introduction.....78
4.1.1 Challenges Using Metal Phthalocyanines as Labeling Reagents 79
4.1.2 Streptavidin-Biotin Binding and Its Use in Bioassays.....80
4.2 Materials and Methods.....81
4.2.1 Reagents and Samples.....81
4.2.2 Conjugation of Zn4CPc Activated Ester (ZnPc-NHS) to Protein 82
4.2.3 Reactivity Binding Assay 83
4.3 Results and Discussion 84
4.3.1 Optimal Conditions for Labeling Streptavidin with ZnPc-NHS.....84
4.4 Conclusions.....92
4.5 References.....92

Chapter 5 The Electrophoretic Behavior of Metal Phthalocyanines and Labeled Complexes Using Capillary Zone Electrophoresis 96
5.1 Theory of Electrophoresis.....96
5.1.1 Instrumentation 100
5.1.2 Modes of Separation 102
5.1.3 Separation of Metal Phthalocyanines (MPc's) 103
5.1.4 Electrophoresis Considerations of MPc's.....105
5.1.4.1 Role of Metal 105
5.1.4.2 Role of Peripheral Groups 105
5.1.4.3 Aggregation Effects of MPc's (buffer issues) 106
5.2 Experimental.....107
5.2.1 Materials and Methods.....107
5.2.2 Instrumentation 108
5.2.2.1 Capillary Electrophoresis.....108
5.3 Results and Discussion 110
5.3.1 Electrophoretic Separation of MPc's.....110
5.3.1.1 Effect of Metal Center on Mobility 110
5.3.1.2 Effect of Peripheral Groups on Mobility 112

5.3.1.3 Effect of Aggregation on Mobility (carrier electrolyte selection) 114
5.3.1.4 Effect of Methanol Concentration 117
5.3.1.5 Effect of pH.....120
5.3.2 Electrophoretic Separation of Labeled Insulin Chain B and Digested β-Casein....121
5.3.2.1 Effect of pH.....129
5.4 Conclusions.....131
5.5 References.....131

Chapter 6 Unsuccessful Approaches, Summary and Future Work.....138
6.1 Unsuccessful Labeling Approaches.....138
6.2 Summary.....142
6.3 Current and Future Work.....145
6.4 References.....146

Vita 148

List of Tables

Table 2.1 Absorption (λ_a) and emission (λ_e) maxima of a metal free (H_2Pc)and several MPc dyes. The dyes were suspended in DMSO. HPLC retention times (t_R) for the MPc's using a reverse phase column and the exact mass as determined by MALDI-TOF-MS of each dye is also listed 35

Table 2.2 Absorption (λ_a) and emission (λ_e) maxima of metal free (H_2Pc) and metal dye pentyl esters. Extinction coefficients (ε) and the exact mass, as determined by MALDI-TOF-MS are also listed 36

Table 2.3 Fluorescence lifetimes (τ_f), fluorescence quantum yields (Φ_f), photobleaching quantum yields (Φ_d), and photon yields per molecule (n_f) for the standard, DOTCI, metal free and several metal Pc dyes. The χ^2 value for each decay profile is also presented. All of these photophysical properties were measured in DMSO, except for the fluorescence quantum yields measured in H_2O (CAPS, pH = 11.0) and the ZnPc**6a**/-streptavidin conjugate, which was measured in HEPES buffer (pH = 8.0) 42

Table 4.1 Optimal method conditions for the general labeling of proteins. Parameters such concentration, pH of buffer and amount of organic content were evaluated.....88

Table 5.1 Electrophoretic mobility, theoretical plates, and standard deviation for the native MPc's studied. All dyes were dissolved in the running buffer at concentration of 10^{-6} M 114

Table 5.2 Sequence of theoretical tryptic peptides for β-casein. 123

List of Figures

Figure 1.1 Simple schematic of the Jablonski diagram depicting the excitation of a molecule by the absorption of light and the relaxation process of the excited molecule. 2

Figure 1.2 Schematic of a spectrofluorometer. The basic components are a light source, excitation and emission monochromators and photomultiplier tube for detection.....8

Figure 1.3 Spectral distribution of irradiance for various arc lamps to include the xenon lamp. (Courtesy of Newport; used with permission) 9

Figure 1.4 Schematic of a time-correlated single photon counting (TCSPC) instrument. The instrument consists of a light source, time-to-amplitude (TAC) converter, constant fraction discriminator (CFD), mutichannel analyzer (MCA), and computer for data analysis.....11

Figure 1.5 Examples of visible dyes, FITC and Alexa 488, commonly used for fluorescent labeling.....16

Figure 1.6 Basic structure of carbocyanine dyes used as fluorescent reporters.....17

Figure 1.7 Structure of tricarbocyanine dye previously reported for use in DNA sequencing applications.[38].....18

Figure 2.1 Schematic of the synthesis of 2,9,16,23-tetrasubstituted Pc's.....28

Figure 2.2 Schematic of the synthesis of 2,3,9,10,16,17,23,24-octasubstituted MPc's.....29

Figure 2.3 Schematic of the synthesis of hexadeca substituted ZnPc.....30

Figure 2.4 Synthesis of ZnPc-N, hydroxysuccinimide ester using DCC in the presence of DMF.....31

Figure 2.5 Absorption (A) and emission (B) spectra of ZnPc dyes along with the ZnPc**6a**/streptavidin complex. The emission spectra were obtained at an excitation wavelength of 675 nm. The emission spectra were normalized to the maxima. All emission spectra were collected in DMSO at a concentration of ~1.0 μM, while the absorption spectra used dye concentrations that varied from 1-100 μM 38

Figure 2.6 Normalized absorption (A) and emission (B) spectra for a metal free Pc and several metal substituted Pc dyes (Zn, Al, Ga) dissolved in DMSO. The emission spectra were excited at the absorption maximum for each dye at a concentration of 1.0 μM. In all cases, the tetra-carboxylated dyes were used in these measurements. 39

Figure 2.7 Absorption spectra for MPc's in HEPES buffer, pH 8. The concentrations of dyes used in these measurements were 1.0×10^{-6} M. The absorption spectra were normalized with respect to the absorption maxima 41

Figure 2.8 Photobleaching profiles for several Zn*x*CPc dyes, IRD700, and DOTCI. The photobleaching decay profiles were collected using 680 nm excitation by constantly irradiating a 1.0 μM solution and continuously monitoring the fluorescence emission.Results taken from experiments in collaboration with Dr. Michael Allen 43

Figure 2.9 Chromatogram showing the elution of (A) ZnPc **6a** by itself(t_r = 19.2 min), ZnPc **6a**/streptavidin conjguate (t_r = 23.1 min, 28.5 min and 35.0 min) along with the ZnPc **12**/streptavidin conjguate (B). The fluorescence detector was set at λ_{ex} = 686 nm and λ_{em} = 693 n. See experimental section for an explanation of the chromatographic conditions 44

Figure 3.1 Structure of EDC and DCC used for converting carboxylic acid functional groups to active O-acylisourea derivative for labeling biomolecules containing primary amines forming stable amide bonds.....57

Figure 3.2 Schematic representing the derivatization of carboxylic acid functionalites using EDC coupling chemistry. The addition of NHS produces a more stable amide bond between primary amines and carboxylic acid groups.....57

Figure 3.3 Structure of tetracarboxylate metal phthalocyanine (Zn4CPc) used for labeling reactions. The synthesis of Zn4CPc has been discussed in detail previously.....59

Figure 3.4 Schematic illustrating the experimental set up for attaching dye labeled streptavidin to biotinylated microspheres.....62

Figure 3.5 ^{13}C NMR spectrum of Zn4CPc dissolved is DMSO. Concentration of the Zn4CPc solution: 3 mM.....63

Figure 3.6 ^{13}C NMR spectrum representing the NMR shift for N, hydroxysuccinimde. The concentration of NHS dissolved in d_6-DMSO was 12 M. 63

Figure 3.7 ^{13}C NMR spectrum illustrating the appearance of an NMR peak indicative of the active ester formation.....64

Figure 3.8 Normalized overlay of the absorption and emission spectra of ZnPc-insulin chain B conjugate in 10%DMSO/HEPES. The fluorescence emission spectrum was obtained using an excitation wavelength of 675 nm. The dye-to-peptide ratio was set at 10:1. Concentration of ZnPc used for conjugation was 10^{-6} M 65

Figure 3.9 Normalized overlay of the absorption and emission spectra for ZnPc-BSA conjugate along with the absorption spectrum for unconjugated BSA. The BSA-to-dye ratio was set at 10:1. The excitation wavelength maximum was 683 nm and the emission maximum was 686 nm. The dye concentration was 1×10^{-6} M.....66

Figure 3.10 Absorption spectra of oligonucleotide and ZnPc-oligonucleotide conjugate in HEPES buffer. The broad peaks at 637 nm and 683 nm are indicative of H-aggregation. The dye-to-primer ratio was 10:1 with a dye concentration of 1×10^{-6} M.....67

Figure 3.11 Fluorescence emission spectrum of ZnPc-streptavidin bound to biotinylated microspheres and a control reaction with no streptavidin added to the solution. Non-specific binding of the dye is minimal. Excitation wavelength: 680 nm, [dye] = 1 x 10^{-6} M; microbeads and Zn4CPc exhibit low non-specific interaction with the solid surface 68

Figure 3.12 Fluorescence decay profile of Zn4CPc-streptavidin in HEPES buffer at pH 8 and the instrument response function (A) along with the fluorescence decay profile of Zn4CPc (B). Weighted residual shown for zinc phthalocyanine only. χ^2 value of 1.34 represents a good fit of the decay profile.....69

Figure 3.13 Mass spectrum of ZnPc-insulin chain B conjugate dissolved in a 1:1 (v/v) solution of 2,4,6 Trihydroxyacetophenone (THAP) matrix. Mass spectrum acquired by MALDI-TOF using a 337 nm nitrogen laser operated in negative mode.....70

Figure 3.14 Chromatogram of unlabeled insulin chain B (**A**) with a retention time of 4.5 min, and Zn4CPc labeled insulin chain B (**B**) with peaks eluting at 5.2 min, unresolved peaks at ~16 min, and a peak eluting at 28 min. Separation was performed using a reverse-phase column and a linear gradient of 0.1%TEAA/ACN for 35 min. Detection was performed using a PDA and fluorescence detector system. Concentration of ZnPc-NHS used in reaction: 10^{-6} M. The dye-to-peptide ratio was 10:1. 71

Figure 3.15 Illustration of the conjugate structure for Zn4CPc labeled with a peptide or protein. The oligonucleotide has an amino modified linker attached to the 5' end. See experimental section for labeling details 73

Figure 3.16 HPLC reverse-phase chromatographic separation of ZnPc-oligonucleotide conjugate using a C6-amino linker (A) and a C12-amino linker (B) attached to the primer. Dye concentration: 10^{-5}M; dye-to-primer ratio: 10-to-1. Chromatographic separation was performed with a linear gradient of 0.1% TEAA/ACN. See experimental details. 74

Figure 4.1 Chemical structure of biotin 80

Figure 4.2 Tetrameric structure of streptavidin used as a model protein for optimization of the conjugation reaction with Zn4CPc. Each subunit has a molecular weight of 15 kDa.....81

Figure 4.3 Molecular structure of the active N-hydroxysuccinimide (NHS) ester form of Zn4CPc. All four carboxyl groups are converted to NHS esters outlined by a procedure published by Koval et al.[36] Synthesis was performed in-house in collaboration with Dr. Hammer's laboratory 82

Figure 4.4 Schematic representing the microplate assay used for evaluating the optimal conditions. Parameters that were evaluated include pH, dye concentrations, dye-to-protein ratio, and amount of aqueous solvent (percentage).....84

Figure 4.5 A comparison of the relative fluorescence intensity of unreacted streptavidin, free Zn4CPc, buffer, and streptavidin-dye conjugate. Results show minimal nonspecific adsorption of the free ZnPc-NHS. Excitation wavelength was 680 nm with an emission wavelength of 693 nm. The samples were incubated in the microwell for 30 minutes prior to rinsing. 85

Figure 4.6 Fluorescence emission of Zn4CPc in the well with immobilized biotin in the absence of streptavidin. Results indicated minimal non-specific interaction of Zn4CPc with immobilized biotin 86

Figure 4.7 Fluorescence emission spectrum of ZnPc-streptavidin conjugate under varying pH conditions. The conjugate reaction mixture was allowed to incubate in the well with immobilized biotin for 30 minutes prior to rinsing 3 times with HEPES. Dye concentration used was 10^{-6} M with a dye-to-protein ratio of 10-to-1.....87

Figure 4.8 Schematic depicting hydrolysis of the N-hydroxysuccinimide active ester by which the ester converts back to the carboxyl group as a competing reaction. At high pH values, the rate of hydrolysis increases.....88

Figure 4.9 Fluorescence analysis of Zn4CPc-streptavidin conjugate as a function of (A) Zn4CPc concentration and (B) pH of HEPES buffer. Excitation, 680 nm; 5 nm slit width. Final volume of the labeling reaction incubated in the microwell was 200 μL at room temperature for 30 min. and the detected at an emission wavelength of 693. This pH range was chosen due to the solubility of Zn4CPc at this pH range.....89

Figure 4.10 Fluorescence intensity of ZnPc-streptavidin conjugate with varying dye-to-protein ratio 90

Figure 4.11 Fluorescence intensity of Zn4CPc-streptavidin conjugate as a function of the amount of HEPES in the reaction solution. The intensity continues to decrease as the amount of organic content lowers 91

Figure 4.12 Absorption spectrum of Zn4CPc-streptavidin conjugate mixture in 80/20 HEPES/DMSO exhibiting extensive aggregation 91

Figure 5.1 Depiction of the formation of a "double layer" near the capillary surface. The direction of the EOF moves all charged species toward the cathode. "N" represents neutral species.....97

Figure 5.2 Schematic of capillary electrophoresis separation mechanism.[29].....98

Figure 5.3 Depiction of electroosmotic flow profile compared to laminar flow profile typically seen for other analytical techniques such as HPLC 98

Figure 5.4 Basic components of a CE separation system. A capillary open on both ends are immersed in buffered solutions, across which a high voltage is applied. Detection is performed on-column 100

Figure 5.5 Structure of MPc with carboxylic acid functional groups substituted on the periphery of the macrocycle. M = Zn, Al, and Ga. 110

Figure 5.6 CZE separation of (A) Zn4CPc, (B) Al4CPc, and (C) Ga4CPc in 80/20 methanol/borate buffer, pH 9. Separation performed in a bare silica capillary column, 75 μm i.d., 375 μm o.d. with a total effective length of 40 cm. Field strength: 300 V/cm. Samples were

introduced using electrokinetic injection at 10 kV for 5 s. UV-Vis detection was monitored at 260 nm. Dye concentrations: Zn4CPc: 1×10^{-5} M, Al4CPc: 1×10^{-6} M, Ga4CPc: 1×10^{-6} M 111

Figure 5.7 CZE separation of Zn8Pc dye with a migration time of 12.47 min. Separation conditions were the same for all MPc dyes. The dye concentration was 2.0×10^{-6} M with detection at 345 nm 112

Figure 5.8 Electropherogram of Zn16Pc with a migration time of 16.39 min. Detection was accomplished with UV detection at 340 nm. Dye concentration: 10^{-6} M.....113

Figure 5.9 Effect of NaCl on the absorption spectra of Zn4CPc in 80/20 methanol/borate mixture. An increase in electrolyte concentration increases aggregation by the increased appearance of an aggregate peak at 640 nm 115

Figure 5.10 Effect of the presence of salt on the CE separation of Zn4CPc. Carrier electrolyte: 40 mM borate buffer, pH 9. Salt concentration: 0.05 M NaCl (A), 0.1 M NaCl (B), and 0.2 M NaCl (C).....116

Figure 5.11 Electrophoretic analysis of Zn4CPc separation in 60/40 methanol/borate running buffer at pH 9. Sample concentration: 1×10^{-5} M. Detection was monitored at wavelength 260 nm. Other separation conditions are given in Figure 5.6.....118

Figure 5.12 Electropherogram of Zn4CPc obtained in 20/80 methanol/borate running buffer. Conditions: 50 cm capillary;40 mM borate buffer pH 9.....119

Figure 5.13 Apparent mobilities of Zn4CPc as a function of the methanol content in the BGE. The CZE conditions are described in the experimental section.....119

Figure 5.14 Effect of pH on the CZE of Zn4CPc. The running buffer consisted of 80/20 methanol/CAPS at pH 11. Dye concentration: 3×10^{-5} M. Other experimental conditions described in the experimental section.....120

Figure 5.15 Amino acid residue sequence of insulin chain B with one N-terminal primary amine and one ε primary amine on the lysine residue available for labeling.....121

Figure 5.16 Electropherogram of insulin chain B dissolved in HEPES pH 8 at a sample concentration of 1 mM. Detection was monitored at a wavelength of 260 nm using a photodiode array (PDA) 121

Figure 5.17 Free solution electropherogram of insulin chain B conjugated to Zn4CPc. The amount of dye used was a 15-fold molar excess over the peptide. Sample was injected using electrokinetic injection for 5 sec. UV detection was monitored at 260 nm. The conjugate reaction mixture was purified using sephadex LH-20 prior to electrophoresis.....122

Figure 5.18 Electropherogram showing the separation of Zn4CPc labeled β-casein in a 40 mM borate buffer at pH 9. Sample was injected onto a bore silica capillary using electrokinetic injection for 5 sec and detected using a PDA monitored at 340 nm.....124

Figure 5.19 Capillary electropherogram of peptides generated from trypsin digestion of β-casein. Capillary electrophoresis was performed at pH 9.1 in 40 mM borate buffer. The sample was electrokinetically injected onto the column at 15 KV for 5 s and separated using a carrier buffer at V = 30 KV. Separation was monitored at 345 nm. Peak labeled "P" represents undigested β-casein.....125

Figure 5.20 A blow up of several regions representing the electropherogram of Zn4CPc labeled β-casein digested with the enzyme trypsin 126

Figure 5.21 Microchip (PMMA) electrophoresis of Zn4CPc active ester without the presence of streptavidin. Dye concentration: 150 μM, injection time: 50 s. Separation was performed in HEPES, pH 8. Detection monitored using laser-induced fluorescence detector at an excitation wavelength of 633 nm.....127

Figure 5.22 Electropherogram of ZnPc-streptavidin conjugate separated on PMMA microchip. Protein concentration: 1 μM, dye-to-protein ratio: 15-to-1, injection time: 50 sec. Separation was performed in HEPES at pH 8 and detection was monitored using a laser-induced fluorescence detector at an excitation wavelength of 633 nm 128

Figure 5.23 Electropherogram of Alexa Fluor-streptavidin conjugate obtained on an uncoated microchip. Sample injection time: 50 sec. Dye concentration: 150 μM. Dye-to-protein ratio for labeling: 15-to-1.....129

Figure 5.24 CZE electropherogram of tryptic peptide fragments produced from β-casein digestion. Separation was performed using 40 mM phosphate buffer at pH 2.....130

Figure 6.1 Schematic illustrating the reaction to convert carboxylic acid groups to active functional esters while reacting with amino modified primer simultaneously 138

Figure 6.2 Anion-exchange chromatogram of a labeling reaction mixture consisting of Zn4CPc, EDC/NHS, and oligonucleotide present in solution. Precipitation formed when carbonate buffer was added. Concentration-10^{-5} M dye: 10^{-6} DNA 139

Figure 6.3 HPLC chromatogram of labeling reaction mixture. Reaction quenched using NaOH. Concentration ratio: 15:1 Dye:DNA (10^{-3} M:10^{-5} M) Analysis method - 0-90 % $NaClO_4$ in 30 minutes using anion exchange column. Black line represents DNA only.....140

Figure 6.4 Anion-exchange chromatography of a 1 mM Zn4CPc-oligonucleotide reaction mixture. Fractions were collected and monitored at 260 nm. Dionex DNAPac anion-exchange (4 × 250 mm analytical column), 13 μm column. Gradient from 0% to 75% 0.375 M $NaClO_4$ in 45 minute, room temperate 140

Figure 6.5 MALDI-TOF of Zn4CPc-oligonucleotide conjugate. MALDI-TOF acquired on a Bruker Pro-Flex equipped with a 337 N_2 laser 141

Figure 6.6 Structure of asymmetrical Pc dyes for labeling biomolecules 146

Abstract

Efforts to improve the technology for DNA analyses stimulated the work presented here to develop a series of fluorescent probes that would aid in the increased multiplexing capabilities allowing the ability to detect multiple targets in a single measurement. Typically, spectral discrimination has been used to identify each DNA fragment in sequencing or diagnostic applications by means of unique emission properties from several labeling dyes. This has been accomplished with labels that fluoresce in the visible region. The limitations with these dyes is the broad emission profile making discrimination difficult, high intrinsic biological fluorescence and structural differences of the dyes leading to differences in the electrophoretic mobility of labeled oligonucleotides, complicating sorting using electrophoresis. The use of labeling dyes that fluoresce in the near-IR has several advantages including reduced background interference, increased sensitivity due to decreases in Raman scattering, and can be excited using inexpensive diode lasers allowing time-resolved measurements to be carried out. Thus, lifetime discrimination in parallel with color discrimination can potentially offer increased multiplexing capabilities for a variety of DNA analysis applications.

Strategies are reported that produce symmetrical metal-free and metallo-phthalocyanine dyes, Pc and MPc, respectively that contain various numbers of water solubilizing carboxylic acid groups on their periphery that provide a dual role by also serving as functional groups to covalently link primary amine-containing targets to these dyes. The influence of the number of solubilizing groups and metal center on the spectral and photophysical properties were evaluated. MPc dyes containing 4, 8, or 16 carboxylic acid groups exhibited similar absorption and emission maxima (677 nm and 686 nm, respectively) with the molar absorptivity of the Q-band $\sim 10^5\ M^{-1}cm^{-1}$. Results indicated that the fluorescence lifetimes and quantum yields varied as a function of the metal center; the degree of carboxylation did not significantly alter these

properties in DMSO, but did mediate the solubility and aggregation states when placed in aqueous solvents. Results also showed that the conjugate, produced by covalently linking an MPc to biological entities, generated a red-shift in the emission maximum with a fluorescence lifetime shorter than that of the native MPc dye.

Chapter 1
Theory of Fluorescence Spectroscopy and Near-IR Detection

1.1 Theory of Fluorescence Spectroscopy

Fluorescence spectroscopy has been recognized as a significant technological achievement over the past years and has permitted new avenues in molecular dynamics to be explored. [1-3] Due to its specificity, high sensitivity to small modifications in the structural dynamics and function of biological complexes, and the ability to detect very low concentrations, fluorescence spectroscopy has become the primary analytical tool in the disciplines of chemistry and biochemistry. [2,4,5] Pioneering work by Stokes and Förster demonstrated the usefulness of fluorescence spectroscopy and in recent years, it has been used in a wide range of applications including cell identification and cell imaging, and detection for DNA sequencing.[6-10] This chapter presents the theory of fluorescence spectroscopy, together with examples of fluorescent probes to illustrate the potential use of this technique as a method for the analysis and identification of fluorescent dye-labeled targets in complex biological systems.

Luminescence occurs when molecules are excited by the absorption of energy and emits light from electronically excited states as it relaxes to the ground state.[1,11] The excitation time is on the order of 10^{-14} to 10^{-15} s, with the rate of emission depending on the nature of the excited state.[1] A simplified schematic of the Jablonski diagram depicting the quantum processes of absorption and emission is shown is Figure 1.1. The electronic states are divided into singlet states, S_0, S_1, and S_2, in which all electron's spin are paired (multiplicity = 1), and triplet states in which two electrons have parallel spins. Each electronic state is associated with vibrational states represented by lighter horizontal lines. Initially, the molecule occupies the lowest singlet state, S_0. After absorption of a photon, the molecule occupies a vibrational level of an excited singlet state (e.g. S_2). The excited molecule then relaxes to a vibrational level of the lowest excited

singlet state within about 10^{-11} s through a process called ″internal conversion.″

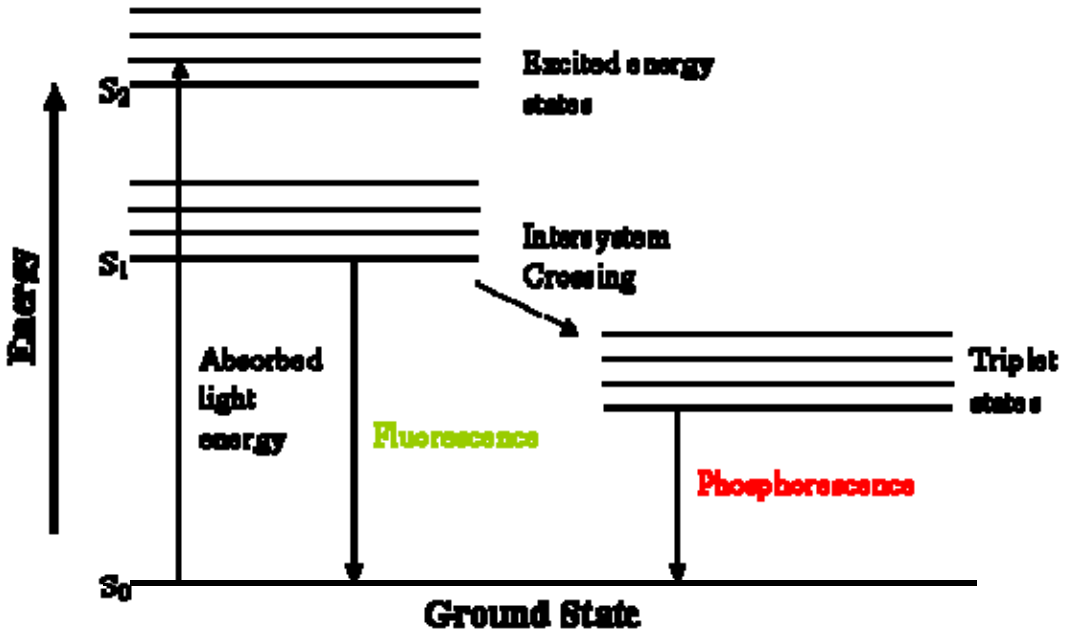

Figure 1.1 Simple schematic of the Jablonski diagram depicting the excitation of a molecule by the absorption of light and the relaxation process of the excited molecule.

Fluorescence emission occurs when the molecule further relaxes to the ground state from the lowest excited singlet state dissipating energy in the form of light.[2,11,12] Typically, the emission process is rapid, occurring in approximately 10^8 s^{-1}. Consequently, when a molecule is in the excited singlet state, an electron can change its spin (spin unpaired) resulting in a transfer of the excited molecule to an excited triplet state through intersystem crossing.[2] The molecule then rapidly relaxes to the lowest vibrational level of the first excited triplet state and emission is observed in the form of phosphorescence, which occurs in 10^{-4} to 10 s. In addition to fluorescence and phosphorescence, other non-radiative deactivation pathways include intramolecular charge transfer and intermolecular processes such as electron transfer and excimer formation (dimers associated with excited electronic states).[13] A characteristic of the fluorescence emission is a shift to a longer wavelength referred to as the Stokes' shift due to loss of energy caused by the rapid decay of the molecule to the lowest vibrational level of the excited state and the molecule decaying to higher vibrational levels of the electronic ground state.[11]

1.1.1 Quantum Efficiency

As mentioned previously, a molecule can return to the ground state through several deactivation pathways. The number of molecules that emit photons after being excited is measured by the fluorescence quantum yield of that fluorophore:

$$\Phi_F = \frac{\text{number of quanta emitted}}{\text{number of quanta absorbed}} \qquad \textbf{(1.1)}$$

The quantum efficiency and the observed fluorescence lifetime (τ_f) are related by the following equation;

$$\Phi_F = \frac{k_r}{k_r + k_{nr}} = k_r \tau_f \qquad \textbf{(1.2)}$$

where k_r is the emissive rate of the fluorophore and k_{nr} is the nonradiative rate. The quantum yield can easily be determined by measuring the fluorescence emission of a dilute sample relative to a standard, which has the same absorption maximum and for which the quantum yield is known.[14] The efficiency of the fluorescence emission is dependent on several variables, which include concentration, temperature and excitation wavelength.[1,14] The fluorescence intensity of a molecule can be decreased as a result of quenching, which can be categorized as either collisional or static.[1,15] Collisional quenching refers to the return of a molecule to the ground state upon interaction with another molecule in solution, referred to as the quencher. Static quenching involves the formation of complexes in the excited state that are not fluorescent.[16]

One of the major bottlenecks to fluorescence detection is the photostability of the fluorophore.[17,18] Photobleaching of a fluorophore refers to the irreversible destruction of a molecule induced by light. The photodestruction quantum efficiency, Φ_d, can be determined by the following equation;

$$\Phi_d = \frac{1}{k_a \tau_b} \qquad \textbf{(1.3)}$$

where τ_b is the average photobleaching lifetime, k_a is the absorption rate, and Φ_d is the photodestruction quantum yield. The absorption rate is expressed by the equation;

$$k_a = \sigma_a I \quad \textbf{(1.4)}$$

where, σ_a is the absorption cross section (3.8×10^{-21} cm^2/molecule) multiplied by the molar absorptivity ($cm^{-1}M^{-1}$) and I is the laser intensity (photons cm^{-2} s^{-1}). The photodestruction quantum efficiency can be assessed directly by monitoring the decrease in fluorescence intensity or by flash photolysis generating photobleaching by short excitation pulses and analyzed using absorbance.[18-20] The stability of a molecule is a dye-dependent property and is significantly affected by environmental conditions such as temperature and atmospheric conditions.[21-23]

1.1.2 Fluorescence Lifetimes

Many biological studies rely on the change in fluorescence intensity to monitor analytes in response to changes such as quantum yields upon binding, and inner filtering effects. However, the fluorescence intensity can vary due to light scattering and photodestruction of fluorophores limiting their use for the aforementioned applications. Thus, several studies have begun to explore lifetime-based technologies for probing molecular targets.[24-26] The fluorescence lifetime is a measure of the amount of time an ensemble of molecules in the excited state returns to the ground state by emission. For lifetime measurements, the fluorescence intensity observed is proportional to the number of excited molecules at time t, according to the following expression;

$$I(t) = I_0 \exp(-t/\tau) \quad \textbf{(1.5)}$$

where I_0 is the intensity at time zero. The lifetime τ is the inverse of the total decay rate expressed by the sum of the rate constants of several first-order processes:

$$\tau_f = \frac{1}{k_r + k_{nr}} \quad \textbf{(1.6)}$$

where k_r (s^{-1}) is the radiative decay rate constant, k_{nr} (s^{-1}) is the non-radiative decay rate constant and τ_f (ns) is the fluorescence lifetime. The non-radiative decay process is composed of several rates, which is expressed by a linear combination of their decay constants;

$$k_{nr} = k_i + k_{ec} + k_{ic} + k_{pd} + k_d \qquad \textbf{(1.7)}$$

where intersystem crossing (k_i), external conversion (k_{ec}), internal conversion (k_{ic}), predissociation (k_{pd}), and dissociation (k_d) are the respective processes. Observed fluorescence lifetimes are typically 10^{-7} – 10^{-10} s.

1.1.3 Radiative Lifetimes

The natural lifetime of a fluorophore represents the fluorescent decay process in the absence of nonradiative decay processes and is expressed by the following equation:

$$\tau_0 = \frac{1}{k_r} \qquad \textbf{(1.8)}$$

The natural lifetime is related to the spontaneous processes of absorption and emission by a fluorescent molecule through the Einstein relation.[27] Einstein's equation was only useful for atomic systems, but in 1962 Strickler and Berg modified this equation to apply it to polyatomic molecules.[27] Thus, the Strickler-Berg equation can be used to calculate the radiative decay rate using the equation;

$$k_r = 2.880 \times 10^{-9} < \nu_f^3 >_{av}^{-1} \left(g_1/g_2\right) \int \varepsilon d \ln \nu \qquad \textbf{(1.9)}$$

where g_1/g_2 is the ratio of degeneracy levels of the electronic states of the compound, $\int \varepsilon d \ln \nu$ is the integrated extinction coefficient multiplied by the reciprocal of the average value of the wavenumber;

$$< \nu_f^3 >_{av}^{-1} = \frac{\int I(\nu) d\nu}{\int \nu^{-3} I(\nu) d\nu} \qquad \textbf{(1.10)}$$

obtained experimentally by taking the integral over the entire fluorescence emission band and multiplying the same integration by the cubed fluorescence intensity, and k_r is the radiative rate constant.[28] In theory, the Strickler-Berg equation provides a means for calculating the probability of spontaneous emission and is directly proportional to the probability of absorption for most transitions. In the case of weak transitions, there may be up to 30% error in this calculation.[11]

1.1.4 Steady-State and Time-Resolved Fluorescence

In addition to spectral information provided by steady-state fluorescence, time-resolved fluorescence is a means that provides time-related information of a particular analyte. Time-resolved fluorescence can reveal information about a molecule's behavior such as decay kinetics, conformational changes, its interaction with other macromolecules, and distinguishes between static and dynamic quenching. Steady-state fluorescence in conjunction with time-resolved fluorescence have become powerful tools for investigating various photophysical phenomena such as structure and dynamics in proteins, rotational diffusion and excited-state proton transfer reactions that are not available when performed in only the steady-state mode.[1] Techniques used for measuring intensity decay profiles are frequency-domain and time-domain methods.[1] Both techniques yield the same information and differ only in how the time-resolved data is obtained. In frequency-domain, the sample is excited with a sinusoidal modulated beam. Fluorescence emission occurs at the same frequency, but it is delayed compared to the modulated excitation. The phase shift (ϕ) and demodulation, M, can then be used to extract the lifetime. In time-domain methods, the sample is excited continuously with a pulsed light. The time-dependent intensity is measured following the excitation pulse, and the lifetime is determined from the slope of a plot of the intensity versus time. Both techniques offer several benefits. Time-domain techniques offer high sensitivity, an outstanding dynamic range and linearity, and

well-defined statistics for proper weighting of each data point. Benefits of frequency-domain include lifetime-based decomposition of spectra into their components is simple compared to time-domain and data collection is generally faster. A challenge associated with time-domain measurements is the pile-up effect in which the number of detected fluorescence photons is high compared to the number of excitation pulses resulting in distorted counting statistics causing the fluorescence decay to appear shorter.[29] The instrumentation for steady state and time-resolved fluorescence is discussed in the following sections.

1.2 Fluorescence Measurements and Instrumentation

1.2.1 Steady-State Fluorescence

Steady-state emission profiles are generally recorded on a single beam spectrofluorometer, that records in the spectral range of 200-1100 nm. The instrument consists of excitation and emission monochromators each containing gratings for specific wavelengths, a light source, a photomultiplier tube (PMT), shutters used to cut out excitation light and a computer for data acquisition and analysis. Figure 1.2 illustrates the standard components of a typical spectrofluorometer with the traditional "L-shape" configuration commonly seen in commercially available instruments to avoid background from non-absorbed radiation.[30] Light sources can be categorized as continuum or line sources depending on the spectral distribution of the emitted radiation.[30] Traditional continuum sources include gas filled arc lamps such as argon, mercury, and xenon lamps, which emit in the UV to visible, typically 200 to 650 nm. The most common source used for fluorescence spectroscopy is a 450 W high pressure Xenon arc lamp, providing a continuous spectrum of light ranging from the ultraviolet (250 nm) to infrared (700 nm). The white light generated is due to ionized Xe atoms colliding with electrons from the atoms yielding continuous emission.[1] Xenon lamps are available in either continuous mode (DC) or pulsed sources (AC).

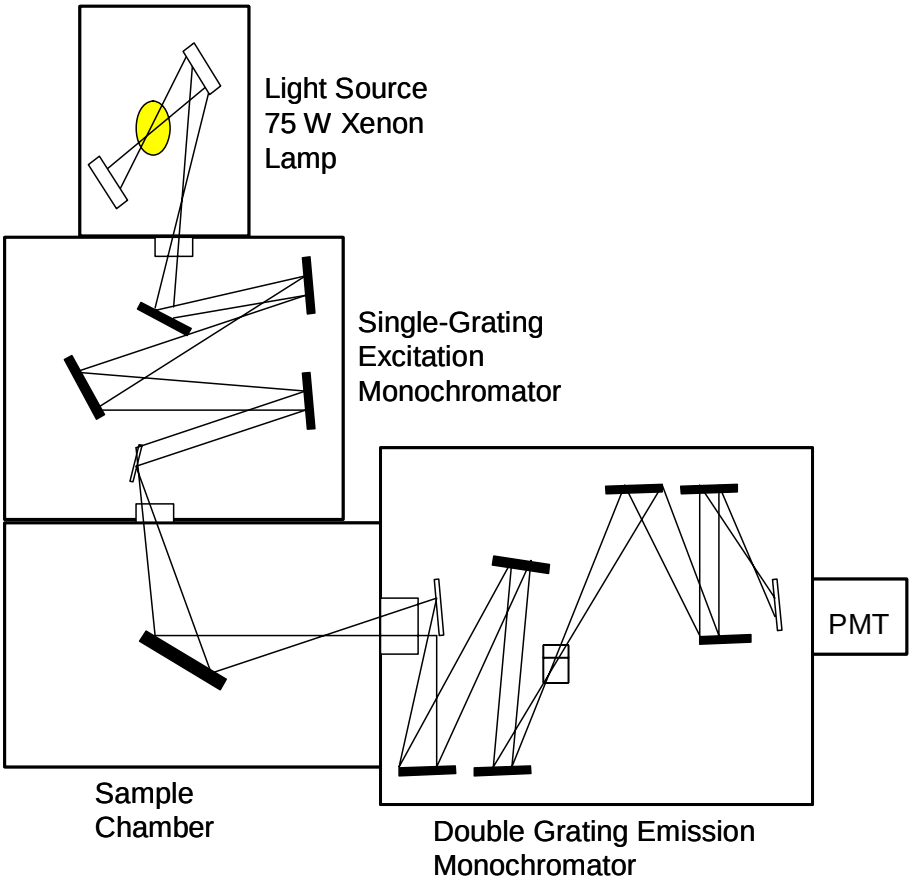

Figure 1.2 Schematic of a spectrofluorometer. The basic components are a light source, excitation and emission monochromators and photomultiplier tube for detection.

They are encased in optically clear glass envelopes due to the danger of explosion because the xenon gas is under high pressure. Additionally, the housing serves to collimate and focus the lamp output into the entrance slits of the monochromators.[1] It is important to mention here that when using xenon arc lamps for steady-state measurements, incorporating a mirror at the back of the lamp directs additional energy toward the output, maximizing the intensity of light that is focused on the entrance slit of the excitation monochromator, thereby increasing the sensitivity of the measurements. [1,30]

Monochromators separate light into various wavelengths accomplished using slits, mirrors that produce a parallel beam of irradiation, and diffraction gratings or prisms.

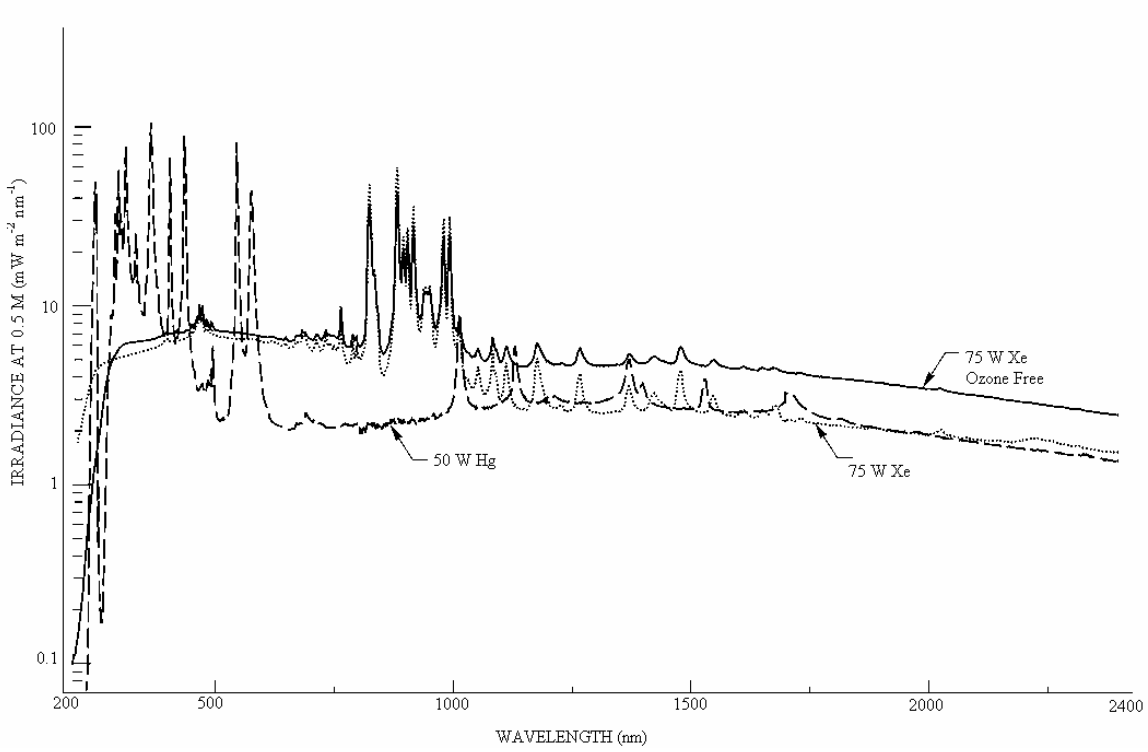

Figure 1.3 Spectral distribution (irradiance) for various arc lamps including the xenon lamp. (Courtesy of Newport; used with permission).

The slit widths are variable and a typical monochromator will have slits for the exit and entrance. Light enters the monochromator through entrance slits and is collimated using lenses or mirrors before striking a dispersing surface, which separates the light into component wavelengths. The two types of dispersing elements found in monochromators are prisms and gratings with the latter being the most common due to low fabrication costs, and better wavelength separation.[30] For prism monochromators, light is dispersed as a result of refraction; in grating monochromators, angular dispersion results from diffraction occurring at the surface of concave or planar gratings. Grating monochromators are widely used due to their high resolution, and dispersion properties that are independent of wavelength. A number of filters are available that transmit selected light or prevent light at certain wavelengths from passing through.[1] Examples of filters include optical filters such as colored glass or quartz and interference.[30]

Characteristics of an ideal detector include high sensitivity, high signal-to-noise ratio, and a rapid and steady response over a range of wavelengths. [30] Photomultiplier tubes (PMT) are widely used and are generally the most preferred detectors in fluorescence spectrometers. Photomultiplier tubes are composed of a photocathode and electrodes called dynodes that are fixed at constant but different negative potentials to amplify the signal. Photons that strike the photocathode cause secondary electrons to be emitted and these electrons then strike the first dynode causing additional electrons to be generated. Depending on the number of dynodes and overall voltage, the current is amplified by this cascade effect and the voltage is then measured.[1] Photomultiplier tubes are highly sensitive to high levels of ultraviolet and visible light. Furthermore, they have extremely fast response times. One limitation of the PMT is the noise from various sources in the tube such as thermal emission, resulting in dark current.

1.2.2 Time-Correlated Single Photon Counting (TCSPC)

This technique is like a "stopwatch" whereby a time clock starts as the excitation pulses begin. The method consists of exciting a fluorescent molecule by a continuous train of light pulses. Each pulse is detected by a photodiode that produces a start signal used to trigger the voltage ramp of a time-to-amplitude converter (TAC). The voltage ramp is stopped upon detection of the first fluorescence photon from the sample. By repeating this sequence an adequate number of times, a histogram of arrival times is compiled. The data are then processed using appropriate deconvolution and fitting procedures. Typically, three curves are associated with a fluorescence decay including the instrument response function, the measured data and the calculated data. The instrument response function is the response of the instrument usually measured using a dilute scattering solution.

1.2.2.1 Components for TCSPC Instrumentation

A block diagram of a TCSPC instrument is shown in Figure 1.3. For conventional TCSPC measurements, one of the most intricate parts of time-resolved fluorescence measurements is the constant fraction discriminator (CFD) that extracts with high precision the arrival time of electrical photon pulses that vary in amplitude. The CFD splits the detector signal into two parts, one part which is an amplified and delayed version of the original signal by about half of the pulse width.

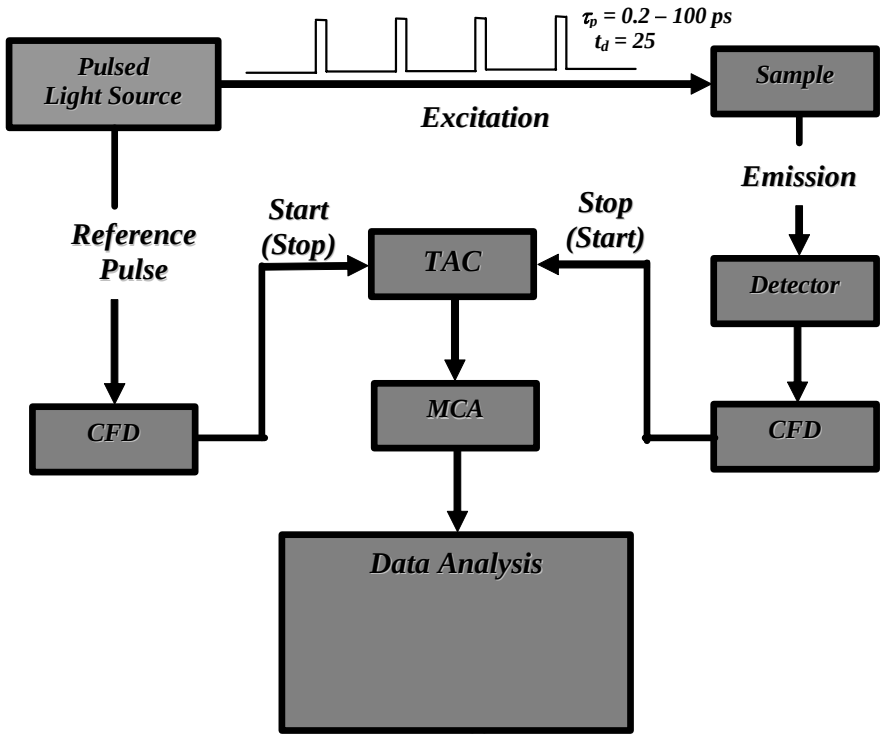

Figure 1.4 Schematic of a time-correlated single photon counting (TCSPC) instrument. The instrument consists of a light source, time-to-amplitude converter (TAC), constant fraction discriminator (CFD), mutichannel analyzer (MCA), and computer for data analysis.

The signal derived from combining the two parts changes polarity when a constant fraction of the pulse height is reached. A zero crossing signal is formed independent of the input pulse.[1] The time-to-amplitude converter (TAC) measures the time interval between the excitation pulse and the arrival time of the emitted photon. The TAC can operate in a reverse start-stop mode,

which enables the TAC to record at reduced speeds due to the cycle rate controlled by the photon detection rate and not the repetition rate of the laser.[1] The multi-channel analyzer (MCA) measures the voltage from the TAC and stores them in a time bin, or channel. MCA's are generally comprised of 2048-8192 channels, which are further divided into smaller parts.[1]

1.2.2.2 Data Analysis Methods for TCSPC Measurements

Two procedures used for fluorescence decay analysis is one based on weighted least-squares and the other based on maximum likelihood estimation (MLE). In the least-squares method, referred to as nonlinear least squares (NLLS), one assumes a model to describe the data. The goal is then to obtain the parameter values that provide the best estimate match between the experimental data and the calculated decay using the parameter values that are assumed. This is accomplished by minimizing the goodness of fit parameter, χ^2 where;

$$\chi^2 = \sum_{k=1}^{n} \frac{[N(t_k) - N_C(t_k)]^2}{N(t_k)} \qquad \textbf{(1.11)}$$

The value of χ^2 is the sum of the squared deviations between the experimental value, $N(t_k)$ and the expected value $N_c(t_k)$ divided by the squared deviations expected. For multiple exponential decays, a procedure that mathematically matches the measured data to the assumed data precisely is iterative reconvolution.

For MLE, the lifetime is calculated according to the following relationship

$$1 + (e^{T/\tau_f} - 1)^{-1} - m(e^{mT/\tau_f} - 1)^{-1} = N_t^{-1} \sum_{1}^{m} iN_i \qquad \textbf{(1.12)}$$

where m is the total number of time channels, T is the time width of each channel, N_t is the total number of photocounts used in calculation, and N_i is the number of photocounts in the time channel. The lifetime is determined from the data using reiterative techniques.

1.3 Factors Affecting Fluorescence

1.3.1 Intramolecular Effects

The molecular structure of a fluorophore can have an effect on the quantum efficiency of fluorescence. For example, structural rigidity plays a key role in the fluorescence intensity of a chromophore with a more rigid structure typically resulting in enhanced fluorescence, whereas lack of rigidity results in enhanced internal conversion and an increase in radiationless decay.[1,30] Structural modifications such as the addition of substituents may influence the fluorescence properties of the compound due to enhanced rates of non-radiative processes which, depend upon the nature and position of the substituent, can alter both the emission profile as well as the quantum efficiency. For example, electron accepting functional groups such as –COOH and -NO_2 possess low-lying π^* orbitals from which an electron can be promoted to an unoccupied orbital of the fluorescent molecule causing the electron density to be shifted from the macrocycle to the substituent as a consequence of the transition quenching the fluorescence. Observed changes include additional bands due to vibrational transitions and bathochromic shifts in the absorption and emission spectrum because of an increase in the extent of the π-electron configuration.

Complexation with a metal ion can also have a profound influence on the fluorescence characteristics of the molecule. Many transition metal ions have electrons that can be promoted to an orbital of the chromophore causing mixing of the electronic states that result in the appearance of charge transfer bands in the fluorescence spectrum. Generally, macrocycles complexed with closed shell diamagnetic metal ions such as zinc and gallium fluorescence strongly, with fluorescence spectra similar to the chromophore. Paramagnetic metal ions however, are found to interact strongly with the atomic orbitals of the macrocycle, resulting in quenching of the fluorescence due to increased efficiency of intersystem crossing, a direct

consequence of unpaired electrons in the d-orbitals.[11] It is also well established that heavy atom substituents also quench the fluorescence because of spin-orbital coupling (heavy atom effect) in which the metals' atomic orbitals conjugate with the first antibonding orbitals of the macrocycle to which an electron is promoted increasing the probability of intersystem crossing. Spin orbital interactions are dependent on the atomic number, Z, to the fourth power, and increase in atomic number increases spin orbit coupling.[31,32]

1.3.2 Environmental Effects

The nature of the environment such as solvent, pH, and temperature has shown to have a great impact on photophysical properties of fluorescent molecules, for example, spectral shifts in the emission wavelengths due to solvent interactions resulting from changes in the dipole moment of the fluorophore and lowering of the excited state energies.[1] Numerous equations have been derived that relate the differences in energy due to such interactions [1,2] Oshima investigated solvent effects on the photophysical properties of aniline dyes and reported marked differences observed in the fluorescence intensity and lifetime due to the hydrophobic nature of the solvent.[33] The intensity generally increases as the solvent viscosity increases since fewer molecules collide, thereby losing energy associated with internal conversion.[34] In addition, solvents that contain heavy atoms decrease the fluorescence of a molecule due to increased rates of intersystem crossing. The effect of a heavy atom as a function of geometry and distance between the heavy atom and chromophore have been studied by Kavarnos and co-workers, who concluded that the position of the heavy atom plays an important role in the interaction between singlet and triplet states.[35] Water as a solvent plays an important role in the fluorescence behavior of dyes because it serves as the preferred medium in biological studies.

1.4 Characteristics of Ideal Probes

The use of fluorescent dye molecules as a means of detecting many complex biological targets allows researchers to investigate complex systems with high sensitivity. When designing fluorescent probes, thermal stability and photostability, molar absorptivity, high quantum yields, and excitation and emission wavelengths are important features to consider for the qualitative and quantitative analysis of biomolecules.[36] Desirably, the absorption and emission maximum of the fluorescent reporter is in a spectral range that biomolecules do not show intrinsic fluorescence, which will increase selectivity and sensitivity. Ideally, a fluorescent probe would possess an extinction coefficient of at least 20,000 L mol^{-1} cm^{-1} , a high quantum yield (>0.1), high photostability, solublity in aqueous media to reduce aggregate formation , and high reactivity toward the target analyte.[37-39] The size of the fluorophore should also be considered, as small, rigid fluorophores are less perturbative of the target's local environment. Additionally, matching the appropriate dye sets with the wavelength of the excitation source is critical and with the advancement in technology, most continuous sources, in which the radiation changes slowly as a function of wavelength, offer flexibility.[40] These properties in combination with sensitive instrumentation can potentially allow label detection at the sub-picomolar level.[41]

Fluorescent probes can be covalently or non-covalently attached to the target molecule.[36,42,43] When a fluorescent dye is covalently bound to a biomolecule, it is desirable that the spectral and photophysical properties of the label are primarily unaffected by attachment to the target molecule.[40,43] A number of covalent fluorescent probes are available that can attach to target molecules through reactive groups such as isothiocyanates and succinimidyl esters that bind to primary amine groups on peptides, proteins and oligonucleotides. Fluorescent probes that attach to target molecules through non-covalent interactions are also available. These fluorophores usually exhibit weak fluorescence until associated to the target . This has proven

useful in a variety of applications such as detection of PCR fragments. Some commonly used fluorescent probes are described below with the choice of probe dependent upon the specific application.

1.4.1 Visible Fluorescent Probes (400-650 nm)

The most common organic dyes used for probing biomolecules are visible fluorophores due to their availability from commercial sources and the availability of excitation sources, such as argon lasers. However, there are disadvantages to working in the visible region. The increase in background noise due to scattering of the exciting photons and autofluorescence by biomolecules interferes with the analytical signal.[38,43] In addition, the fluorescence can be quenched on conjugation to biomolecules and their conjugates are pH sensitive.[44] Lefevre and coworkers reported on the use of several Texas red and rhodamine derivatives in an effort to improve conjugation reactions using these labels.[55] Sjöback characterized the properties of fluorescein conjugated to nucleic acids and determined the conjugates existed in two conformational states at neutral pH, which are important for biological studies.[45]

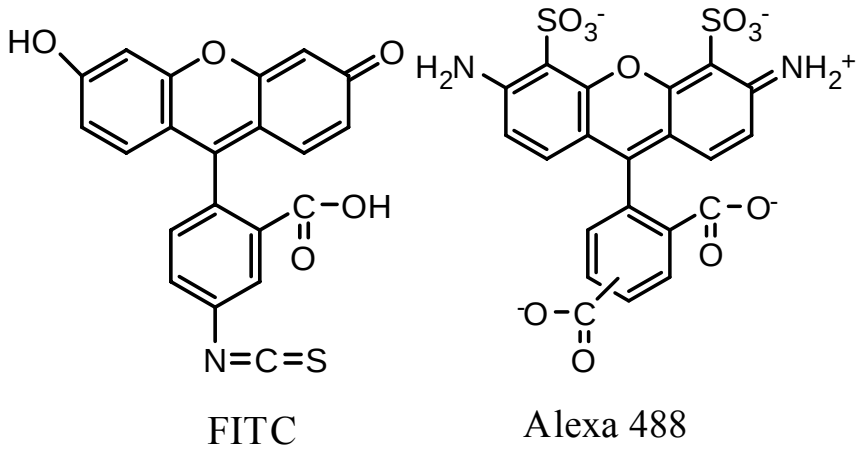

Figure 1.5 Examples of visible dyes, FITC and Alexa Fluor 488, commonly used for fluorescent labeling.

1.4.2 Near-Infrared (NIR) Probes (650-1000 nm)

Near-IR fluorescence has become a promising alternative to visible fluorescence for a variety of applications. Advantages include an increased signal-to-noise ratio arising from significant reductions in the background, since only a few molecules show intrinsic fluorescence in the near-IR spectral region. In addition, Raman cross sections are reduced compared to visible wavelengths.[46] Traditional fluorescent dyes used in covalent attachment to biomolecules are the carbocyanine dyes, consisting of an aromatic or heteroaromatic ring structures linked by a conjugated polymethine chain (see Figure 1.6). These dyes demonstrate a shift in the absorption and emission maximum wavelengths resulting from increasing the length of the polymethine chain.

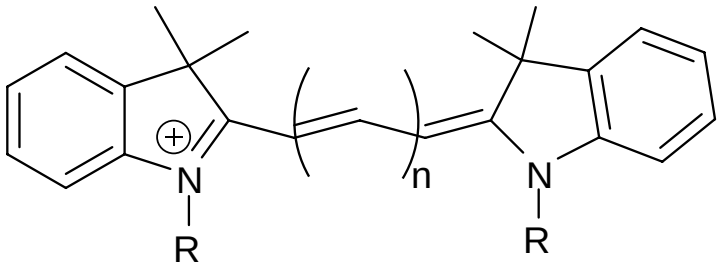

Figure 1.6 Basic structure of carbocyanine dyes used as fluorescent reporters.

Tricarbocyanine dyes have been used for a variety of biological applications, including DNA sequencing,[47] PCR,[48] and labeling of amino acids,[49] peptides[50] and proteins (see Figure 1.7). However, the major limitations associated with the carbocyanine dyes are their poor chemical and photochemical stabilities, low quantum yields in aqueous media and major spectral changes when placed in aqueous solutions.[38,51-54 39] Recently, Alexa Fluor dyes have been made commercially available that exhibit strong absorption in the near-IR region and have high extinction coefficients. The use of Alexa fluor dyes for a number of biological applications including immunofluorescence staining and flow cytometry has been reported.[23,44]

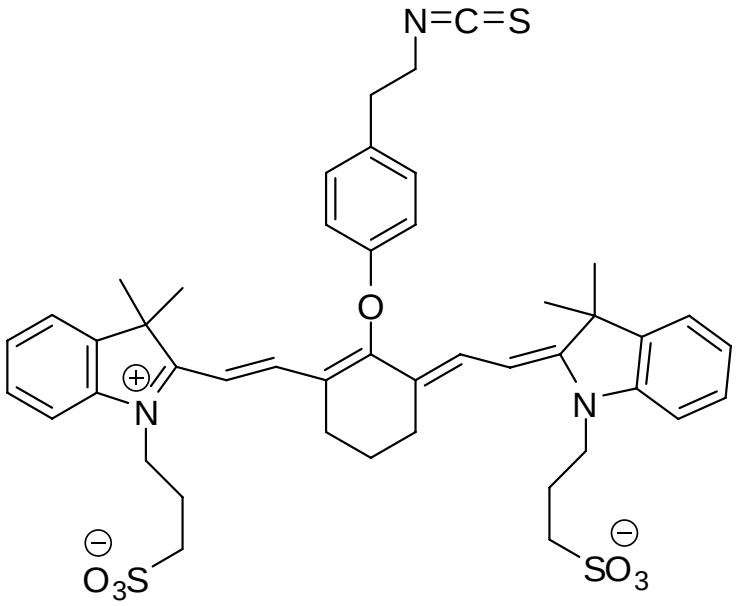

Figure 1.7 Structure of tricarbocyanine dye previously reported for use in DNA sequencing applications.[38]

1.4.3 Metal Phthalocyanines (MPc's) as Near-IR Fluorescent Probes

Although the availability of fluorescent probes has increased in the last decade, the existence of stable fluorescent probes for use in sensitive biological systems and DNA multiplexing is unsatisfactory due to poor water solubility and broad emission profile. The ability to tailor the spectral and photophysical properties make MPc dyes excellent candidates for use in complex biological assays. MPc dyes exhibit unique properties that, together with sophisticated time-resolved instrumentation, allow sensitive detection that exceeds what is obtainable with conventional near-IR dye-systems. Therefore, the aim of this research presented herein is to develop near-IR fluorescent, photostable MPc's that can be readily conjugated to biological targets and to characterize their photophysical and photochemical properties for labeling peptides, proteins, and oligonucleotides. The applications of these dyes includes labeling single stranded DNA for increased multiplexing capabilities in DNA sequencing and FRET based detection techniques for molecular diagnostics.

1.5 References

(1) Lakowicz, J. R. *Principles of fluorescence spectroscopy*; Plenum Press: New York, 1983.

(2) Guilbault, G. G.; Guilbault, G. G. *Practical fluorescence*; 2nd ed.; M. Dekker: New York, 1990.

(3) Varley, P. G. *Methods in molecular biology (Clifton, N.J.)* 1994, *22*, 203-18.

(4) Dewey, T. G. *Biophysical and biochemical aspects of fluorescence spectroscopy*; Plenum Press: New York, 1991.

(5) Hwang, L. C.; Wohland, T. *ChemPhysChem* 2004, *5*, 549-551.

(6) Soper, S. A.; Nutter, H. L.; Keller, R. A.; Davis, L. M.; Shera, E. B. *Photochem. Photobiol.* 1993, *57*, 972-977.

(7) Hof, M.; Hutterer, R.; Fidler, V. *Fluorescence spectroscopy in biology : advanced methods and their applications to membranes, proteins, DNA, and cells*; Springer: Berlin, Germany; New York, 2005.

(8) Soper, S. A., Williams, D. *Analytical Chemistry* 1995, *67*, 3427-3432.

(9) Soper, S. A., Owens, C, Lassiter, S., Xu, Y. *Topics in Fluorescence Spectroscopy* 2003, 1-68.

(10) Giepmans, B. N. G.; Adams, S. R.; Ellisman, M. H.; Tsien, R. Y. *Science* 2006, *312*, 217-224.

(11) Guilbault, G. G.; American Chemical Society. Division of Analytical Chemistry. *Fluorescence : theory, instrumentation, and practice*; M. Dekker: New York,, 1967.

(12) Becker, R. S. *Theory and interpretation of fluorescence and phosphorescence*; Wiley Interscience: New York,, 1969.

(13) Valeur, B. *Molecular fluorescence : principles and applications*; Wiley-VCH: Weinheim, 2002.

(14) Fery-Forgues, S.; Lavabre, D. *J. Chem. Educ.* 1999, *76*, 1260-1264.

(15) Hirschfeld, T. *Appl. Opt.* 1976, *15*, 3135-3139.

(16) Johansson, M. K.; Cook, R. M. *Chemistry-a European Journal* 2003, *9*, 3466-3471.

(17) Mathies, R. A.; Peck, K.; Stryer, L. *Analytical Chemistry* 1990, *62*, 1786-1791.

(18) Deschenes, L. A.; Bout, D. A. V. *Chemical Physics Letters* 2002, *365*, 387-395.

(19) Dittrich, P. S.; Schwille, P. *Applied Physics B-Lasers and Optics* 2001, *73*, 829-837.

(20) White, J. C.; Stryer, L. *Analytical Biochemistry* 1987, *161*, 442-452.

(21) Eggeling, C.; Volkmer, A.; Seidel, C. A. M. *Chemphyschem* 2005, *6*, 791-804.

(22) Heilemann, M.; Margeat, E.; Kasper, R.; Sauer, M.; Tinnefeld, P. *Journal of the American Chemical Society* 2005, *127*, 3801-3806.

(23) Berlier, J. E.; Rothe, A.; Buller, G.; Bradford, J.; Gray, D. R.; Filanoski, B. J.; Telford, W. G.; Yue, S.; Liu, J. X.; Cheung, C. Y.; Chang, W.; Hirsch, J. D.; Beechem, J. M.; Haugland, R. P.; Haugland, R. P. *Journal of Histochemistry & Cytochemistry* 2003, *51*, 1699-1712.

(24) Maliwal, B. P. *Analytical Chemistry* 2001, *73*, 4277-4285.

(25) McIntosh, S. L.; Nunnally, B. K.; Nesbit, A. R.; Deligeorgiev, T. G.; Gadjev, N. I.; McGown, L. B. *Analytical Chemistry* 2000, *72*, 5444-5449.

(26) Waddell, E.; Wang, Y.; Stryjewski, W.; McWhorter, S.; Henry, A. C.; Evans, D.; McCarley, R. L.; Soper, S. A. *Analytical Chemistry* 2000, *72*, 5907-5917.

(27) Strickler, S. J.; Berg, R. A. *Journal of Chemical Physics* 1962, *37*, 814-22.

(28) Soper, S. A.; Chamberlin, S.; Johnson, C. K.; Kuwana, T. *Applied Spectroscopy* 1990, *44*, 858-863.

(29) Gratton, E.; Breusegem, S.; Sutin, J.; Ruan, Q. Q. *Journal of Biomedical Optics* 2003, *8*, 381-390.

(30) Skoog, D. A.; Holler, F. J.; Nieman, T. A. *Principles of instrumental analysis*; 5th ed.; Saunders College Pub.; Harcourt Brace College Publishers: Philadelphia; Orlando, Fla., 1998.

(31) Harriman, A. *Journal of the Chemical Society, Faraday Transactions 2: Molecular and Chemical Physics* 1981, *77*, 1281-91.

(32) Pavlopoulos, T.; El-Sayed, M. A. *The Journal of Chemical Physics* 1964, *41*, 1082-1092.

(33) Oshima, J.; Shiobara, S.; Naoumi, H.; Kaneko, S.; Yoshihara, T.; Mishra, A. K.; Tobita, S. *Journal of Physical Chemistry A* 2006, *110*, 4629-4637.

(34) Ogunsipe, A.; Nyokong, T. *J. Mol. Struct.* 2004, *689*, 89-97.

(35) Kavarnos, G.; Cole, T.; Scribe, P.; Dalton, J. C.; Turro, N. J. *Journal of the American Chemical Society* 1971, *93*, 1032-&.

(36) Beddard, G. S.; West, M. A. *Fluorescent probes*; Academic Press: London ; New York, 1981.

(37) Haugland, R. P. *Handbook of Fluorescent Probes and Research Chemicals*; 6th ed.; Molecular Probes Inc.: Eugene, OR, 1996.

(38) Flanagan, J. H.; Khan, S. H.; Menchen, S.; Soper, S. A.; Hammer, R. P. *Bioconjugate Chemistry* 1997, *8*, 751-756.

(39) Hammer, R. P.; Owens, C. V.; Hwang, S. H.; Sayes, C. M.; Soper, S. A. *Bioconjugate Chemistry* 2002, *13*, 1244-1252.

(40) Kapanidis, A. N.; Weiss, S. *Journal of Chemical Physics* 2002, *117*, 10953-10964.

(41) Slavík, J. *Fluorescence microscopy and fluorescent probes*; Plenum Press: New York, 1996.

(42) Slavík, J. *Fluorescent probes in cellular and molecular biology*; CRC Press: Boca Raton, 1994.

(43) Owens, C. V.; Louisiana State University (Baton Rouge La.). Dept. of Chemistry. Thesis (Ph.D.), Louisiana State University, Baton Rouge, 2000., 2000.

(44) Voloshina, N. P.; Haugland, R. P.; Bishop, J.; Bhalgat, M.; Millard, P.; Mao, F.; Leung, W. Y.; Haugland, R. P. *Molecular Biology of the Cell* 1997, *8*, 2017-2017.

(45) Sjoback, R.; Nygren, J.; Kubista, M. *Biopolymers* 1998, *46*, 445-453.

(46) Williams, D. C., Soper, S.A. *Analytical Chemistry* 1995, *67*, 3427-3432.

(47) Shealy, D. B.; Lipowska, M.; Lipowski, J.; Narayanan, N.; Sutter, S.; Strekowski, L.; Patonay, G. *Analytical Chemistry* 1995, *67*, 247-251.

(48) Schwartz, H. E.; Ulfelder, K. J. *Analytical Chemistry* 1992, *64*, 1737-1740.

(49) Flanagan, J. H.; Legendre, B. L.; Hammer, R. P.; Soper, S. A. *Analytical Chemistry* 1995, *67*, 341-347.

(50) Williams, R. J.; Lipowska, M.; Patonay, G.; Strekowski, L. *Analytical Chemistry* 1993, *65*, 601-605.

(51) Flanagan, J. H.; Owens, C. V.; Romero, S. E.; Waddell, E.; Kahn, S. H.; Hammer, R. P.; Soper, S. A. *Analytical Chemistry* 1998, *70*, 2676-2684.

(52) Soper, S. A.; Legendre, B. L.; Huang, J. P. *Chemical Physics Letters* 1995, *237*, 339-345.

(53) Davidson, Y. Y.; Gunn, B. M.; Soper, S. A. *Applied Spectroscopy* 1996, *50*, 211-21.

(54) Fouassier, J. P.; Lougnot, D. J.; Faure, J. *Optics Communications* 1976, *18*, 263-7.

(55) Lefevre, C.; Kang, H. C.; Haugland, R. P.; Malekzadeh, N.; Arttamangkul, S.; Haugland, R. P. *Bioconjugate Chemistry* 1996, 7, 482-489.

Chapter 2
Water Soluble Metal Phthalocyanines: The Role of the Functional Groups on the Spectral and Photophysical Properties

2.1 Introduction

Phthalocyanines (Pc) and their metal complexes (MPc) have attracted considerable interest and have been found to be highly promising candidates for a variety of uses such as liquid crystals,[1,2] photosensitizers,[3-5] and in various chemical sensing applications.[6,7] The properties that make Pc/MPc dyes particularly attractive as potential bioassay reagents include their high molar absorptivity,[8,9] resistance to chemical and photochemical degradation,[10] absorption and emission in the deep red region of the electromagnetic spectrum,[9,10] long lifetimes with high quantum yields,[10] and a wide range of accessible chemical structures allowing the design of compounds capable of meeting certain needs.[11] The difficulties associated with these dyes includes their propensity to form aggregates due to molecular stacking resulting in low quantum yields,[12,13] limited solubility in aqueous media, formation of mixed isomers during synthesis,[14,15] and difficulties in purifying these dyes to homogeneity using standard chromatographic methods.[16] Unfortunately, these limitations have severely limited the use of Pc and MPc dyes as potential labeling reagents for ultra-sensitive fluorescence-based measurements.

MPc's and Pc's are chemically robust and photochemically stable due in part to the nitrogens located within the aromatic macrocycle and the peripherally-fused benzene rings.[17,18] These dyes possess a strong absorption band in the near-IR due to the extended π–conjugation system around the ring structure.[3,10] Pc's can coordinate a variety of metals in their central cavity, which further enables tailoring their spectral and photophysical properties because the metal can affect the pathways of the excited MPc returning to the ground state, in particular the rate of intersystem crossing resulting from metal-ligand spin-orbit coupling.[19,20] In addition,

interaction of the metal with the π system of the Pc can modify the electron distribution of the macrocycle resulting in additional absorption bands and/or bathochromic shifts in existing bands, which are highly dependent upon the paramagnetic properties of the central metal.

Several examples have appeared in the literature in which Pc derivatives have been described with emphasis placed on the synthesis of the Pc with a primary goal of tuning the water solubility and aggregation effects for their use in photodynamic therapy.[21,22] For example, Vicente and coworkers reported on the synthesis and cell uptake of ZnPc's bearing 16-carboxylic acids to reduce aggregation for use as a potential photosensitizer for cancer therapy.[5] Ng *et al.* synthesized dendritic phthalocyanines and studied their aggregation behavior, which was influenced by interactions with surfactants.[23] Margaron *et al.* synthesized several different ZnPc dyes to evaluate their use for photodynamic therapy.[4] Results indicated that the phototoxicity increased with decreasing number of sulfonate groups on the periphery. Sener *et al.* reported on the synthesis and spectroscopic studies of MPc's substituted with dicarboxyethyl substituents designed to control intermolecular dimerization of the MPc's in solution.[24] Spectroscopic evaluation indicated a high propensity of these compounds to dimerize at pH > 6. Unfortunately, none of the aforementioned work described the role of the solubilizing groups on the photophysical properties of the MPc or Pc dyes or has used the peripheral water solubilizing groups (i.e., symmetrical Pc dyes) as an attachment scaffold to biomolecular targets. Several groups have reported the use of asymmetrical MPc derivatives as fluorescent labeling reagents bearing a single isothiocyanato group for tagging monoclonal antibodies or oligonucleotides.[25,26] Asymmetrical MPc's, which are comprised of water solubilizing groups and a functional group, however, are difficult to prepare and isolation of the desired product is often challenging as a result of statistical mixtures of substituted Pc's obtained during synthesis.

Herein, we report on the synthesis, spectroscopic and photophysical properties of several symmetrical Pc's and MPc's that can potentially serve as fluorogenic labeling reagents for near-IR fluorescence applications that exhibit favorable water solubility, minimal aggregation effects in aqueous media and facile conjugation routes to primary-amine containing targets. We made use of symmetrical MPc's as the labeling reagents for conjugation due to their ease of preparation and simplified purification methods. We examined alkoxy substituted MPc's having peripheral four, eight and sixteen carboxylate groups and a variety of central metal ions (Al(OH), Ga(OH), Zn, Ni, Pt and Pd) as well as metal-free Pc's in order to evaluate the spectroscopic and photophysical effects of these substitutions on the base chromophore and aggregation properties. These water solubilizing groups were also used for the covalent attachment of biomolecules to the fluorophore. Fluorescence quantum yields, radiative lifetimes and photobleaching quantum yields, which are crucial in determining the feasibility of using any dye as reporters for high sensitivity analyses of biological molecules, will be reported and related to the degree of carboxylation of the MPc. In addition, the spectral and photophysical properties will be examined upon conjugating an MPc dye to a biological target (i.e., streptavidin).

2.2 Materials and Methods

2.2.1 Reagents and Samples

Spectral grade dimethyl sulfoxide (DMSO) and dimethylformamide (DMF) were obtained from Aldrich Chemical Co. (Milwaukee, WI). N-hydroxysuccinimide ester (NHS), and N,N-dicyclohexylcarbodiimide (DCC) was purchased from Sigma-Aldrich Co. (Milwaukee, WI). 3-(Cyclohexylamino)-1 propanesulfonic acid (CAPS) and 4-(2-Hydroxyethyl) piperazine-1-ethanesulfonic acid (HEPES) were obtained from Sigma. HPLC grade acetonitrile was purchased from Aldrich Chemical Co. and used without further purification. Triethylammonium acetate (TEAA) buffer and streptavidin from streptomyces avidinii were purchased from Fluka

(St. Louis, MO). Zinc acetate and nickel acetate tetrahydrate were finely ground, dried at 110 ºC under vacuum for 30 h and stored in sealed vials; palladium (II) chloride, platinum (II) chloride, anhydrous aluminum chloride, anhydrous gallium chloride, anhydrous tin (IV) chloride were used as received.

Chromatographic separations were obtained using a Jasco HPLC (Jasco, Inc., Easton, MD) equipped with a diode array and fluorescence detector. Reverse-phase HPLC chromatography was performed using a Supelco C-18 column (Bellefonte, PA) with a linear gradient of 5-95% acetonitrile/0.1% TEAA for 45 min. at a flow rate of 1 mL/min. Analysis of the HPLC data was performed using EZChrom software provided by JASCO. The purity of MPc's was verified by the observance of a single peak detected at 680 nm. Thin Layer Chromatography (TLC) was performed using silica gel as the stationary phase. Flash chromatography was performed with silica gel of particle size 60 μm. Melting points were determined using a Fisher-Johns melting point apparatus. NMR spectra were recorded on a Bruker DPX-250. GC-MS spectra were recorded on a Hewlett Packard 5971A mass spectrometer in EI mode at 70 eV. MALDI mass spectra were recorded on a Bruker ProFLEX III MALDI-TOF mass spectrometer.

2.2.2 Synthesis of Metal and Metal-Free Phthalocyanines (MPc's)

The synthesis of the MPc's was performed in collaboration with Dr. Hammer's laboratory by Dr. Guifa Su and Dr. Serhii Pakhomov. A mixture of 4-nitrophthalonitrile (for the synthesis of **1**, see Scheme 2.1), 4,5-dichlorophthalonitrile (7 mmol, for the synthesis of **2** and **3**, see Scheme 2.2 and 2.3, respectively), substituted 4-hydroxybenzoate (for **1**, 7.5 mmol and for **2** and **3**, 15.4 mmol) and dried potassium carbonate (6.38 g, 46.2 mmol) in anhydrous DMF (50 mL) was stirred overnight at 85°C in an inert atmosphere. After cooling to room temperature, the mixture was diluted with ethyl acetate (60 mL) and water (40 mL). The organic layer was

separated and the aqueous phase was extracted with ethyl acetate (2 x 50 mL). The combined organic layers were washed with a saturated solution of $NaHCO_3$ (40 mL), brine (40 mL) and dried over Na_2SO_4. The solvents were removed *in vacuo*, and the crude product was purified by column chromatography on silica gel using dichloromethane/acetonitrile mixture (20/1) as an eluent to furnish **1-3**.

4-(4-Pentoxycarbonyl) phenoxyphthalonitrile (**1**)*:* 88 %, mp 48-49 °C, ^{1}H NMR ($CDCl_3$) δ 8.15 (d, 2H, J = 8.7 Hz), 7.77 (d, 1H, J = 8.7 Hz), 7.35 (d, 1H, J = 2.3 Hz), 7.30 (d, 1H, J = 8.7 Hz), 7.12 (d, 2H, J = 8.7 Hz), 4.34 (2H, t, OCH_2, J = 6.7 Hz), 1.79 (m, 2H, CH_2), 1.42 (m, 4H, CH_2CH_2), 0.94 (t, 3H, J = 7 Hz, CH_3).

4,5-Bis(4-pentoxycarbonyl) phenoxyphthalonitrile (**2***):* 88 %, mp 77-78 °C, ^{1}H NMR ($CDCl_3$) δ 8.11 (dd, 4H, J = 2.1, 6.8 Hz), 7.35 (s, 2H), 7.03 (dd, 4H, J = 2.1, 6.8 Hz), 4.33 (t, 4H, J = 6.7 Hz, 2 CH_2O), 1.78 (m, 4H, 2 CH_2), 1.41 (m, 8H, 2 $(CH_2)_2$), 0.94 (t, 6H, 2 CH_3, J = 7.1 Hz).

4,5-Bis(3,5-dimethoxycarbonyl) phenoxyphthalonitrile (**3**): 74 %, mp 202-203 °C, ^{1}H NMR (CD_3CN) δ 8.33 (t, 2H, J = 1.45 Hz), 7.75 (d, 4H, J = 1.45 Hz), 7.63 (s, 2H, J = 1.45 Hz), 3.87 (s, 12 H, 4 CO_2CH_3). FAB (glycerol) 544.8 (M^+) (calculated on $C_{28}H_{20}N_2O_{10}$ 544.47).

Syntheses of Phthalocyanines (typical procedure). 2,9,16,23-Tetrakis(4-carboxyphenoxy)-phthalocyanato zinc (II)(**6a**, Scheme 2.1, Path B): A mixture of 4-(4-pentyloxycarbonylphenoxy)phthalonitrile (0.670 g, 2.0 mmol), anhydrous zinc acetate (0.183 g, 1.0 mmol) and dry pentanol (5 mL) was heated to 65°C under argon. DBU (0.4 mL, 2.5 mmol) was added dropwise to the mixture, which was subsequently refluxed for 24 h. The solvents were removed *in vacuo* and the residue was purified by column chromatography on silica gel using hexanes/ethyl acetate mixtures (3/1) as the eluent. The fractions were combined and the solvents were evaporated to dryness. The residue was dissolved in THF (40 mL) and added dropwise to a solution of $LiOH{\cdot}H_2O$ (1.568 g, 36.6 mmol) in 70% aqueous methanol (100 mL). The mixture

was stirred at 60°C for 17 h. The organic solvents were removed *in vacuo*, the aqueous phase washed with chloroform (3 x 20 mL) and acidified to pH 2 with HCl (4 M). The resultant precipitate was centrifuged, washed with chloroform (3 x 20 mL) and oven dried at 60°C.

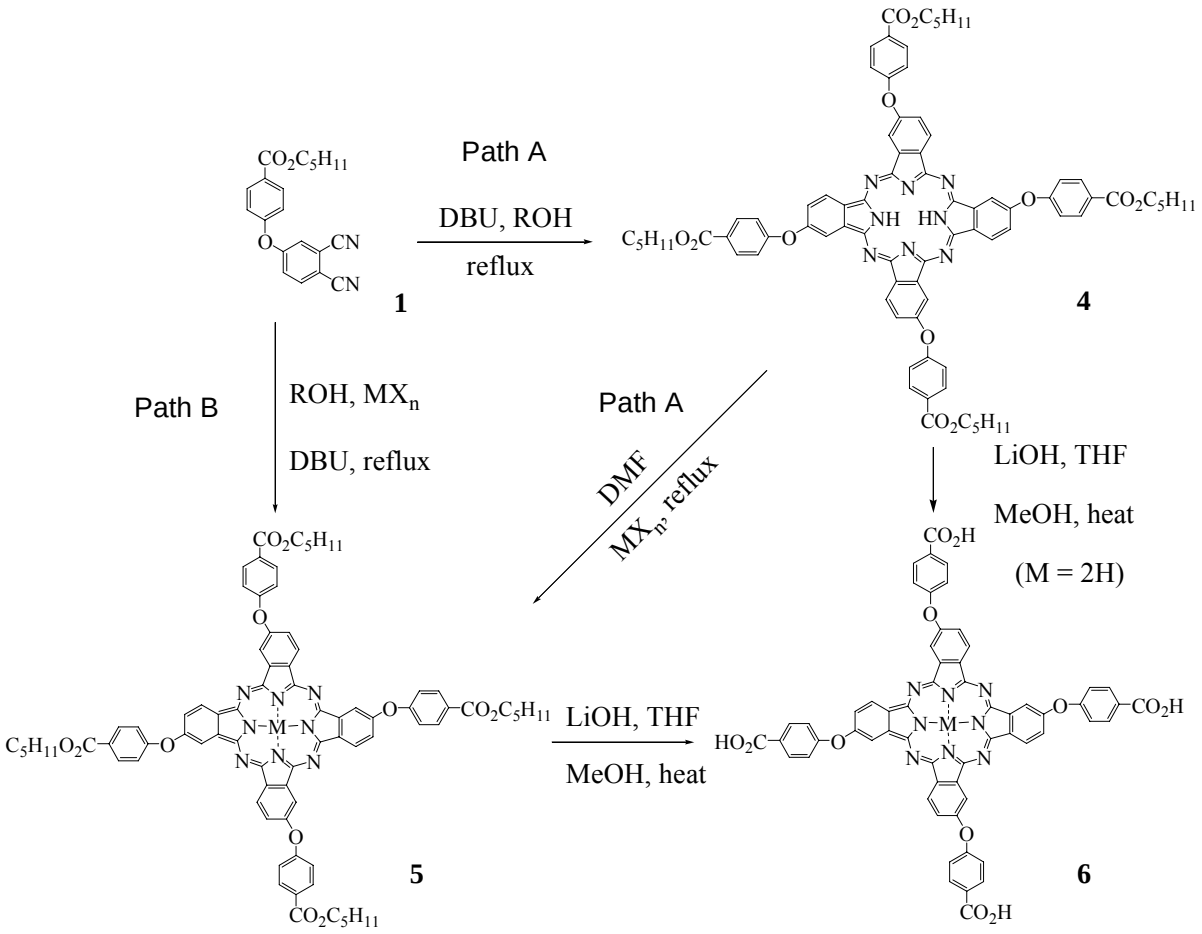

Figure 2.1 Schematic of the synthesis of 2,9,16,23-tetrasubstituted Pc's.

Syntheses of Phthalocyanines (typical procedure). 2,9,16,23-Tetrakis(4-carboxyphenoxy)-phthalocyanato zinc (II) (**6a,** Scheme 2.1, Path A): A solution of 2,9,16,23-tetrakis(4-pentoxycarbonylphenoxy)phthalocyanato zinc (II) (***5a*)**, 0.430 g, 0.307 mmol) in THF (40 mL) was added dropwise to a solution of $LiOH{\cdot}H_2O$ (1.568 g, 36.6 mmol) in 70% aqueous methanol (100 mL). The mixture was stirred at 60°C for 17 h.

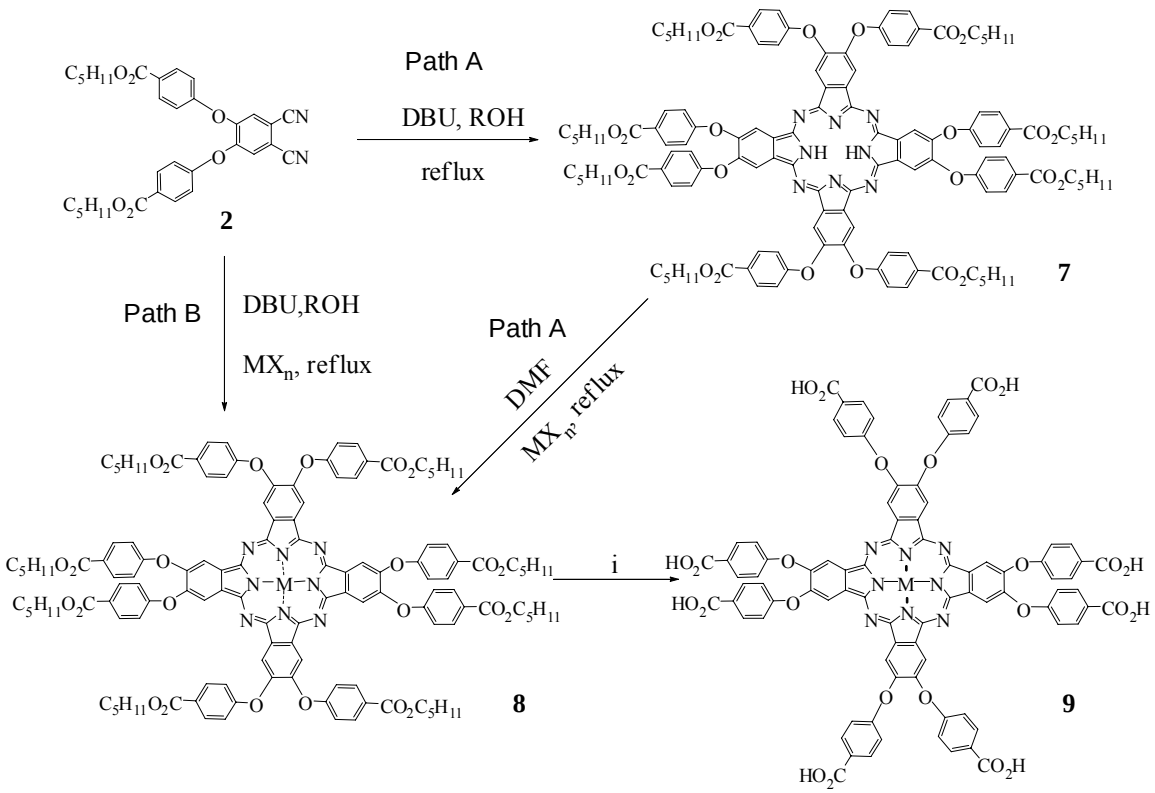

Figure 2.2 Schematic of the synthesis of 2,3,9,10,16,17,23,24-octabsubstituted MPc's

The reaction mixture work-up was done as above. MS (MALDI-TOF, anthracene) produced an isotopic cluster peak at *m/z* 1120.88 (MH^+). ^{1}H NMR (DMSO-d^6) δ 9.04 (br, 4H), 8.65 (br, 4H), 8.13 (m, 8 H), 7.85 (br, 4H), 7.48 (m, 8H). 2,3,9,10,16,17,23,24-Octakis(4-pentoxycarbonyl)-phenoxyphthalocyanine (**7**, Scheme 2, Path A): A mixture of 4,5-*bis*(4-pentoxycarbonylphenoxy)phthalonitrile (***2***, 1.08 g, 2 mmol) in dry *n*-pentanol (10 mL) was stirred at 90^{o}C under argon and DBU (0.32 mL, 2 mmol) was added dropwise. The mixture was refluxed for 38 h. *n*-Pentanol was removed *in vacuo* and the crude product was purified by column chromatography (silica gel, eluent hexane/ethyl acetate 9:1 to 4:1). MS (MALDI-TOF, anthracene) yielded an isotopic cluster peak at *m/z* 2164.47 (M^+).

2,3,9,10,16,17,23,24-Octakis(4-pentoxycarbonylphenoxy)phthalocyanato zinc (II) (**8a**, Path A, see Scheme 2.2):A mixture of 2,3,9,10,16,17,23,24-octakis(4-pentoxycarbonylphenoxy)-phthalocyanine (**7**, 110 mg, 0.05 mmol), anhydrous zinc acetate (37 mg, 0.2 mmol) and dry DMF (10 mL) was refluxed under argon (12 h).

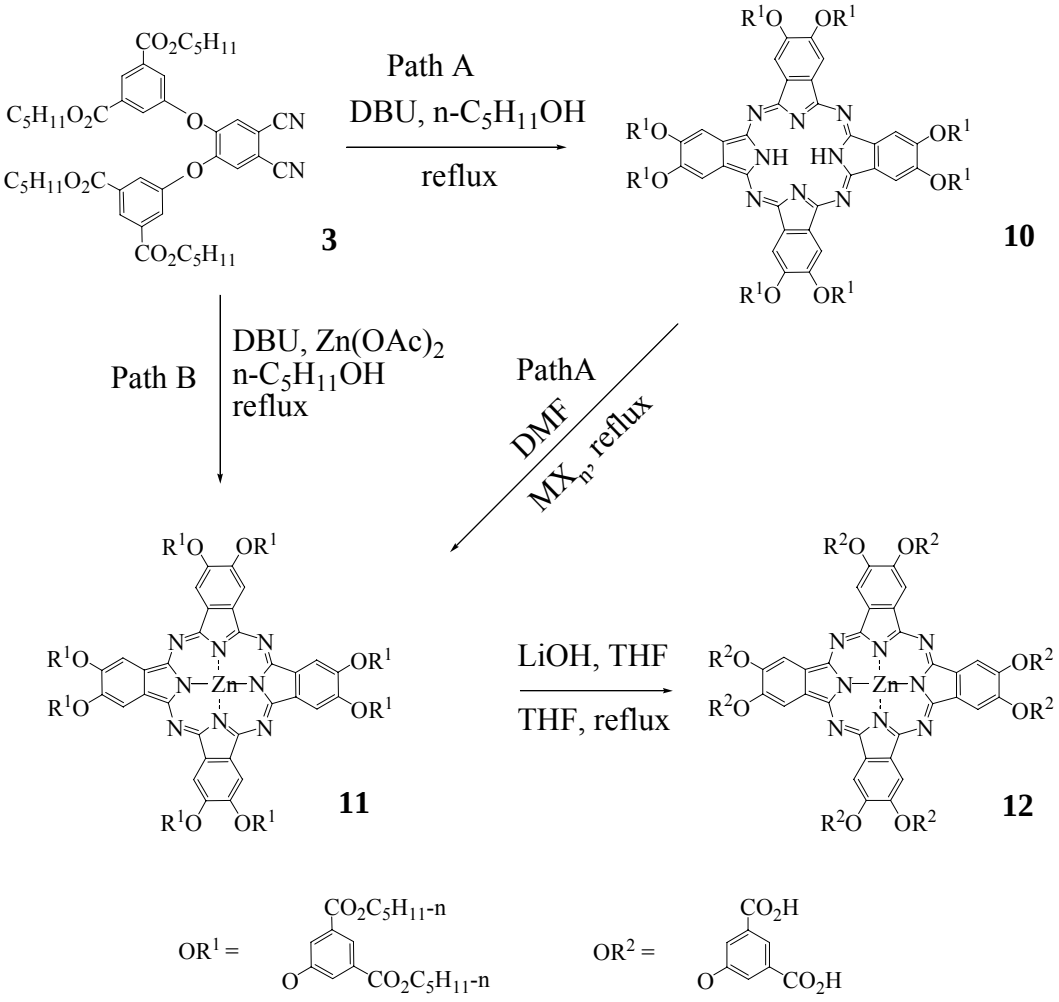

Figure 2.3 Schematic of the synthesis of hexadeca substituted ZnPc.

The flask was cooled on an ice-water bath for 20 min. The mixture was poured into a beaker containing 13 g of crushed ice and the precipitate was filtered and washed with cold water, and then air dried. The crude product was purified by column chromatography (silica gel, eluent: hexane/ethyl acetate, 4:1 to 3:1). MS (MALDI-TOF, anthracene) yielded an isotopic cluster peak at *m/z* 2227.84 (M^+).

Synthesis of zinc phthalocyanine N, hydroxysuccinimide ester. The synthesis of NHS ester derivatives of carboxylate zinc-Pc ***6a*** was adapted from a published procedure and will only be described briefly here.[27] A solution of carboxylate Pc ***6a*** was dissolved in dry DMF and added to a solution of NHS and DCC (1.5 equiv. each) in dry DMF.

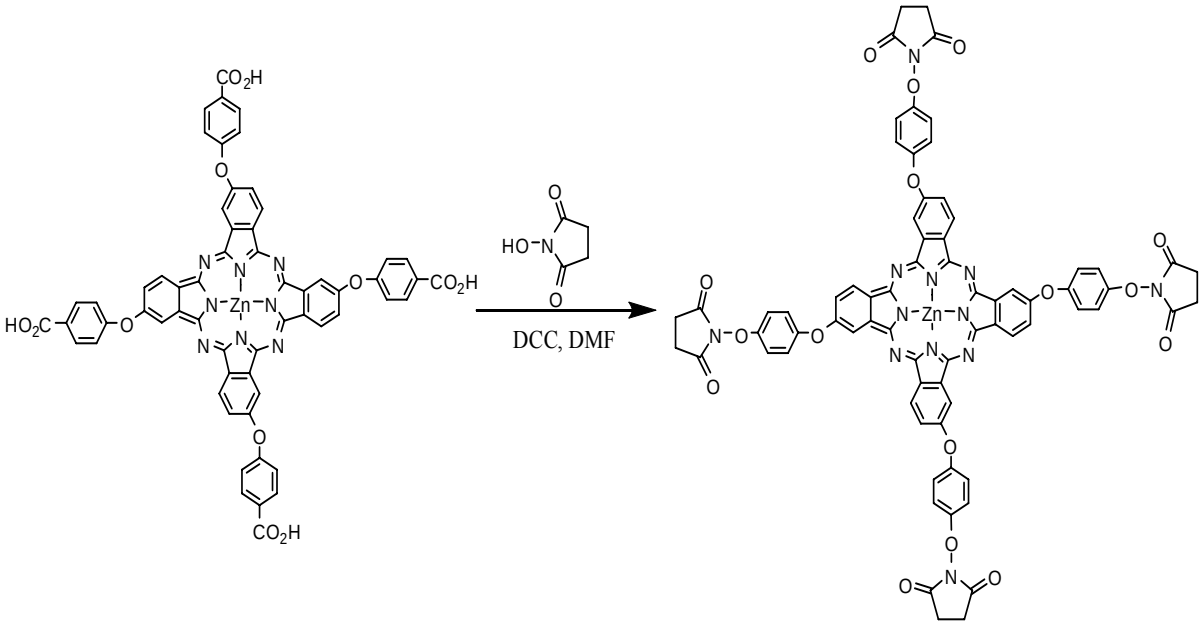

Figure 2.4 Synthesis of ZnPc-N, hydroxysuccinimide ester using DCC in the presence of DMF. The reaction was carried out at room temperature under agitation and allowed to react overnight. The reaction was then pooled and the product was precipitated by the addition of diethyl ether, isolated by centrifugation and dried under vacuum for several hours (see Figure 2.4).

2.2.3 Spectral and Fluorescence Measurements of Metal-Free and MPc's

▪ UV/Vis Spectra. Absorption spectra were collected on an Ultrospec 4000 single beam UV/Visible spectrophotometer (Amersham Biosciences, Piscataway, NJ) with 1-cm quartz cuvettes using SWIFT software (Amersham Biosciences). The concentrations of the MPc dyes used in these measurements were 1 - 100 x 10^{-6} M to minimize the formation of aggregates.[28] The molar absorptivity was calculated from a least squares fit of the absorbance versus concentration for each dye. An absorption spectrum of the reference solvent, which was DMSO, was obtained and subtracted prior to the acquisition of each spectrum.

▪ Fluorescence Measurements. Steady-state fluorescence spectra were acquired using a Spex Fluorolog-3 equipped with a 450 W Xenon light source (Horiba Jobin Yvon, Edison, NJ) and a Hamamatsu R928 photomultiplier tube (Bridgewater, NJ). DM300 software was used for data analysis. Fluorescence spectra were obtained using an excitation wavelength of 680 nm for Pc and MPc dyes with a bandpass of 2 nm for both the excitation and emission monochromators.

The quantum yields were determined relative to a secondary standard using the equation;[29,30]

$$\Phi_{f(x)} = (A_{standard}/A_{sample})\,(F_{sample}/F_{standard})\,(n_{sample}/n_{standard})^2\,\Phi_{standard} \qquad (\mathbf{1})$$

where F_{sample} and $F_{standard}$ are the measured fluorescence for the sample and standard respectively, $A_{standard}$ and A_{sample} are the measured absorbance, n_{sample} and $n_{standard}$ are the refractive index of the solvent used for the sample and standard, respectively, and $\Phi_{standard}$ is the quantum yield of the secondary standard. The secondary standard used in these experiments was diethyloxatricarbocyanine iodide (DOTCI). The quantum yield of DOTCI has been reported to be 0.63 in DMSO.[31] For the determination of the quantum yields, the secondary standard was excited at 680 nm to avoid post correction analysis. To minimize any error due to reabsorption or aggregation, all measurements were made with highly dilute solutions having an absorbance between 0.04 and 0.05 for a 1 cm path length.

▪ Time-Resolved Fluorescence Measurements. Time-resolved fluorescence decays were collected using time-correlated single photon counting (TCSPC) acquired on a Fluotime 200 instrument (Picoquant, Berlin Germany). The excitation source was a 680 nm pulsed diode laser (PDL 800, Picoquant). Since rotational diffusion could lead to distortion of the fluorescence decay, a polarizer was inserted into the system and set at the magic angle of 54.7°. The spectrometer consisted of a monochromator (ScienceTech 9030) and a photomultiplier tube (PMS 182-M single photon detection). All electronics for TCSPC were situated on a single PC card resident on the bus of the PC and consisted of a constant fraction discriminator and time-to-digital converter with an instrument response function of ~450 ps (FWHM). Time-resolved data were analyzed using FluoFit software (Picoquant, Berlin Germany). The fluorescence decays

were collected until ~10,000 counts were accumulated in the time channel with the most counts and fit to single or multi-exponential functions by an iterative reconvolution algorithm using nonlinear least squares. The instrument response function was always collected to the same maximum number of counts as the fluorescence decay data. The quality of the fit was determined by the randomness of the weighted residuals and the value of χ^2.

▪ Photobleaching Measurements. Bleaching curves were recorded by continuously irradiating several MPc dyes, and commercially available dicarbocyanine, IRD700, and tricarbocyanine, DOTCI for several minutes under air using a 680 nm diode laser (Picoquant, Berlin Germany) as the excitation source. The beam waist was measured by mounting a razor blade on a translation stage and measuring the beam power using a laser power meter. The product of $I_0\sigma$ (laser intensity in photons s^{-1} cm^{-2} × absorption cross section in cm^2) was kept constant for all samples to eliminate absorption rate (k_a) differences in the bleaching curves. The absorption cross section was determined by multiplying 3.8×10^{-21} by the molar extinction coefficient. The dyes were dissolved in DMSO at a concentration of 1.0 μM and were not degassed. A linear least squares fit to a semi-log plot of time versus the fluorescence intensity was used to calculate the photobleaching rate. The quantum yield of photobleaching was determined from the following equation:

$$\tau_b = \frac{1}{k_a \Phi_d} \qquad \textbf{(2)}$$

where, τ_b is the photobleaching lifetime (s), k_a is the absorption rate (s^{-1}), and Φ_d is the photobleaching quantum yield. An estimation of the photon yield per molecule was calculated from the ratio of the fluorescence quantum yield to the photo-destruction quantum yield.

▪ Labeling of Streptavidin with ZnPc **6a** Active Ester. Conjugation of ZnPc ***6a*** to streptavidin was performed in 0.1 M HEPES buffer, pH 8, using a streptavidin concentration of 10μM. A solution of N-hydroxysuccinimide tetraester of ZnPc ***6a*** in DMSO was added to the streptavidin solution to achieve the desired dye-to-protein molar concentration ratio of 10:1. The reaction was incubated at room temperature for 24 h followed by analysis and purification using reverse-

phase HPLC. Separation of the products was performed on a C18 column using a linear gradient of 30-75 % acetonitrile/0.1TEAA for 30 minutes at a flow rate of 1 mL/min. The elution of the conjugates was monitored using fluorescence detection at 686 nm for excitation and 693 nm for emission.

2.3 Results

2.3.1 Synthesis of Metal and Metal-Free Phthalocyanines

Figure 2.1-2.3 describes the methods used to prepare tetra-, octa-, and hexadeca-carboxylate Pc's and MPc's. The metal-free analogues, which can serve as precursors for various MPc's, are usually prepared by base-promoted cyclization of phthalonitriles. For the synthesis of MPc's one can imagine two routes: one through the introduction of the central metal into the metal-free Pc (Path A in Schemes 2.1-2.3) or direct metal templated MPc preparation (Path B in Figures 2.1-2.3).

The starting substituted phthalonitriles **1-3** were prepared from 4-nitrophthalonitrile or 4,5-dichlorophthalonitrile and appropriate phenols according to literature protocols.[5,32,33] Synthesis of the previously reported Zn-tetracarboxylate Pc **6a** starts with phthalonitrile **1** as the pentyl ester.[34,35] Refluxing of **1** in pentanol in the absence of a metal salt (Scheme 2.1, Path A) gives the metal-free, tetra-ester Pc **4**. Refluxing of it in DMF in the presence of an excess (>10 equiv.) of $Zn(OAc)_2$ converts it to the ZnPc tetra-pentyl ester **5a**.

The preparation of this compound is more directly accomplished by refluxing of phthalonitrile **1** in pentanol in presence of DBU and $Zn(OAc)_2$ (Scheme 2.1, Path B). This direct synthetic route also works well for the preparation of Ni, Pd and Pd MPc's as tetra-pentyl esters **5d-5f**. Because Path B consists of one less step than Path A, the overall yields of the compounds prepared by this method were higher than those for Path A. Moreover, the cyclization itself is

facilitated in the presence of the metal giving higher yields for the synthesis of MPc's than for metal-free Pc's.

For Group IIIa MPc's, direct synthesis of tetracarboxylates GaPc **6b** and AlPc **6c** by refluxing the substituted phthalonitrile and the appropriate metal salt in *n*-pentanol in an inert atmosphere with the subsequent hydrolysis of MPc's esters **5b** and **5c** failed. Thus, only Path B was available for the synthesis of these derivatives which consists in the reaction of metal free Pc (tetra-ester) **4** refluxed with $GaCl_3$ or $AlCl_3$ to give esters metallated Pc's esters **5b** and **5c**, correspondingly.

Table 2.1 Absorption (λ_a) and emission (λ_e) maxima of a metal free (H_2Pc) and several MPc dyes. The dyes were suspended in DMSO. HPLC retention times (t_R) for the MPc's using a reverse phase column and the exact mass as determined by MALDI-TOF-MS of each dye is also listed.

Compound	λ_a[a] (nm)	λ_f[a] (nm)	ε[a] ($M^{-1}cm^{-1}$)	Molecular formula	MALDI-MS		t_R[b]
					Calculated	Found	
ZnPc **6a**	677	687	2.85×10^5	$C_{60}H_{33}N_8O_{12}Zn$ (MH^+)	1121.15 (MH^+)	1120.88	19.2
GaPc **6b**	680, 696	689	2.94×10^4	$C_{60}H_{32}N_8O_{12}Ga$ [$(M\text{-}OH)^+$]	1125.14 ($M\text{-}OH^+$)	1124.76	19.1
AlPc **6c**	677	683	3.00×10^4	$C_{60}H_{33}N_8O_{13}Al$ (M^+)	1100.20 (M^+)	1099.82	19.3
NiPc **6d**	673	*Weak Fluorescence*	2.71×10^4	$C_{60}H_{32}N_8O_{12}Ni$ (M^+)	1115.15 (M^+)	1114.82	19.1
PdPc **6e**	665	*Weak Fluorescence*	N.M.[c]	$C_{60}H_{32}N_8O_{12}Pd$ (M^+)	1162.12 (M^+)	1162.37	19.1
PtPc **6f**	696	*Weak Fluorescence*	N.M.[c]	$C_{60}H_{32}N_8O_{12}Pt$ (M^+)	1251.18 (M^+)	1250.98	19.1
ZnPc **9a**	678	686	2.75×10^5	$C_{88}H_{48}N_8O_{24}Zn$ (M^+)	1665.22 (M^+)	1665.34	22.5
ZnPc **12**	676	689	2.67×10^5	$C_{96}H_{48}N_8O_{40}Zn$ (M^+)	2018.13 (M^+)	2018.50	26.1
H_2Pc **6g**	654, 675	686	3.3×10^4	$C_{60}H_{35}N_8O_{12}$ (MH^+)	1059.24 (MH^+)	1059.45	

a. All measurements were made at a concentration of 1 x 10^{-6} M. Molar absorptivities were calculated at λ_{max}. b. HPLC conditions: 5-95% acetonitrile/0.1 M TEAA at a flow rate of 1 mL/min. c. N.M., not measured. Cannot be determined reliably due to aggregations

The methyl ester of phthalonitrile **1** works well for either Path A or Path B, but gives mixtures of esters in the resulting Pc (or MPc) ester products, complicating their purification. In

order to avoid such complications, we prefer to match the ester group to the preferred alcohol. Pentanol gives the most flexibility in terms of temperature range for the reaction and thus, the pentyl ester of starting phthalonitriles (**1-3**) has become our standard. To generate either the metal-free Pc or MPc tetracarboxylates, their pentyl esters are saponified with LiOH in a tertiary mixture of water, THF and methanol. Both the MPc esters and the lithium salts generally stay soluble in this medium and upon acidification with aqueous HCl, the pure free acids are readily obtained in quantitative yields. Purification of these compounds can be accomplished by washing the precipitate with chloroform and dissolving the solid in aqueous hydroxide solution and re-precipitating the free acid (Pc or MPc) into aqueous acid (HCl).

Table 2.2 Absorption (λ_a) and emission (λ_e) maxima of metal free (H_2Pc) and MPc dye pentyl esters. Extinction coefficients (ε) and the exact mass, as determined by MALDI-TOF-MS are also listed.

Compound	**# of COOH groups**	**Solvent**	**λ_a (nm) [ε ($M^{-1}cm^{-1}$)]**	**Molecular formula**	**MALDI-MS**	
					Calculated	**Found**
H_2Pc **4**	4	$CHCl_3$	664 (5.67×10^4), 701 (6.50×10^4)	$C_{80}H_{74}N_8O_{12}$	1338.54 (M^+)	1338.30
ZnPc **5a**	4	$CHCl_3$	677	$C_{80}H_{72}N_8O_{12}Zn$	1400.46 (M^+)	1400.69
GaPc **5b**	4			$C_{80}H_{73}ClN_8O_{12}Ga$	1441.43 $(M+H)^+$	1441.22
AlPc **5c**	4			$C_{80}H_{73}ClN_8O_{12}Al$	1399.49 $(M+H)^+$	1399.68
NiPc **5d**	4	$CHCl_3$	670.5 (9.27×10^4)	$C_{80}H_{73}N_8O_{12}Zn$	1395.47 $(M+H)^+$	1395.10
PdPc (methoxy-ethyl ester) **5e**	4	pyridine DMSO	664 (5.70×10^4) 665.5	$C_{72}H_{57}N_8O_{16}Pd$	1395.29 $(M+H)^+$	1394.87
H_2Pc **7**	8	$CHCl_3$	664 (1.04×10^5), 700.5 (1.21×10^5)	$C_{60}H_{32}N_8O_{12}Pt$	2162.92 (M^+)	2163.06
ZnPc **8a**	8	$CHCl_3$	680.5	$C_{128}H_{128}N_8O_{24}Zn$	2224.83 (M^+)	2225.12
GaPc **8b**	8	$CHCl_3$	697 (1.90×10^5)	$C_{128}H_{129}ClN_8O_{24}Ga$	2268.61 $(M+H)^+$	2268.69
H_2Pc **10**	16	$CHCl_3$	662.5 (1.47×10^5), 699. 5 (1.64×10^5)	$C_{176}H_{210}N_8O_{40}$	3077.47 (M^+)	3077.64
ZnPc **11**	16	DMSO	643 (4.65×10^4)			

Alternatively, a DMF solution of the free acid can be precipitated into an excess of diethyl ether. Because the central atom of the group IIIa MPc's is trivalent, the MPc's should

have axial ligands. According to the MALDI data, the ligand of Ga and Al MPc's (esters) is chloride (see Table 2). Under the subsequent hydrolysis reaction conditions, chloride is substituted by a hydroxyl group. This transformation is seen in the MALDI analysis of tetracarboxylate AlPc **6c**, where the molecular ion $C_{60}H_{33}N_8O_{13}Al$ is observed. The corresponding GaPc **6b** does not exhibit molecular peaks in MALDI-TOF as only $(M\text{-}OH)^+$ peaks are observed. Despite the absence of mass spectral evidence for the hydroxyl ligand on the GaPc **6b**, we assume its presence in analogy with AlPc **6c** and its requirement for filling of the Ga valencies.

For the synthesis of the octa and hexadeca substituted MPc's **9** and **12** (see Figures 2.2 and 2.3, respectively), we used the same synthetic routes. It is possible to use both paths A and B, but again the use of path B gave higher yields. Phthalonitriles **2** and **3** used in the syntheses of MPc's esters **8** and **11**, are more sterically hindered and having different aromatic electron density because of substitution, so their cyclization reaction gave lower yields of Pc's and MPc's. Increasing the reaction temperature did not increase the yields of the final compounds. The rate of hydrolysis of pentyl esters of such MPc's **8** and **11** is slower and required up to 5 times higher concentrations of the hydroxide of to achieve complete saponification.

2.3.2 Spectral Properties

Absorption spectra of Pc dyes typically have two main bands, one in the UV and another in the near-IR. The higher energy band (~350 nm) is known as the B or Soret band.[17,36] The lower energy band, typically appearing around 680 nm, is often referred to as the Q-band. The Q-band exhibits vibronic structure in solution between 610 and 640 nm.[17,37,38]

The absorption and fluorescence emission properties, including the molar absorptivities for the Pc and MPc's containing various degrees of carboxylation are listed in Table 2.1. The absorption and emission spectra of the ZnPc dyes with different degrees of carboxylation are shown in Figures 2.5A and 2.5B, respectively.

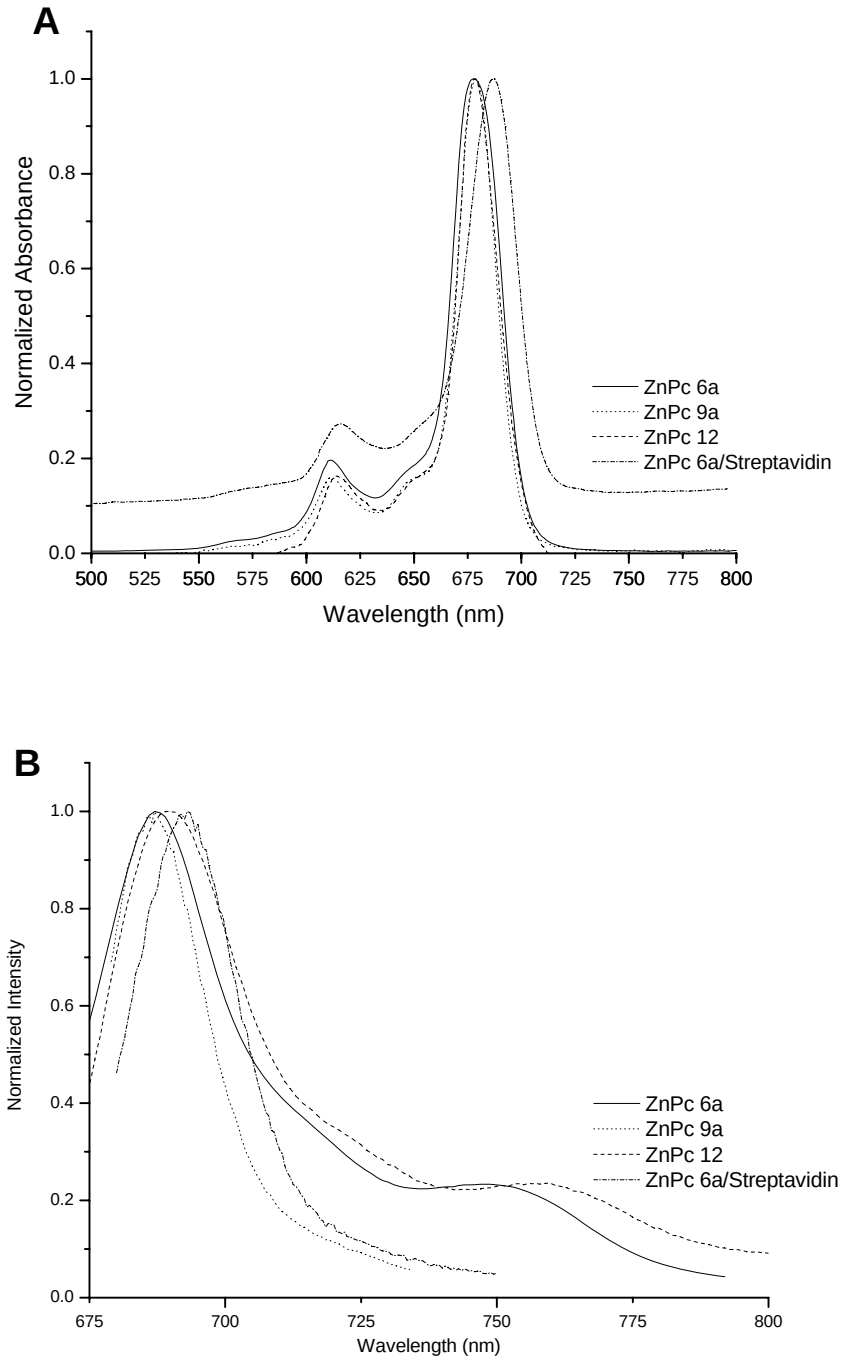

Figure 2.5 Absorption (A) and emission (B) spectra of ZnPc dyes along with the ZnPc **6a**/streptavidin complex. The emission spectra were obtained at an excitation wavelength of 675 nm. The emission spectra were normalized to the maxima. All emission spectra were collected in DMSO at a concentration of ~1.0 μM, while the absorption spectra used dye concentrations that varied from 1-100 μM.

Tetracarboxylate ZnPc **6a** shows a single absorption peak at 677 nm with a blue-shifted band at 610 nm. Upon excitation at 675 nm, **6a** exhibited strong fluorescence with a maximum at 687 nm and a shoulder at 759 nm. The absorption and emission spectra for octa and hexadecacarboxylate ZnPc **9a** and **12** in DMSO were similar to those exhibited by tetracarboxylate ZnPc **6a**. However, the emission shoulder appearing at ~759 nm for **6a** and **12** was absent in the case of **9a**.

The absorption and emission spectra of the following tetracarboxylates - metal free Pc **6g**, GaPc **6b** and AlPc **6c** in DMSO are shown in Figures 2.6A and 2.6B, respectively. GaPc **6b** exhibited a split in its Q-band with absorption maxima at 680 nm and 696 nm, while AlPc **6c** showed only a singlet Q-band with an absorption maximum at 677 nm. In the case of metal free Pc **6g**, a very broad absorption spectrum was observed with a Q-band split showing a maximum at 675 nm.

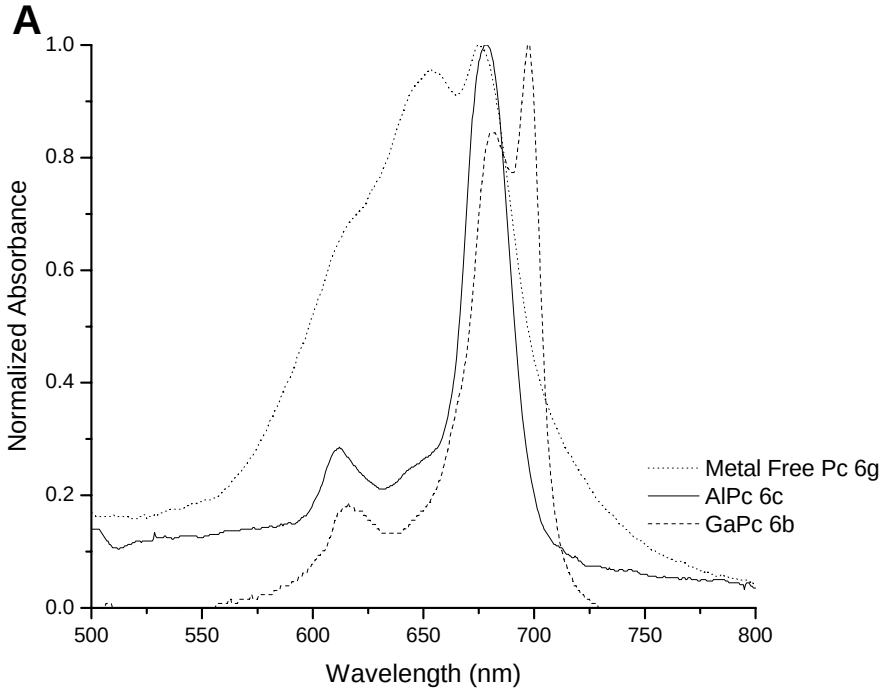

Figure 2.6 Normalized absorption (A) and emission (B) spectra for a metal free Pc and several metal substituted Pc dyes (Zn, Al, Ga) dissolved in DMSO. The emission spectra were excited at the absorption maximum for each dye at a concentration of 1.0 μM. In all cases, the tetra-carboxylated dyes were used in these measurements.

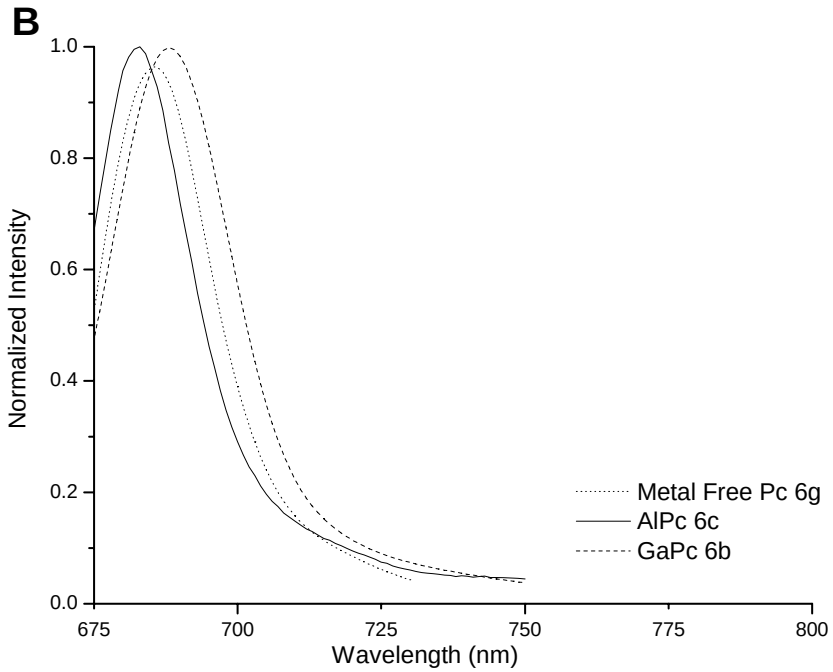

Figure 2.6 Continued

GaPc **6b**, AlPc **6c** and metal free Pc **6g** showed emission maxima that ranged between 683 and 689 nm with a slight red-shift seen for the maxima in the series, Al, H_2 and Ga. The absorption maxima, extinction coefficients and MALDI-MS data for the MPc esters **5**, **8** and **11** are also listed in Table 2.2. The absorption characteristics are consistent with the data seen for the free acids. In addition, the calculated mass agreed favorably to that obtained from the MALDI-MS, indicating the assigned molecular structure of the dye was correct.

The absorption spectra of tetra-, octa- and hexadecacarboxylate ZnPc **6a**, **9a** and **12**, tetracarboxylate AlPc **6c** and GaPc **6b** in HEPES at pH 8 are illustrated in Figures 2.7. The absorbance was also measured in CAPS at pH 11 and the results were the same as those shown in Figure 2.7. Most of these compounds showed similar absorption maxima, but broader absorption envelopes compared to the same spectra in DMSO with the absorption maximum slightly blue-shifted (~645 nm in HEPES compared to ~675 nm in DMSO). However, **9a** and **12** showed absorption characteristics in both HEPES and CAPS buffer that were very similar to those observed in DMSO, both in terms of the spectral widths and absorption maxima.

2.3.3 Photophysics of MPc's

The fluorescence quantum yields of the MPc complexes were measured with respect to a secondary standard, diethyloxatricarbocyanine iodide (DOTCI), in DMSO, which has a documented quantum yield of 0.63 [31]. The quantum yields for ZnPc **6a**, **9a** and **12** with different degree of carboxylation ranged from 0.40 – 0.41, while the quantum yields for GaPc **6b** and AlPc **6c** were 0.58 and 0.60, respectively.

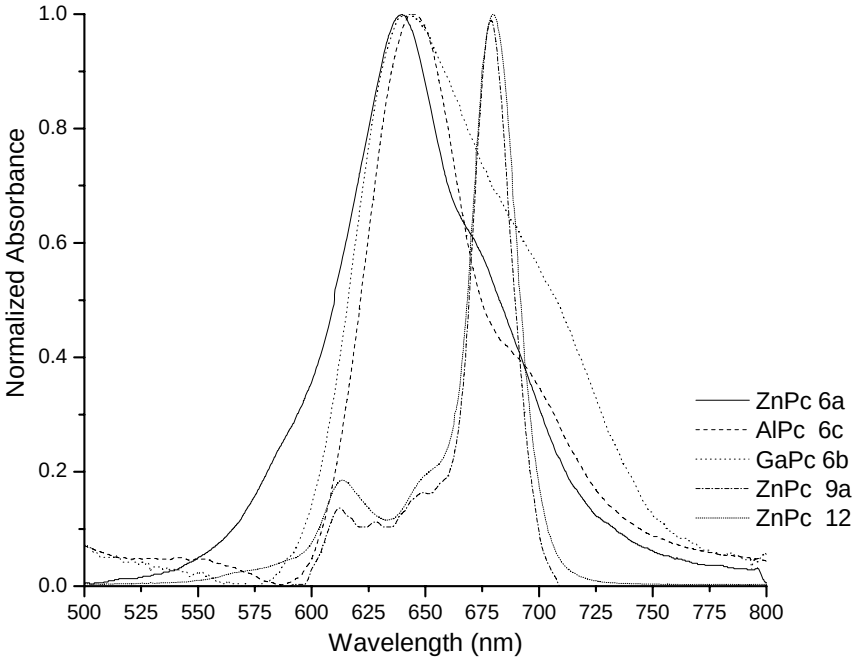

Figure 2.7 Absorption spectra for MPc's in HEPES buffer, pH 8. The concentrations of dyes used in these measurements were 1.0 x 10^{-6} M. The absorption spectra were normalized with respect to the absorption maxima.

The quantum yields were also determined for the MPc's in CAPS buffer at pH 11 with the result shown in Table 2.3. The quantum yields for the ZnPc's **6a**, **9a** and **12** and GaPc **6b** were 0.10, whereas the quantum yield for AlPc **6c** was determined to be 0.30. The radiative decay rates for several of the MPc's were estimated using the emission and extinction profiles and the Strickler-Berg equation [39], which yielded rates calculated for ZnPc **6a**, GaPc **6b** and AlPc **6c** of 0.64 × $10^9 s^{-1}$, 0.58 × 10^9 s^{-1}, and 0.48 × 10^9 s^{-1}, respectively (see Table 2.3).

The fluorescence lifetimes for each MPc dye are given in Table 2.3. ZnPc **6a** had a lifetime of 3.1 ns with its decay kinetics adequately described by a single exponential function. AlPc **6c** was best fit to a double exponential function yielding fluorescence lifetimes of 5.0 and 0.64 ns. In addition, GaPc **6b** exhibited a multi-exponential decay with the longest lifetime being 3.5 ns. Octacarboxylate ZnPc **9a** was best fit to a monoexponential function with a lifetime of 2.9 ns while hexadecacarboxylate ZnPc **12** displayed a lifetime of 2.8 ns (see Table 2.2).

Table 2.3 Fluorescence lifetimes (τ_f), fluorescence quantum yields (Φ_f), photobleaching quantum yields (Φ_d), and photon yields per molecule (n_f) for the standard, DOTCI, metal free and several metal Pc dyes. The χ^2 value for each decay profile is also presented. All of these photophysical properties were measured in DMSO, except for the fluorescence quantum yields measured in H_2O (CAPS, pH = 11.0) and the ZnPc **6a**/streptavidin conjugate, which was measured in HEPES buffer (pH = 8.0).

Compound	τ_f **(ns)**	τ_2 **(ns)**	Φ_f	Φ_f **H_2O**	Φ_d	n_f	k_r **(ns^{-1})**	χ^2
ZnPc **6a**	3.1		0.41	0.11	5.0×10^{-7}	1.3×10^6	0.64	1.43
ZnPc **9a**	2.9		0.40	0.11	4.3×10^{-7}	1.4×10^6		1.49
ZnPc **12**	2.8		0.40	0.12	1.3×10^{-7}	5.0×10^6		1.27
GaPc **6b**	3.5	0.57	0.58	0.14	2.3×10^{-6}	2.7×10^5	0.58	1.48
AlPc **6c**	5.0	0.64	0.60	0.31	2.8×10^{-5}	2.1×10^4	0.48	1.09
DOTCI	n.d*	n.d*	0.63		7.0×10^{-3}	90.0		
IRDye 700	n.d*	n.d*	0.70		4.6×10^{-6}	1.5×10^5		
ZnPc **6a**/ streptavidin	2.85			0.16				

NOTE: Radiative rates were calculated using the Strickler-Berg relationship. Samples were prepared to have an optical density of ≤ 0.05 at the λ_{max}.
*The fluorescence lifetimes for DOTCI and IRD700 were not determined (n.d.).

The photodestruction quantum yields along with the photon yields per molecule for tetra-, octa- and hexadecacarboxylate ZnPc **6a**, **9a** and **12**, as well as AlPc **6c** and GaPc **6b** are listed in Table 2.3. The results indicate decreased photostability for AlPc **6c** compared to ZnPc **6a** with a photobleaching quantum yield of 2.8×10^{-5} for AlPc and 5.0×10^{-7} for ZnPc. For the ZnPc's **6a**, **9a** and **12**, increasing the degree of carboxylation provided dyes with increased photostabilities and consequently, improved photon yields on a per molecule basis. A qualitative

examination of the photobleaching data showed that these ZnPc dyes were significantly more photostable than a commercially available tricarbocyanine dye (see Figure 2.8).

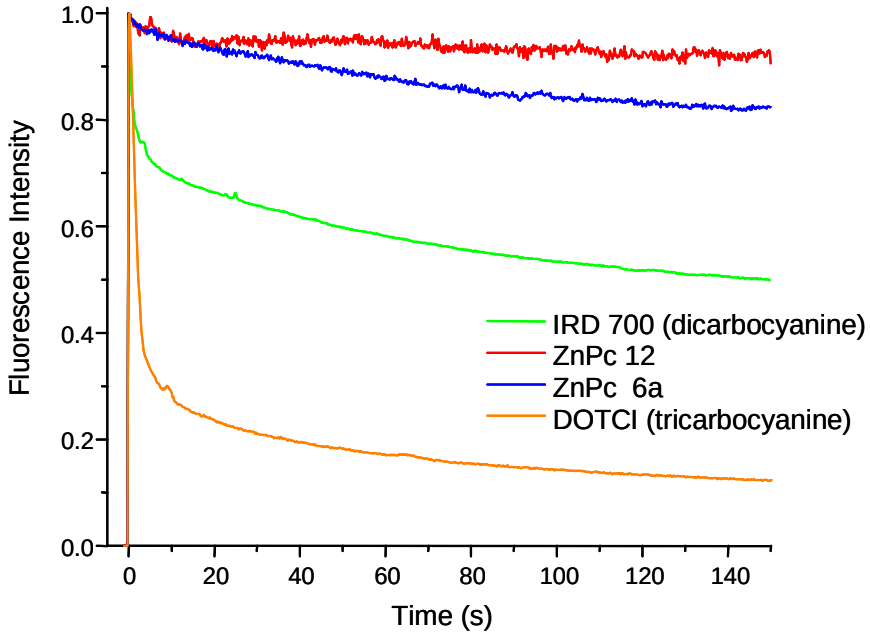

Figure 2.8 Photobleaching profiles for several Zn*x*CPc dyes, IRD700, and DOTCI. The photobleaching decay profiles were collected using 680 excitation by constantly irradiating a 1.0 µM solution and continuously monitoring the fluorescence emission. Results taken from experiments performed in collaboration with Dr. Michael Allen.

The photophysical and spectral properties were also investigated when tetracarboxylate ZnPc **6a** was covalently attached to streptavidin, a 55 kDa protein. Results indicated a slight shift in the absorption and emission maxima for the conjugate compared to the dye with the absorption maxima appearing at 687 nm and the emission maxima at 693 nm (see Figures 2.9A). In addition, the fluorescence lifetime of the conjugate was found to be 2.85 ns, slightly shorter than that seen for the ZnPc dye. Evaluation of the ZnPc-streptavidin conjugation mixture was analyzed using reverse-phase chromatography with fluorescence detection used to monitor both the conjugate and free ZnPc dye. The chromatograms for the reaction mixtures of ZnPc **6a** only and streptavidin conjugated to **6a** and **12** are shown in Figures 2.9A and 2.9B. The labeling reaction as can be seen, the free dye peak is visible in the ZnPc/streptavidin reaction since the dye was available at a 10-fold molar excess compared to the protein.

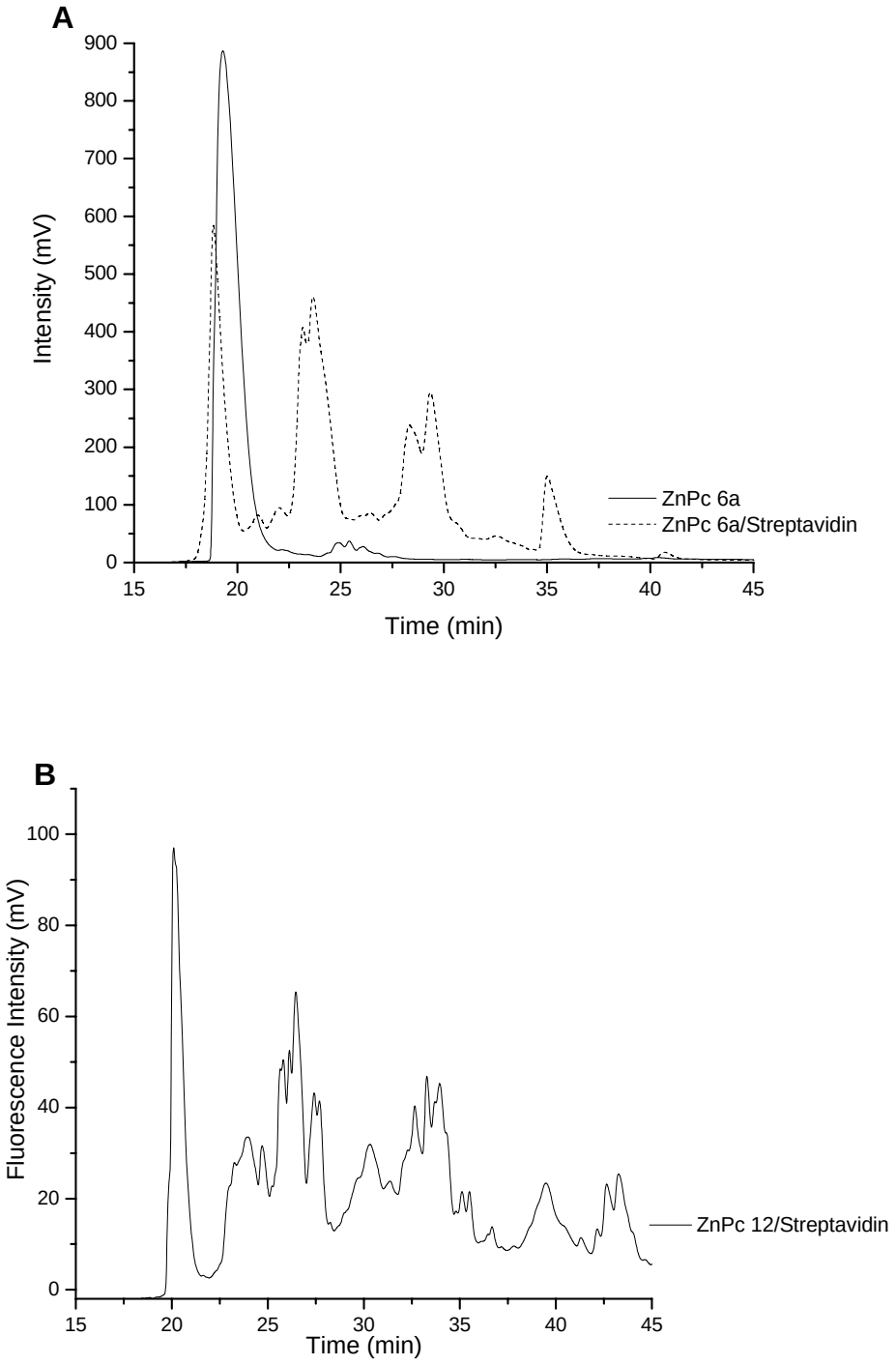

Figure 2.9 Chromatogram showing the elution of (A) ZnPc **6a** by itself (t_r = 19.2 min), ZnPc **6a**/streptavidin conjugate (t_r = 23.1 min, 28.5 min and 35.0 min) along with ZnPc **12**/streptavidin conjugate (B). The fluorescence detector was set at λ_{ex} = 686 nm and λ_{em} = 693 nm. See experimental section for an explanation of the chromatographic conditions.

Also, the chromatogram demonstrated the presence of multiple peaks that were not present for the reaction mixture containing no streptavidin, indicating that streptavidin molecules are multiply labeled with ZnPc **6a**.

2.4 Discussion

Modeling and experimental evaluation of the electronic properties of Pc's and MPc's have been reported.[40-42] As a starting point, Gouterman's model provides useful background in predicting the origin of the main spectral features of metal and metal free Pc's in terms of four orbitals, HOMO-1, HOMO, LUMO, and LUMO+1.[43,44] The Q band is assigned to the a_{1u} (π) to e_g (π^*) transition, while the B band is assigned to an a_{2u} (π) to e_g (π^*) transition. In Pc's, the 1_{a1u} and 1_{a2u} orbitals become widely separated in energy resulting from the presence of the aza bridges and consequently, the Q and B bands appear at approximately 680 nm and 350 nm, respectively.[45,46] For metal free Pc's, Q-band splitting is indicative of D_{2h} symmetry with the orbital degeneracy lifted, while the symmetry of MPc's is generally D_{4h}.[47] Depending on the size of the metal ion, accommodation of the metal can result in doming or ring expansion in the macrocycle causing the symmetry of the molecule to become distorted [48], inducing electronic perturbations that are manifested by bathochromic shifts in the absorption bands and/or Q-band splitting. Significant mixing of the transition metal d-orbitals and the π orbitals of the macrocycle produce changes in the electronic features of the MPc's as well with the extent of interaction dependent upon the nature of the central metal. The metal-macrocycle interaction has been analyzed in detail by Rosa *et al*.[49]

For the MPc's investigated in this paper, the absorption spectra for tetra-, octa- and hexadecacarboxylate ZnPc **6a**, **9a** and **12** and tetracarboxylate AlPc **6c** are typical for MPc compounds exhibiting a sharp and narrow Q band suggesting monomeric species and a higher energy Soret band when placed in DMSO solvents (see Figures 2.5 and 2.6). In addition, they showed an additional shoulder to the blue of the Q-band, which can be attributed to combination overtones of Q-band electronic transitions.[49] For gallium phthalocyanine, it has been reported that the Ga center is approximately 0.45 Å out of plane; the Q-band split observed in this study suggested that doming did occur in this MPc causing a split in the orbital degeneracy due to

symmetry changes.[50] The absorption spectrum with a split in the Q-band for metal free Pc **6g** is also consistent with D_{2h} symmetry.

Pc complexes with a light closed-shell central metal ion are typically highly fluorescent.[19] The fluorescence emission of the Pc's studied in this report in DMSO have strong emission peaks around 687 nm with the emission profile for tetracarboxylate ZnPc **6a** showing a small shoulder around 750 nm, which may indicate ligand-to-metal charge transfer. Excitation at 696 nm for GaPc **6b** resulted in no detectable fluorescence, suggesting vibronic splitting of the S_1 electronic state. The NiPc **6d**, PdPc **6e** and PtPc **6f** showed weak fluorescence (see Table 2.1) due to these metals larger atomic numbers compared to the Zn, Al, and Ga metal centers, resulting in higher rates of intersystem crossing from spin orbit coupling artifacts.

For many MPc compounds, self-association occurs readily in aqueous solutions due to intermolecular association with the degree of association dependent upon the identity of the metal ion and the peripheral substitutions on the benzo groups.[17,51] For example, introduction of substituents in the 1,3 positions produces a shift to the red as opposed to substituents placed at the 1,4 positions. Aggregation effects of several Pc dyes have been documented.[52,53] Two main aggregate species have been identified as J and H aggregates with J-aggregates marked by a red-shift in the monomer peak due to head-to-tail aggregation, while H-aggregates correspond to face-to-face dimerization marked by a blue shift.[54,55] The absorption spectra for ZnPc **6a** in HEPES buffer at pH 8 (see Figure 2.7) exhibited extensive broadening of the Q band with a blue shift in the absorption maximum indicative of H-aggregate formation. In addition, AlPc **6c** and GaPc **6b** showed the same artifacts in their absorption profiles collected in HEPES buffer. However, as the degree of carboxylation increased, the absorbance spectra more resembled those in DMSO, where aggregation effects were expected to be minimal. For example, octa- and hexadecacarboxylate ZnPc **9a** and **11** showed narrow absorption envelopes with the absorption maximum very similar to that seen in DMSO. Therefore, high degrees of carboxylation (>4 carboxylate groups) seem to be fairly effective in minimizing ground state aggregation for ZnPc dyes. Interestingly, tetracarboxylate ZnPc **6a** in CAPS buffer (pH = 11.0) showed a narrower absorption profile compared to this same compound in HEPES, suggesting a smaller propensity

to aggregate at higher pH, which could be ascribed to a higher population of deprotonated species at higher pH values.

The trends observed in the quantum yields for each MPc in DMSO can be explained in terms of heavy atom effects.[19,46] As the atomic number of the heavy atom, which in this case is the metal center, increases one would expect the quantum yield to decrease due to increases in the intersystem crossing rate resulting from heavy-atom induced spin-orbit coupling. For the data collected herein, the quantum yields for Zn, Ga, and Al did show an increase as the atomic number decreased for this series. Indeed, previous reports on MPc's have indicated that Al-analogs typically show relatively larger quantum yields compared to other MPc's due to its smaller atomic number.[56] Inspection of the data in Table 2.3 also indicated that the degree of carboxylation added to the ZnPc macrocycle did not significantly affect the fluorescence quantum yields for this series of dyes when in DMSO.

In HEPES (pH = 8.0), the quantum yields for the MPc compounds studied herein were observed to be less than 1% (data not shown). However, when the buffer pH was increased (CAPS, pH = 11.0) the fluorescence quantum yields for all of these dyes improved dramatically (see Table 2.3).[57] The fluorescence quantum yield for the ZnPc **6a** /streptavidin conjugate was also found to be significantly higher compared to the free dye only in HEPES buffer. If we assume that the quantum yields for the ground state aggregated forms of these dyes are negligible compared to their monomeric counterparts, the relatively small quantum yields seen for these dyes in HEPES buffer is most likely due to a lower ground state population of the monomeric form. While differences in extinction should correct for this population difference, the broad absorption profiles associated with the aggregates produce an apparent extinction coefficient that does not correct for the lower number of monomeric species (see equation 1).

The fluorescence lifetimes for the MPc's showed the same trend as that seen for the fluorescence quantum yields, with the lifetime of AlPc **6c** significantly longer than that of ZnPc **6a** and GaPc **6b**, which have larger atomic numbers compared to Al and thus, would be

expected to show shorter fluorescence lifetimes based on heavy-atom mediated effects. As can also be noticed in the data displayed in Table 2.3, the fluorescence lifetimes were generally independent of the number of substituents added to the periphery of the ZnPc dyes. The identity of the short-lived component observed for Al and Ga is uncertain.

The nature of MPc intermolecular interactions intimately affects the photostability of MPc's and plays a central role in determining the number of photons generated per molecule, a key parameter in a number of ultra-sensitive fluorescence measurements and imaging as well.[17] Among the MPc's investigated in this work, tetracarboxylate AlPc **6c** was nearly 2 orders of magnitude less photochemically stable compared to the same tetracarboxylate ZnPc **6a** and one order of magnitude less stable than GaPc **6b.** Interestingly, the photodestruction quantum yields for tetra-, octa- and hexadecacarboxylate ZnPc **6a**, **9a** and **12** showed increased photostability with higher degrees of carboxylation. It is clear that a high degree of carboxylation mitigates intermolecular interactions resulting in enhanced photostabilities. The photobleaching quantum yields reported in Table 2.3 illustrate the superiority of the Pc dyes compared to their cyanine counterparts as they dyes are less photochemically stable and thus, provide fewer photons on a per molecule basis. A detailed investigation of the photostability of several metal phthalocyanines has been discussed previously.[58] The authors examined factors that influenced the photobleaching process suggesting that photobleaching was related to the change in the electronic distribution of the molecular structure influenced by the identity of the metal center.

The carboxylic groups not only provided a means for improving the water compatibility of the Pc dyes investigated herein, but could serve the dual function of allowing for their chemical modification by reacting the peripheral carboxylate groups with N-hydroxysuccinimide and DCC to form an activated ester for the covalent binding of targets bearing primary amine groups, such as streptavidin. Inspection of the spectral properties of the ZnPc **6a**/streptavidin complex indicated a slight bathochromic shift in its absorption maximum compared to the free dye in DMSO as well as a slight red-shift in its emission maximum. The dye-to-protein concentration ratio was set to 4 to 1 in order to minimize multiple streptavidin molecules strapped to a single molecule **6a** due to the four active sites around the periphery of the dye.

However, there was still the appearance of several peaks within the chromatographic trace (see Figure 2.9A) besides the free dye and single dye/protein conjugate peak indicating the existence of multiple streptavidins attached to the dye. While hexadecacarboxylate ZnPc **12** could be viewed as a better labeling fluor due to its improved water compatibility and photochemical stability, the presence of these spurious conjugates, besides the 1:1 complex, would make purification and quantification difficult (see Figure 2.9B).

2.5 Conclusions

This work presented facile routes for the preparation of heavily carboxylated MPc-type dyes and also, the photophysical and spectral properties of several metal free and MPc derivatives and the effects of the metal and ring substituents on these properties. In general, the MPc dyes exhibited higher photostability compared to other commercially available fluorophores used for near-IR applications, which will have important ramifications in ultra-sensitive measurements as well as imaging. The fluorescence quantum yields and lifetimes were found to depend on the metal substituent, but not on the degree of carboxylation.

The challenge with the use of MPc-based dyes is their poor compatibility with aqueous solvents due to their high propensity to undergo self-aggregation. However, aggregation artifacts could be mitigated through modification of the periphery of the macrocycle by appending large numbers of polar/ionic groups that inhibit dye-dye interactions. For the dyes investigated here, incorporating carboxylic acid groups proved to be an effective approach for minimizing ground state aggregation as observed from the spectral properties of octa- and hexadecacarboxylate ZnPc's **9a** and **12** in buffered media. Interestingly, high degrees of carboxylation also provided better photochemical stabilities. The initial results obtained for the conjugation studies has prompted future work to focus on the optimization of labeling conditions with various ZnPc dyes, especially those that are heavily carboxylated to provide high quantum yield and photostable conjugates that can be easily purified.

2.6 References

(1) Bryant, G. C.; Cook, M. J.; Ryan, T. G.; Thorne, A. J. *Journal of the Chemical Society-Chemical Communications* **1995**, 467-468.

(2) Piechocki, C.; Simon, J.; Skoulios, A.; Guillon, D.; Weber, P. *Journal of the American Chemical Society* **1982**, *104*, 5245-5247.

(3) Tedesco, A. C. *Current Organic Chemistry* **2003**, 187-196.

(4) Margaron, P.; Gregoire, M. J.; Scasnar, V.; Ali, H.; van Lier, J. E. *Photochemistry and photobiology* **1996**, *63*, 217-23.

(5) Liu, W.; Jensen, T. J.; Fronczek, F. R.; Hammer, R. P.; Smith, K. M.; Vicente, M. G. H. *Journal of Medicinal Chemistry* **2005**, *48*, 1033-1041.

(6) Gopel, W. *Synthetic Metals* **1991**, *41*, 1087-1093.

(7) Zhou, R.; Josse, F.; Gopel, W.; Ozturk, Z. Z.; Bekaroglu, O. *Applied Organometallic Chemistry* **1996**, *10*, 557-577.

(8) Langlois, R.; Ali, H.; Brasseur, N.; Wagner, J. R.; Vanlier, J. E. *Photochemistry and Photobiology* **1986**, *44*, 117-123.

(9) Hu, M.; Brasseur, N.; Yildiz, S. Z.; van Lier, J. E.; Leznoff, C. C. *Journal of Medicinal Chemistry* **1998**, *41*, 1789-1802.

(10) Spikes, J. D. *Photochemistry and Photobiology* **1986**, *43*, 691-699.

(11) Hanack, M.; Gul, A.; Hirsch, A.; Mandal, B. K.; Subramanian, L. R.; Witke, E. *Molecular Crystals and Liquid Crystals* **1990**, *187*, 365-382.

(12) Abramczyk, H.; Szymczyk, I. *Journal of Molecular Liquids* **2004**, *110*, 51-56.

(13) Kuznetsova, N. A.; Gretsova, N. S.; Derkacheva, V. M.; Kaliya, O. L.; Lukyanets, E. A. *Journal of Porphyrins and Phthalocyanines* **2003**, *7*, 147-154.

(14) Hanack, M.; Schmid, G.; Sommerauer, M. *Angewandte Chemie-International Edition in English* **1993**, *32*, 1422-1424.

(15) Hanack, M.; Meng, D. Y.; Beck, A.; Sommerauer, M.; Subramanian, L. R. *Journal of the Chemical Society-Chemical Communications* **1993**, 58-60.

(16) Leznoff, C. C.; Hall, T. W. *Tetrahedron Letters* **1982**, *23*, 3023-3026.

(17) Leznoff, C. C. *Phthalocyanines: Properties and Applications*; VCH Publishers, 1989; Vol. 1.

(18) McCubbin, I.; Phillips, D. *Journal of Photochemistry* **1986**, *34*, 187-195.

(19) Huang, T. H.; Rieckhoff, K. E.; Voigt, E. M. *Chem. Phys.* **1977**, *19*, 25-33.

(20) Wu, S. K.; Zhang, H. C.; Cui, G. Z.; Xu, D. N.; Xu, H. J. *Acta Chimica Sinica* **1985**, *43*, 10-13.

(21) Cuellar, E. A.; Marks, T. J. *Inorganic Chemistry* **1981**, *20*, 3766-3770.

(22) Sakamoto, K.; Kato, T.; Ohno-Okumura, E.; Watanabe, M.; Cook, M. J. *Dyes and Pigments* **2005**, *64*, 63-71.

(23) Ng, A. C. H.; Li, X. Y.; Ng, D. K. P. *Macromolecules* **1999**, *32*, 5292-5298.

(24) Sener, M. K. *Journal of Porphyrins and Phthalocyanines* **2005**, 617-622.

(25) Duan, W. B.; Smith, K.; Savoie, H.; Savoie, H.; Greenman, J.; Boyle, R. W. *Organic & Biomolecular Chemistry* **2005**, *3*, 2384-2386.

(26) Hammer, R. P.; Owens, C. V.; Hwang, S. H.; Sayes, C. M.; Soper, S. A. *Bioconjugate Chemistry* **2002**, *13*, 1244-1252.

(27) Koval, V. V.; Chernonosov, A. A.; Abramova, T. V.; Ivanova, T. M.; Fedorova, O. S.; Knorre, D. G. *Bioorganicheskaya Khimiya* **2000**, *26*, 118-125.

(28) Patonay, G.; Antoine, M. D.; Devanathan, S.; Strekowski, L. *Applied Spectroscopy* **1991**, *45*, 457-461.

(29) Demas, J. N.; Crosby, G. A. *Journal of Physical Chemistry* **1971**, *75*, 991-&.

(30) Fery-Forgues, S.; Lavabre, D. *Journal of Chemical Education* **1999**, *76*, 1260-1264.

(31) Davidson, Y. Y.; Gunn, B. M.; Soper, S. A. *Applied Spectroscopy* **1996**, *50*, 211-21.

(32) Keller, T. M.; Price, T. R.; Griffith, J. R. *Synthesis-Stuttgart* **1980**, 613-613.

(33) Yanagisawa, M.; Korodi, F.; Bergquist, J.; Holmberg, A.; Hagfeldt, A.; Akermark, B.; Sun, L. C. *Journal of Porphyrins and Phthalocyanines* **2004**, *8*, 1228-1235.

(34) Negri, R. M.; Zalts, A.; Roman, E. A. S.; Aramendia, P. F.; Braslavsky, S. E. *Photochemistry and Photobiology* **1991**, *53*, 317-322.

(35) Ogunsipe, A.; Chen, J. Y.; Nyokong, T. *New Journal of Chemistry* **2004**, *28*, 822-827.

(36) Darwent, J. R.; Douglas, P.; Harriman, A.; Porter, G.; Richoux, M. C. *Coordination Chemistry Reviews* **1982**, *44*, 83-126.

(37) Li, Y. F.; Li, S. L.; Jiang, K. E.; Yang, L. M. *Chemistry Letters* **2004**, *33*, 1450-1451.

(38) McKeown, N. B.; Chambrier, I.; Cook, M. J. *Journal of the Chemical Society-Perkin Transactions 1* **1990**, 1169-1177.

(39) Strickler, S. J.; Berg, R. A. *Journal of Chemical Physics* **1962**, *37*, 814-22.

(40) Morley, J. O.; Charlton, M. H. *J. Phys. Chem.* **1995**, *99*, 1928-1934.

(41) Stillman, M.; Mack, J.; Kobayashi, N. *Journal of Porphyrins and Phthalocyanines* **2002**, *6*, 296-300.

(42) Kobayashi, N.; Konami, H. *Journal of Porphyrins and Phthalocyanines* **2001**, *5*, 233-255.

(43) Minor, P. C.; Gouterman, M.; Lever, A. B. P. *Inorg. Chem.* **1985**, *24*, 1894-1900.

(44) Gouterman, M.; Wagniere, G. H.; Snyder, L. C. *J. Mol. Spectrosc.* **1963**, *11*, 108-127.

(45) Keizer, S. P.; Mack, J.; Bench, B. A.; Gorun, S. M.; Stillman, M. J. *Journal of the American Chemical Society* **2003**, *125*, 7067-7085.

(46) Huang, D.; Liu, E. S.; Yang, S. L.; Chen, N. S.; Huang, J. L.; Duan, J. P.; Chen, Y. *Spectroscopy and Spectral Analysis* **2000**, *20*, 95-98.

(47) Cook, M. J.; Dunn, A. J.; Howe, S. D.; Thomson, A. J.; Harrison, K. J. *Journal of the Chemical Society-Perkin Transactions 1* **1988**, 2453-2458.

(48) Tackley, D. R.; Dent, G.; Smith, W. E. *Physical Chemistry Chemical Physics* **2001**, *3*, 1419-1426.

(49) Rosa, A.; Baerends, E. J. *Inorg. Chem.* **1994**, *33*, 584-595.

(50) Wynne, K. J. *Inorg. Chem.* **1984**, *23*, 4658-4663.

(51) Phillips, D.; Dhami, S.; Ostler, R.; Petrasek, Z. *Progress in Reaction Kinetics and Mechanism* **2003**, *28*, 299-420.

(52) Ogunsipe, A.; Nyokong, T. *J. Mol. Struct.* **2004**, *689*, 89-97.

(53) Kobayashi, N.; Lever, A. B. P. *Journal of the American Chemical Society* **1987**, *109*, 7433-7441.

(54) Isago, H. *Chemical Communications* **2003**, 1864-1865.

(55) Li, X. Y.; Ng, D. K. P. *Tetrahedron Lett.* **2001**, *42*, 305-309.

(56) Ogunsipe, A.; Nyokong, T. *Journal of Photochemistry and Photobiology a-Chemistry* **2005**, *173*, 211-220.

(57) Martin, P. C.; Gouterman, M.; Pepich, B. V.; Renzoni, G. E.; Schindele, D. C. *Inorg. Chem.* **1991**, *30*, 3305-3309.

(58) Slota, R.; Dyrda, G. *Inorg. Chem.* **2003**, *42*, 5743-5750.

Chapter 3
Labeling Peptides, Proteins and Oligonucleotides with Metal Phthalocyanines for Highly Sensitive Fluorescence Detection Applications

3.1 Introduction to Fluorescence Labeling Techniques

Technology that relies on the use of fluorescent probes for the sensitive detection of biological substances is becoming increasingly important in the fields of genomic and proteomics that aims at high throughput screening and quantifying biological processes at the single molecule level.[1,2] When used with a sensitive detection device, fluorescent labeling is an excellent strategy that can provide a direct method as a means for identifying, assaying and visualizing biomolecules with high precision and resolution.[2-4] However, the limitation in using this technique is the availability of suitable fluorescent compounds that possess functional groups that are chemically reactive towards functional groups on the biomolecule. We have recently shown the potential of MPc's as fluorescent probes for labeling streptavidin.[5] This chapter briefly discusses the fundamental of labeling chemistry and illustrates the use of MPc's in labeling proteins and peptides, and results are compared to labeling with commercially available fluorophores.

Two primary approaches that can be used for tagging biomolecules are covalent and non-covalent coupling. Non-covalent labeling involves ionic, electrostatic, hydrophobic, and hydrogen bonding interactions, while covalent coupling requires a reactive functional group on the fluorophore to covalently attach to the biomolecule.[6-11] Legendre and coworkers separated proteins that were non-covalently labeled with two commercially available near-IR dyes, diethylthiatricarbocyanine iodide (DTTCI) and IR-125.[12] In their studies, changes in the absorption/emission spectra and fluorescence lifetimes were observed due to hydrophobic interactions with the bound protein.[12] Davidson et al. investigated the spectroscopic and binding properties of tricarbocyanine dyes, hexamethylindotricarbocyanine iodide (HITCI) and

diethylthiatricarbocyanine iodide (DTTCI) to double-stranded DNA. Results showed a significant enhancement in the fluorescence intensity in the presence of double-stranded DNA labeled with HITCI, and a 128-fold enhancement with DTTCI compared to intercalating dyes such as ethidium bromide.[10] Williams and coworkers investigated both non-covalent and covalent labeling of human serum albumin (HSA) with indocyanine green and found that covalently labeled HSA was more stable compared to noncovalently labeled HSA.[7] Flanagan et al. reported on covalent labeling of amino acids with tricarbocyanine dyes, while Duan and coworkers demonstrated covalent labeling of monoclonal antibodies with phthalocyanines bearing a single isothiocyanate group.[10] Recently, Peng and coworkers reported on the covalent attachment of SiPc to antibodies.[13]

Both modification techniques, however, suffer from drawbacks. Although non-covalent reactions occur at a faster rate, they are generally less stable compared to covalent labeleing.[7,14] For covalent labeling, the chemistry is often complex and laborious compared to non-covalent methods that only require mixing the fluorescent dye and biomolecule with no additional steps needed.[8,9,14,15] Commonly used fluorescent probes in non-covalent labeling include naphthalene dyes and squarylium dyes that are highly fluorescent in a complex biological system mainly due to the environment in which these dyes exist and a variety of fluorescent staining dyes such as acridine orange, comassie blue, and colloidal gold.[7,14,16] Fluorophores commonly used for covalent bonding include Alexa Fluor and cyanine dyes that can be synthesized to react towards a number of functionalities.[17]

Functional groups that bind to biomolecules containing primary amines are the most common functional groups on modification reagents. For example, isothiocyanate is a functional group that reacts with nucleophiles such as amines and sulfhydryls. The reaction involves attack of the nucleophile on the electrophilic carbon of the isothiocyanate group and the resulting

electron shift creates a thiourea linkage between the isothiocyanate and the amine group. The only stable product of these reactions is with primary amines however, and they are relatively unstable in aqueous conditions.[18] Aryl halide reagents such as fluorobenzene can also be used to form covalent bonds between a fluorophore and amine-containing biomolecules. This reaction, however, is not specific for primary amines. The most widespread used method for covalently labeling a biomolecule with a fluorescent dye is the use of carbodiimides that can be used to form highly reactive O-acylisourea derivatives, known to react selectively with primary amine groups to create stable amide bonds.[18] Although, the O-acylisourea derivative is also relatively short-lived, the addition of an N-hydroxysuccinimide (NHS) ester increases the stability of the derivative. The latter method was chosen for these studies due to the ability of carbodiimides to activate the carboxylic acids located on the periphery of the MPc's dyes and create a stable amide bond between the MPc dye and the target biomolecule.

3.1.1 Fundamental Aspects of Carbodiimide Coupling Chemistry

Carbodiimides react with carboxylic acids to form a stable covalent bond between the fluorescent dye and the biomolecule containing primary amines. The general use of these compounds was first introduced by the pioneering research of Khorana and his investigation into their role in peptide and nucleotide synthesis.[19,20] These cross-linking reagents have since remained a popular choice for labeling because these compounds mediate the linkage between primary amines and carboxylic acid groups through the formation of amide bonds with no intervening linker necessary. Carbodiimides are either organic soluble or water-soluble, with the latter being the preferred choice for modification reactions because of the hydrophilicity of most biological targets. The structure of these compounds is shown in Figure 3.1 1-Ethyl-3(3-dimethylaminopropyl) carbodiimide hydrochloride (EDC) is typically used due to its water solubility and any excess reagent can easily be removed by simple purification techniques such

as gel filtration, while N,N'-dicyclohexyl-carbodiimide (DCC) is generally used for labeling reactions employing hydrophobic fluorescent dyes.[18] A drawback to using EDC and DCC is the lability of the intermediate and the susceptibility of hydrolysis back to carboxylic acid groups as a competing reaction.[21]

The reaction mechanism illustrating the steps involved in converting carboxylic acids to active esters using EDC is shown in Figure 3.2.

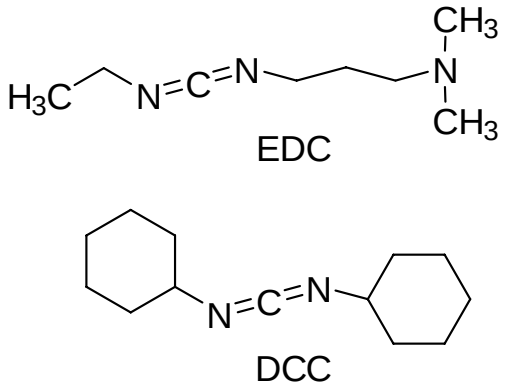

Figure 3.1 Structure of EDC and DCC used for converting carboxylic acid functional groups to active O-acylisourea derivative for labeling biomolecules containing primary amines forming stable amide bonds.

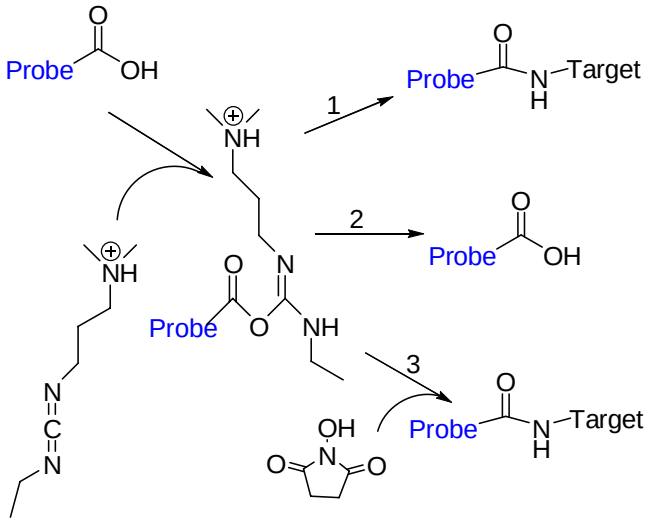

Figure 3.2 Schematic representing the derivatization of carboxylic acid functionalities using EDC coupling chemistry. The addition of NHS produces a more stable amide bond between primary amines and carboxylic acid groups. (1) reaction with EDC without the addition of NHS; (2) hydrolysis reaction; (3) reaction with EDC and NHS.

The reaction takes place by reacting an equimolar amount of EDC to a solution containing the fluorophore creating an O-acylisourea intermediate. In the presence of an active nucleophile, an amide bond is formed and the urea derivative is released as a byproduct that can easily be removed using chromatographic purification techniques.[22] A modified approach is to use a succinimidyl ester derivative (i.e. N-hydroxysuccinimide (NHS)) in conjunction with EDC to create a more stable intermediate. The coupling chemistry using EDC/NHS is highly efficient under optimal conditions and the conjugate yield increases compared to using only EDC.[23] Liu and coworkers reported on the preparation of luminescent silica nanoparticles using EDC and NHS coupling to covalently immobilize monoclonal antibodies for cell imaging applications.[24] Hua demonstrated the use of EDC/NHS coupling to label immunoglobulin antibodies with water-soluble quantum dots.[25] A detailed review of carbodiimide chemistry has been reported by Williams and coworkers.[26]

This chapter discusses the use of carbodiimide coupling as a means to label biological moieties with metal phthalocyanines (MPc's) by converting the carboxylic acids located on the periphery of MPc's to functional succinimidyl esters. Here, we show the feasibility and versatility of labeling with zinc tetracarboxylate phthalocyanine (Zn4CPc) by reacting Zn4CPc with several biomolecules, and examine the effect of a biomolecule on the intrinsic properties of Zn4CPc dye (see Figure 3.3). We also demonstrate the chromatographic separation of the bioconjugates using reverse-phase chromatography.

3.2 Materials and Methods

N, N-dicyclohexal carbodiimide (DCC), N-hydroxysuccinimide (NHS), Dimethylsulfoxide (DMSO), triethylammonium acetate (TEAA), and HEPES were purchased from Sigma-Aldrich (St. Louis, MO). HPLC grade acetonitrile was obtained from Fluka (St. Louis, MO) and used without further purification. Amine modified M13mp18 universal primers

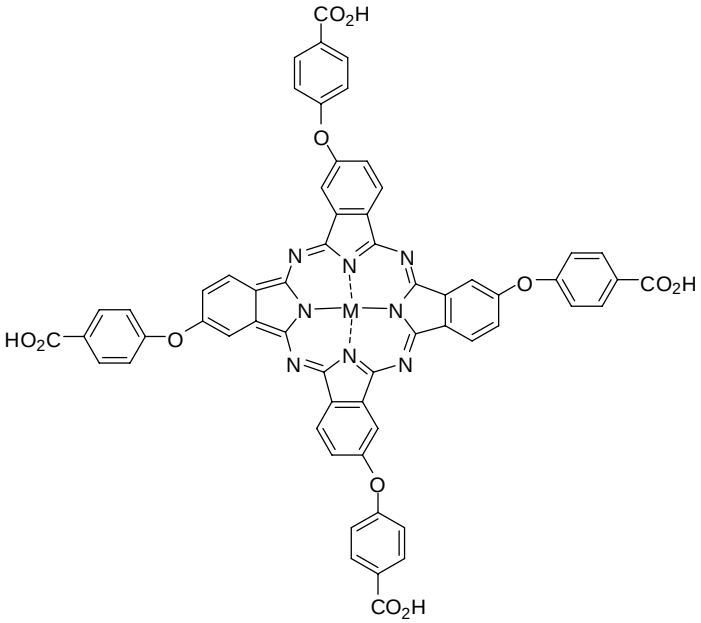

Figure 3.3 Structure of tetracarboxylate metal phthalocyanine (Zn4CPc) used for labeling reactions. The synthesis of Zn4CPc has been discussed in detail previously.[5]

(sequence: GTAAAACGACGACCAGT) with a six or a twelve-carbon chain linker were purchased from IDT DNA (Coralville, IA). Streptavidin and bovine serum albumin (BSA) were acquired from Sigma-Aldrich (St. Louis, MO). Insulin chain B was obtained from Fluka (St. Louis, MO). The active NHS ester derivatives of Zn4CPc (ZnPc-NHS) was synthesized according to a published procedure and is discussed in detail elsewhere.[5] Since ZnPc-NHS ester is in the active form, solutions of the derivatives were prepared immediately before labeling procedures. Labeling was carried out by dissolving insulin chain B, oligonucleotide or BSA in 0.1 M HEPES buffer pH 8, at a concentration of 0.1 mg/mL. A stock solution of ZnPc-NHS was prepared by weighing a small amount of ZnPc-NHS and dissolving the dye in DMSO at a concentration of 1 mg/mL. An aliquot of the dye solution was immediately added to the protein solution dropwise to achieve a dye-to-protein ratio of 10:1. The reaction was vortexed at room temperature overnight. After incubation, the reaction mixtures were desalted using sephadex G-25 desalting columns.

The fractions were then collected and further analyzed using ion-paring reverse-phase HPLC.

3.2.1 Instrumentation

▪ MALDI Analysis. Samples were desalted using $ZipTip_{C18}$ desalting columns prior to analysis. Trihydroxyacetophenone (THAP) matrix solution was prepared at a concentration of 10 mg mL-1 in a 1:1 (v/v) EDTA/ACN. A 5 mL aliquot of the ZnPc-conjugate sample was mixed with 5 mL of matrix solution. The final mixture was spotted on the silicon sample plate and allowed to dry using a heat gun for 10 sec. The ZnPc-conjugate samples were spotted directly onto a sample plate with 2,4,6 Trihydroxyacetophenone (THAP) as the matrix, prepared as a 50:50 mixture of EDTA and acetonitrile. MALDI-TOF was acquired on a Bruker ProFlex MALDI-TOF mass spectrometer (Bruker Daltonics Inc., Billerica, MA) with delayed ion extraction equipped with a N_2 laser (λ = 337 nm). The instrument was operated in both positive and negative mode. The mass spectra were recorded in the range of m/z 1500-7500.

▪ ^{13}C NMR analysis. A stock solution of Zn4CPc was prepared by dissolving 3 mg in DMSO-d_6 to make a final concentration of 3 mM. A diluted sample of Zn4CPc was prepared and DCC and NHS were added in a 4 molar excess of the dye. The solution was mixed and allowed to react for 45 minutes. Using a microsyringe, all samples were transferred to NMR tubes and analyzed on a Bruker DPX 400 ^{13}C NMR equipped with a 5 mm Z-gradient inverse probe.

▪ Reverse-Phase Chromatography. Chromatographic separation was performed on a JASCO HPLC (Jasco, Inc., Easton, MD) equipped with a photodiode array and fluorescence detector. Separation was performed on a C18 reverse phase column (Supelco, Pennsylvania USA). The data was acquired using EZChrom software provided by JASCO. HPLC buffer A was 0.1% TEAA in water and buffer B was 0.1% TEAA in acetonitrile. The conditions used for separation was a linear gradient for 45 min. at a flow rate of 1 mL/min. The detection was monitored using

photodiode array (PDA) at wavelengths 260 nm and 680 nm, and fluorescence detection at 677 nm for excitation and 683 nm for emission.

▪ Spectroscopic Analysis. Absorbance measurements were acquired on an Ultrospec 4000 UV/Visible spectrophotometer (Piscataway, NJ) equipped with deuterium and tungsten lamps. Analysis was performed using SWIFT II software provided by the manufacturer. Steady-state fluorescence measurements were acquired on a Spex Fluorolog 3 (Edison, NJ). Fluorescence lifetime measurements of the labeled conjugates were acquired on a time-correlated single photon counting (TCSPC) instrument previously described in Chapter 2.

▪ Functional Activity Test. Functional activity tests for ZnPc-streptavidin were performed using biotin labeled microspheres purchased from Molecular Probes (Eugene, Oregon). The microspheres (0.2 μm) are supplied as aqueous suspensions containing 1 % solid and 0.02 % Tween, which serves as a blocking agent to minimize nonspecific binding. The number of microspheres per mL of solution was determined to be 7.2×10^8 using the following equation;

$$\frac{6C \times 10^{12}}{\rho \times \pi \times \phi^3} \qquad \textbf{(1.1)}$$

where, C is the concentration (g/mL) of the suspended beads, ϕ is the diameter of the microspheres (μm), and ρ is the density of the microspheres in g/mL. Zn4CPc-Streptavidin conjugate was added to a 5 mL aqueous suspension of the microspheres for 30 minutes at room temperature and then centrifuged for 20 min at 3000 × g to separate the protein-labeled microspheres from unreacted dye. The supernatant was discarded and the formed pellet was resuspended in buffer and gently vortexed and centrifuged as described previously 3 times (three washes). The protein conjugate microsphere was then resuspended in HEPES and further analyzed by measuring the steady-state fluorescence. To determine non-specific binding of Zn4CPc to the solid surface, a control reaction was performed in which ZnPc was added without

the presence of streptavidin in the same fashion (Figure 3.4). In addition, a control reaction of streptavidin incubated with the biotinylated microspheres was carried out to determine any background fluorescence from streptavidin.

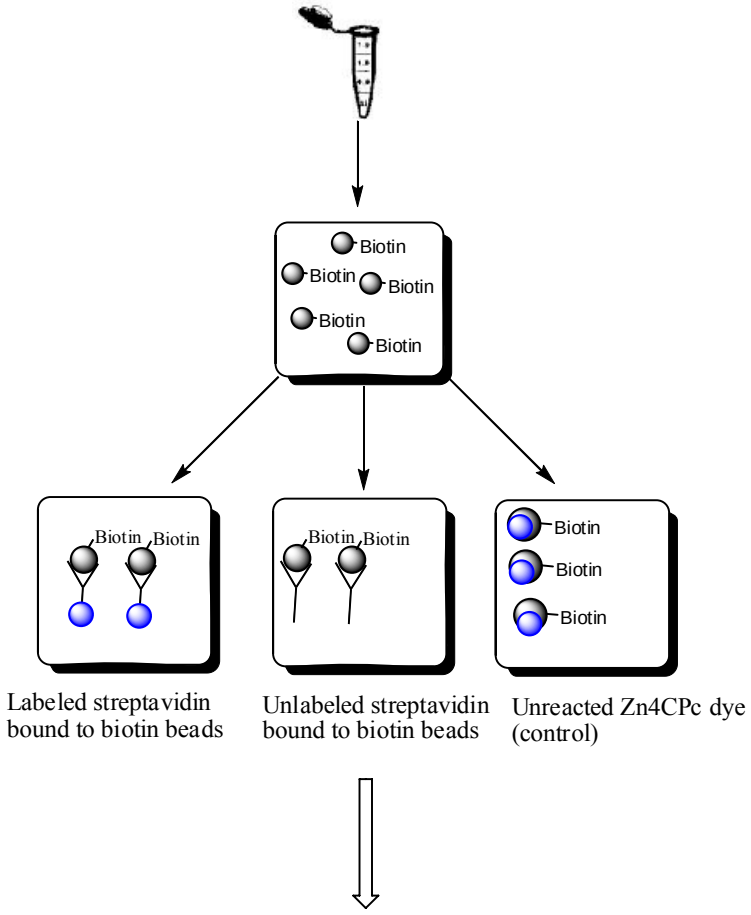

Figure 3.4 Schematic illustrating the experimental set up for attaching dye labeled streptavidin to biotinylated microspheres.

3.3 Results and Discussion

3.3.1 ^{13}C NMR Analysis of Derivatized Zn4CPc

^{13}C NMR is a powerful and useful tool for providing structural information of both organic and inorganic species as well as information on the motion of such species.[10] Structural elucidation of the formation of ZnPc-NHS was performed using ^{13}C NMR. In Figure 3.5 is the

^{13}C NMR spectrum for Zn4CPc dissolved in DMSO-d_6. A chemical shift at 166.67 ppm corresponds to the carboxylic acid functional groups located on the periphery of the phthalocyanine dyes. The peak observed at 131 ppm is due to the solvent.

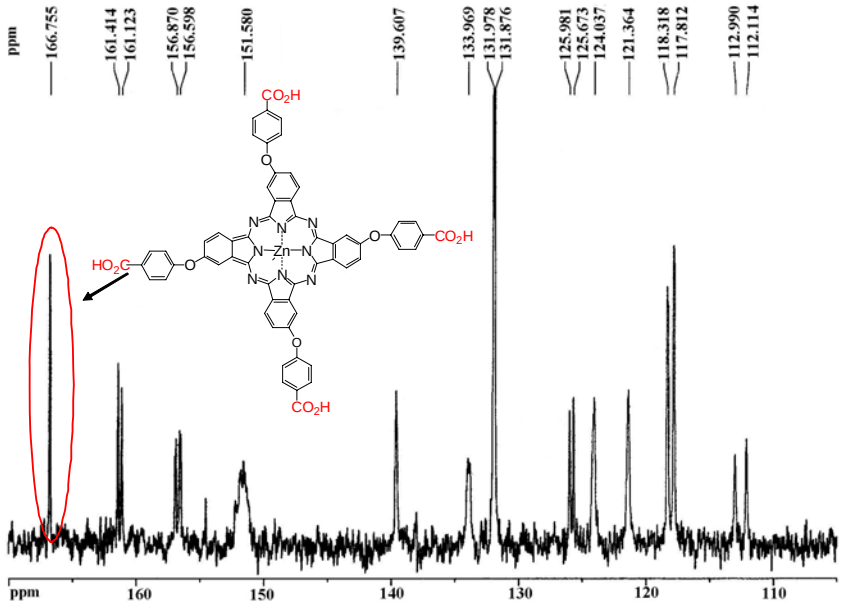

Figure 3.5 ^{13}C NMR spectrum of Zn4CPc dissolved is DMSO. Concentration of the Zn4CPc solution: 3 mM.

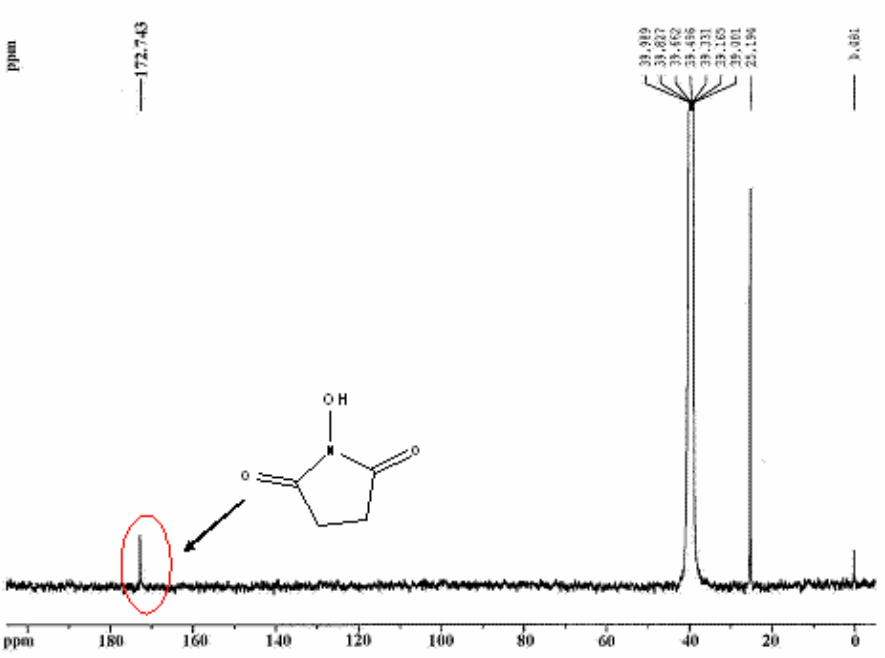

Figure 3.6 ^{13}C NMR spectrum representing the NMR shift for N, hydroxysuccinimide. The concentration of NHS dissolved in d_6-DMSO was 12 M.

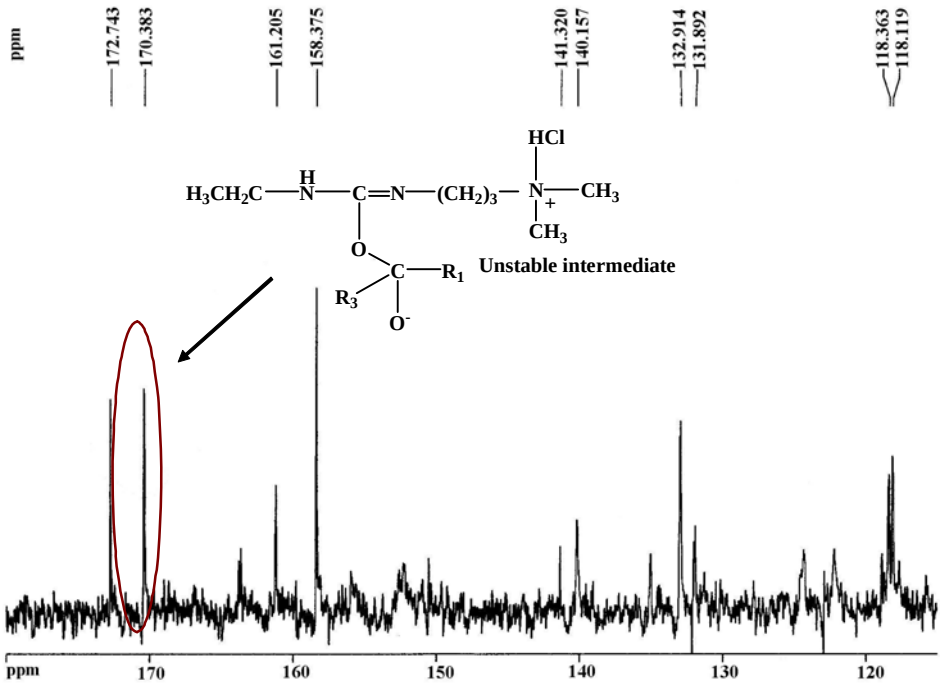

Figure 3.7 ^{13}C NMR spectrum illustrating the appearance of an NMR peak indicative of the active ester formation.

The NMR spectrum for N, Hydroxysuccinimide (NHS) is shown in Figure 3.6 exhibiting a peak shifted further downfield at 172.74 ppm corresponding to the carboxyl group. In Figure 3.7 is the NMR spectral results for ZnPc-NHS with the appearance of a new peak observed slightly further downfield with a chemical shift at 170.38 ppm due to the carboxylic acids being converted to active NHS esters. The disappearance of the carboxyl groups is significant in that it suggests all four carboxylic acid groups have been converted to NHS esters.

3.3.2 Spectral Properties of Labeled BSA, Insulin Chain B and Oligonucleotide

The tetracarboxylated Zn phthalocyanine (Zn4CPc) dye provided a means for their chemical modification by reacting the peripheral carboxylic acids with NHS and DCC to form an activated ester for the covalent binding of targets bearing primary amine groups. Streptavidin, BSA, Insulin Chain B, and a 6-carbon amino modified oligonucleotide were chosen as model

systems due to these compounds possessing a number of primary amines and their commercial availability. BSA is a single chain polypeptide consisting of 530 amino acid residues with a high content of cysteine residues. Insulin chain B possesses two primary amine groups available for labeling and streptavidin is tetrameric protein with several primary amines.

Figure 3.8 shows the absorption and emission spectra for ZnPc-Insulin Chain B in 10%DMSO/HEPES at pH 8. The spectra exhibits a small shift in the absorption and emission

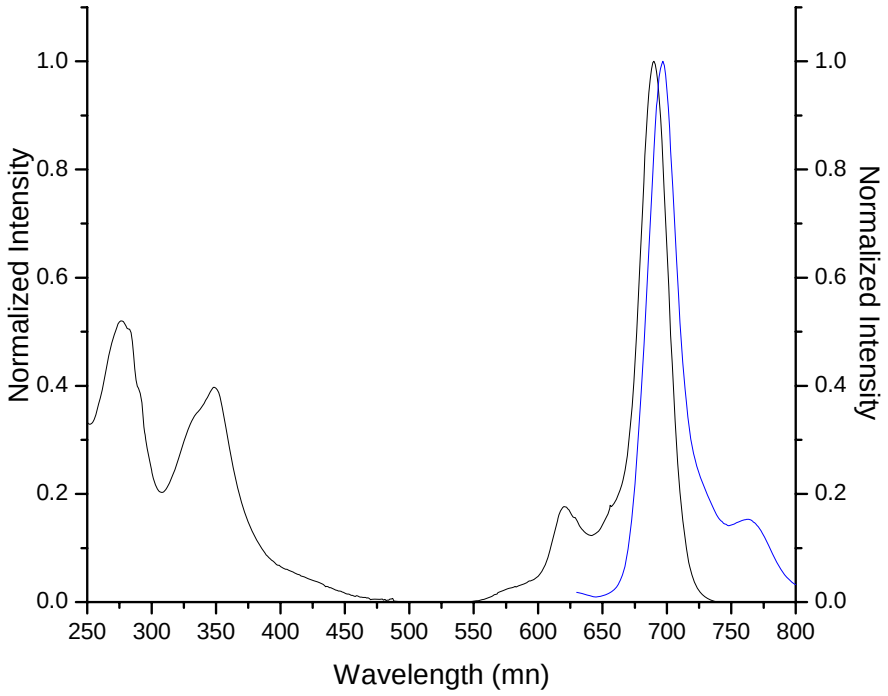

Figure 3.8 Normalized overlay of the absorption and emission spectra of ZnPc-insulin chain B conjugate in 10%DMSO/HEPES. The fluorescence emission spectrum was obtained using an excitation wavelength of 610 nm. The dye-to-peptide ratio was set at 10:1. Concentration of ZnPc used for conjugation was 10^{-6} M.

maxima at wavelengths 680 nm and 686 nm, respectively compared to the absorption and emission maximum of the unreacted Zn4CPc in HEPES at pH 8 that shows significant broadening indicative of extensive aggregation (please refer to Chapter 2).

In figure 3.9 is shown the absorption and emission spectrum of the ZnPc-BSA conjugate in DMSO/HEPES that displays an absorption and emission maxima of 683 nm and 686 nm. In

addition, we examined the absorbance and emission of ZnPc-oligonucleotide in HEPES and the resulting spectra, Figure 3.10, shows an extra peak at 637 nm and the monomeric peak at 683 nm. An overlay of the unlabeled oligonucleotide is shown for comparison of the peak at 254 nm due to the oligonucleotide. The peak observed at 637 nm is due to the formation of H-aggregates marked by a broad peak blue-shifted from the monomer.[11]

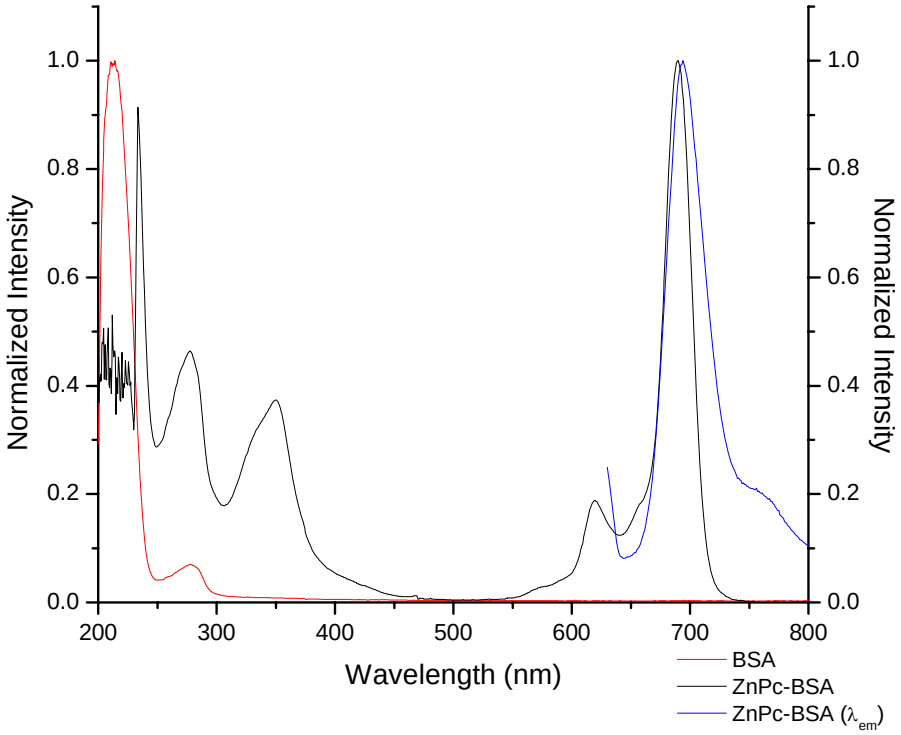

Figure 3.9 Normalized overlay of the absorption and emission spectra for ZnPc-BSA conjugate along with the absorption spectrum for unconjugated BSA. The BSA-to-dye ratio was set at 10:1. The excitation wavelength maximum was 683 nm and the emission maximum was 686 nm. The dye concentration was 1×10^{-6} M.

The bathochromic shift observed in the absorption and emission maximum is due to an increased solubility of the ZnPc in aqueous buffer due to the presence of the oligonucleotide. These results agree with previous studies by Owens and coworkers that reported a chemical shift to longer wavelengths for oligonucleotides labeled with asymmetrical Pc's.[11] The broadening of the absorption spectra observed for the ZnPc-oligonucleotide conjugate in aqueous buffer

solution resulted from extensive ground state aggregation. Addition of a small amount of DMSO to the aqueous solution of ZnPc-conjugates increased their solubility resulting in preference for the monomer compared to pure aqueous media.

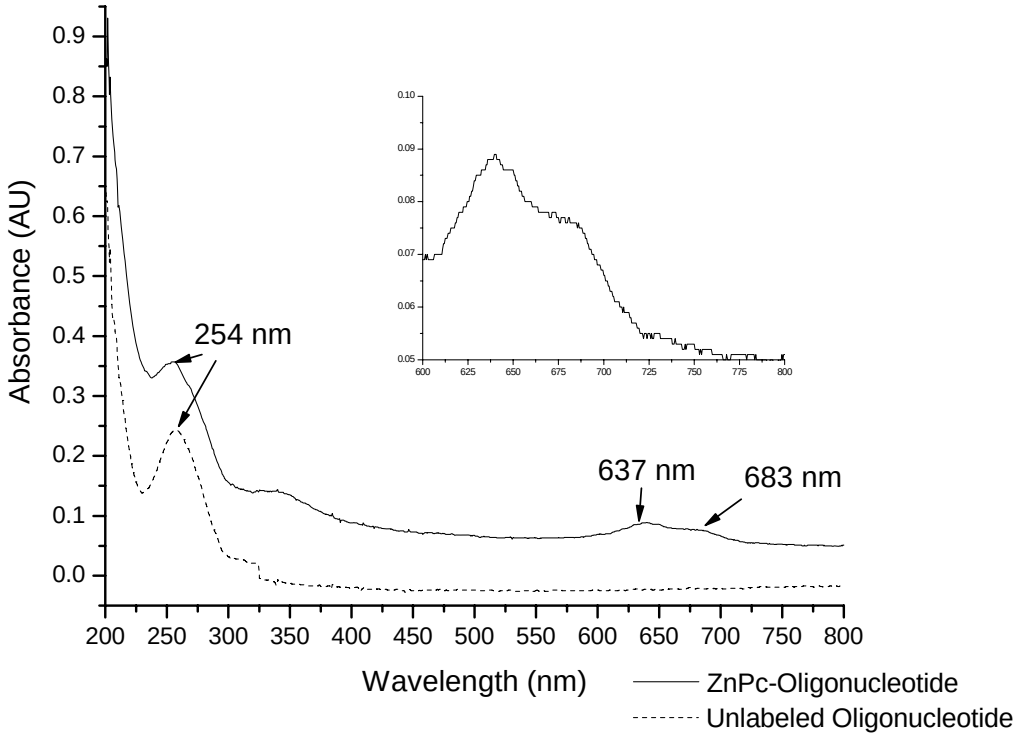

Figure 3.10 Absorption spectra of oligonucleotide and ZnPc-oligonucleotide conjugate in HEPES buffer. The broad peaks at 637 nm and 683 nm are indicative of H-aggregation. The dye-to-primer ratio was 10:1 with a dye concentration of 1×10^{-6} M.

Streptavidin has the unique ability to bind to biotin, naturally occurring vitamin H, with high affinity ($Ka = 10^{15}M^{-1}$) and specificity.[12] The ability of ZnPc-streptavidin conjugate to bind with biotin was tested in a biotin-binding assay with the use of biotin microbeads. Free Zn4CPc was used as a control reaction to determine the extent of non-specific binding of Zn4CPc on the polystyrene-based microspheres, which retains some hydrophobic characteristics. The fluorescence spectra for the Zn4CPc control and the ZnPc-streptavidin conjugate is shown in Figure 3.11. Our results indicate that the ZnPc-streptavidin conjugate binds to the biotinylated

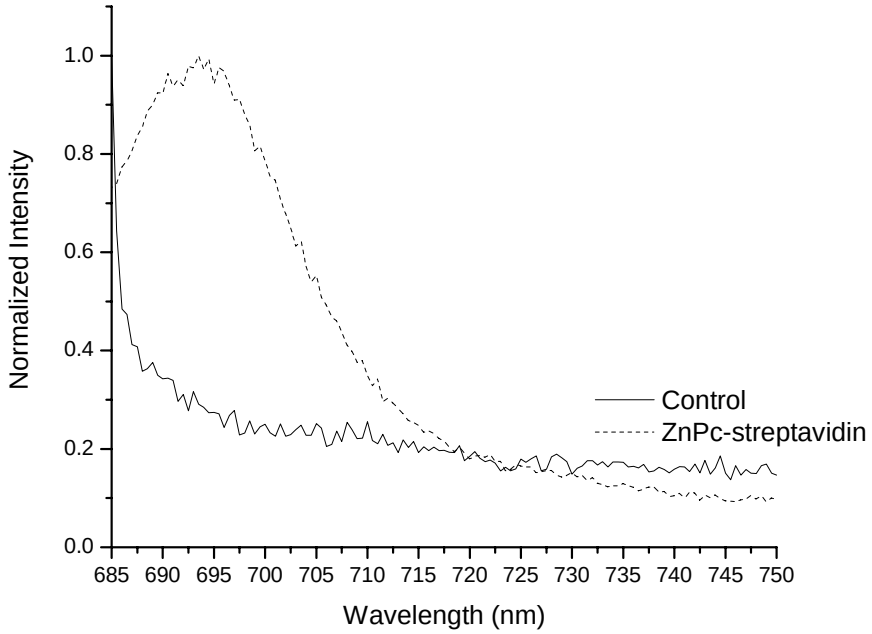

Figure 3.11 Fluorescence emission spectrum of ZnPc-streptavidin bound to biotinylated microspheres and a control reaction with no streptavidin added to the solution. Non-specific binding of the dye is minimal. Excitation wavelength: 680 nm, [dye] = 1×10^{-6} M. microbeads and that Zn4CPc exhibits low non-specific interaction with the solid surface.

3.3.3 Fluorescence Lifetime of Labeled Streptavidin

The fluorescence lifetime is a parameter that has been used in biological assays due to the lack of lifetime data available for fluorescent dyes and the availability of dyes that show unique lifetime characteristics upon derivatization. The measured lifetime for ZnPc-streptavidin was 2.85 ns in comparison to the fluorescence decay of free ZnPc found to be 3.1 ns (see Figure 3.12). The lifetimes were fit to monoexponential decay. The χ^2 value for Zn4CPc-streptavidin conjugate and the Zn4CPc was determined to be 1.34 and 1.43, respectively. Attempts to fit the lifetimes to a double-exponential decay did not increase the goodness of the fit.

In an attempt to characterize the conjugates using MS analysis, MALDI-TOF was carried out as a soft ionization technique to verify the covalent attachment of the biomolecule to ZnPc-NHS.

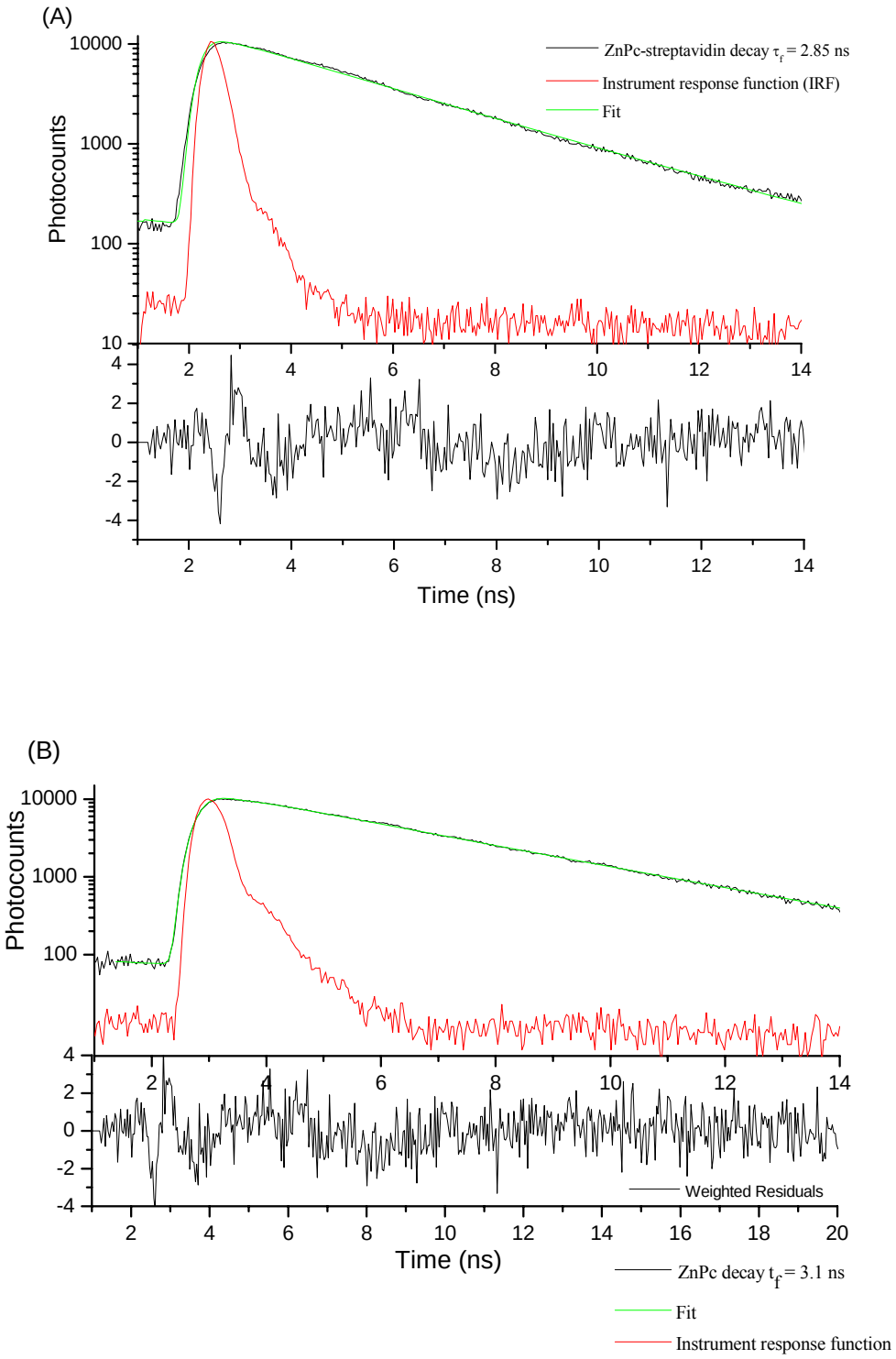

Figure 3.12 Fluorescence decay profile of ZnPc-streptavidin in HEPES buffer at pH 8 and the instrument response function (A) along with the fluorescence decay profile of Zn4CPc (B). Weighted residual shown for zinc phthalocyanine and the conjugate. χ^2 values of 1.34 and 1.43 represents a good fit of the decay profile.

Mass data was unobtainable for ZnPc-streptavidin and ZnPc-oligonucleotide possibly due to an increased amount of the ZnPc-insulin conjugate present in solution. MALDI analysis was obtained for ZnPc-insulin chain B and the result is shown in Figure 3.13. The spectrum gave a major signal at m/z 1546.67 and 4678.12 corresponding to the unreacted ZnPc-NHS and insulin chain B conjugate, respectively.

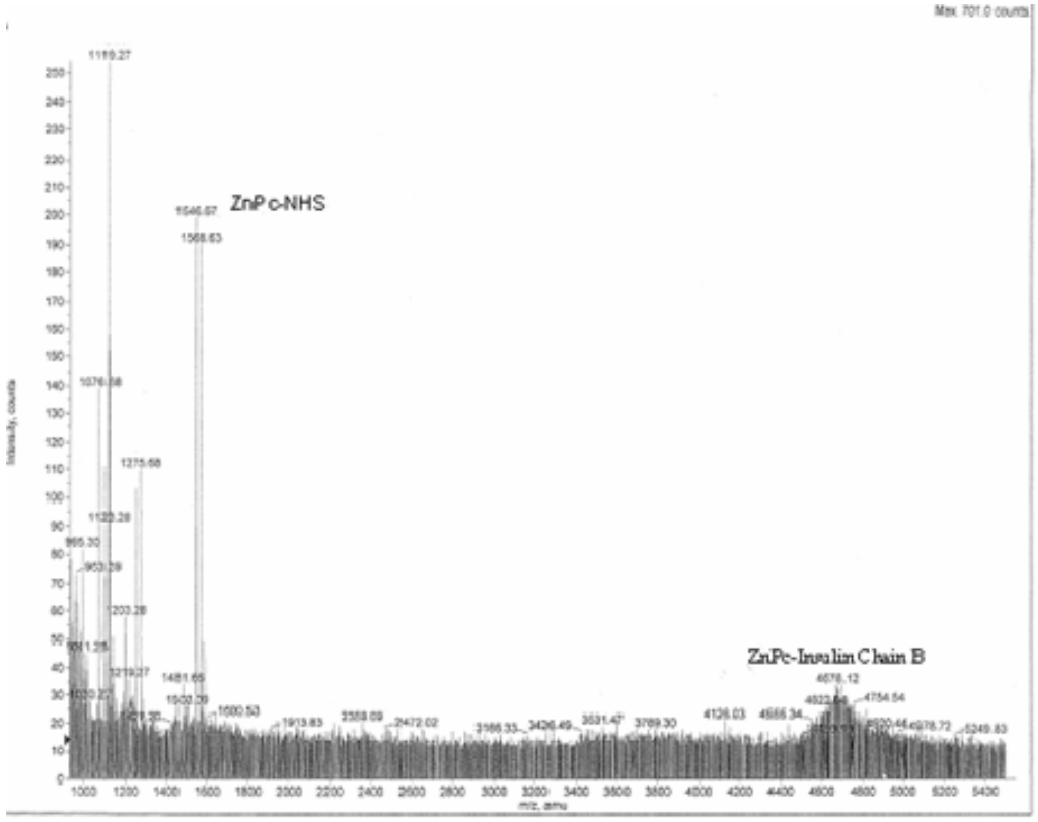

Figure 3.13 Mass spectrum of ZnPc-insulin chain B conjugate dissolved in a 1:1 (v/v) solution of 2,4,6 Trihydroxyacetophenone (THAP) matrix. Mass spectrum acquired by MALDI-TOF using a 337 nm nitrogen laser operated in negative mode.

3.3.4 Separation of Labeled Conjugates Using Reverse Phase Chromatography

The chromatographic separation for ZnPc-insulin chain B conjugate is shown in Figure 3.14. As can be seen, insulin chain B eluted at 4.5 min (Figure 3.14A). The chromatogram for the ZnPc-conjugate is shown in Figure 3.14 B. The detection of insulin chain B was performed using a photodiode array (PDA) with detection monitored at wavelength 260 nm, and ZnPc-insulin chain B was monitored using fluorescence detection at 686 nm.

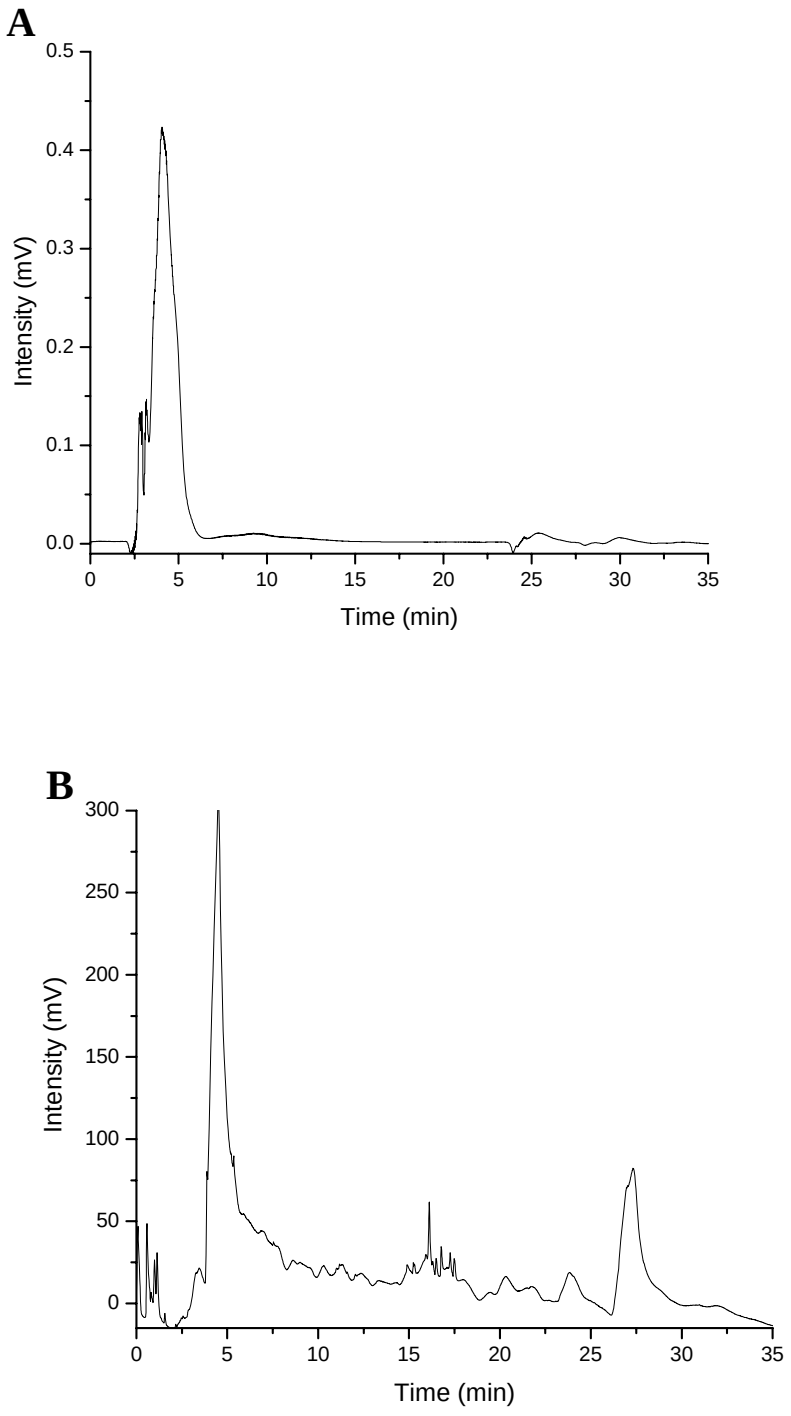

Figure 3.14 Chromatogram of unlabeled insulin chain B (**A**) with a retention time of 4.5 min, and Zn4CPc labeled insulin chain B (**B**) with peaks eluting at 5.2 min, unresolved peaks at ~ 16 min, and a peak eluting at 28 min. Separation was performed using a reverse-phase column and a linear gradient of 0.1%TEAA/ACN for 35 min. Detection was performed using a PDA and fluorescence detector system. Concentration of ZnPc-NHS used in reaction: 10^{-6} M. The dye-to-peptide ratio was 10:1.

Two resolved peaks are present in the separation of the Zn4CPc labeled insulin chain B with an elution time of 5.2 min. and 30 min. with unresolved peaks eluting around 20 min. Insulin chain B contains two primary amines that are available for labeling with pKa's of 8.4 and 9.8, respectively. ZnPc possesses four active ester groups that are available for labeling. The peak observed at 5.2 min can be due to monosubstituted insulin chain B and the unresolved peaks at 20 min can be indicative of multiply labeled insulin chain B. Under reverse-phase HPLC conditions, free ZnPc is expected to elute later compared to the conjugate, therefore, the peak at 30 min. is possibly due to unreacted ZnPc. The dye-to-protein concentration ratio was set to 10-to-1 in order to minimize multiple molecules strapped to a single Zn4CPc molecule due to the four active sites around the periphery of the dye.

3.3.5 Influence of Amino Linker Chain Length on the Conjugation of Amine Modified Oligonucleotides

Depending on the length of the amine linker, the biological functionality of the biomolecule can be compromised due to intramolecular interaction of the dye molecules.[27,28] It has been demonstrated previously that an increase in the length of the linker unit between the biomolecule and the functional moiety significantly reduces intramolecular interaction between the two molecules serving as a simple means to restore the biological function of the biomolecule.[28] Soini reported on the preparation of palladium (II) coproporphyrin as labeling reagents and the effect of the linker unit on the reaction kinetics ad biological activity of Ig conjugates.[29] An increase in the linker length resulted in increased phosphorescence of the conjugate and the biological activity was maintained. We investigated the influence of the length of the carbon chain amino linker on the labeling of oligonucleotides determined based on the intensity of the fluorescence detection using HPLC. Figure 3.15 illustrates the schematic of a single ZnPc molecule attached to a single strand oligonucleotide modified with a six-carbon chain amino linker. An increase in the amine linker appeared to give an increased amount of the

conjugate observed in the chromatogram (Figure 3.16). A possible reason for the decreased amount of conjugate seen with the C6-amine linker may be the ability of the linker to quench the excited state of the conjugate or the decreased symmetry of the conjugate.[28, 29] For the metal phthalocyanine used in the experimental, all four carboxyl groups are activated, however due to steric hindrance only two oligonucleotides are capable of being linked to the dye moiety. Nesterova et al. recently determined the labeling efficiency by HPLC method (unpublished data).[30]

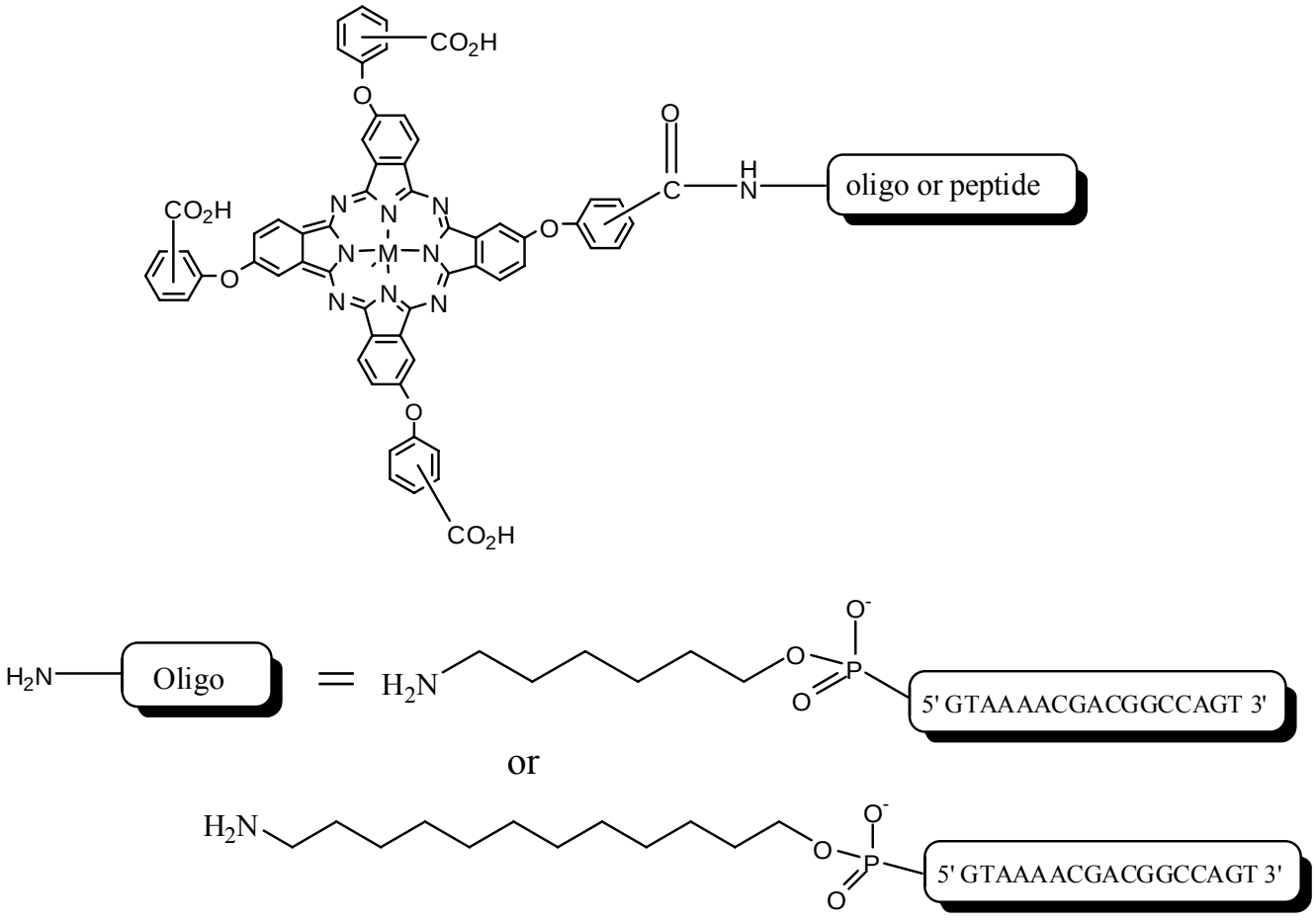

Figure 3.15 Illustration of the conjugate structure for Zn4CPc labeled with an oligonucleotide or peptide. The oligonucleotide has an amino modified linker attached to the 5' end. See experimental section for labeling details.

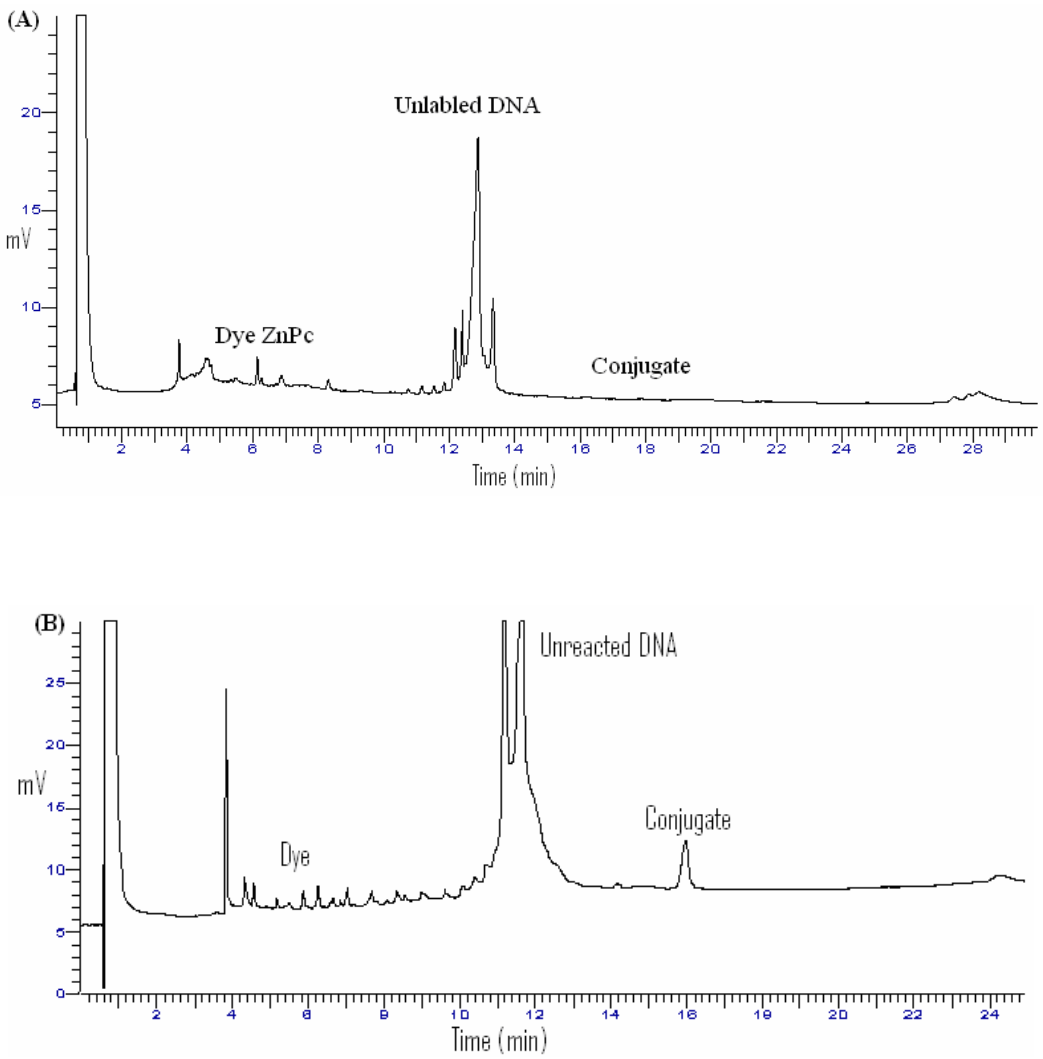

Figure 3.16 HPLC reverse-phase chromatographic separation of ZnPc-oligonucleotide conjugate using a C6-amino linker (A) and a C12-amino linker (B) attached to the primer. Dye concentration: 10^{-5} M; 10:1 dye-to-primer ratio. Chromatographic separation was performed with a linear gradient of 0.1% TEAA/ACN (see experimental for details).

3.4 Conclusions

In conclusion, we have demonstrated the ability to label several biomolecules with Zn4CPc labeling dyes ideal as fluorescent tags for biological assays requiring highly sensitive detection. Zn4CPc was chosen for these studies because it is highly fluorescent and showed favorable water solubility compared to the other MPc's synthesized for this work. Converting the carboxylic acids on the periphery of the dye to functional N, hydroxysuccinimide (NHS) esters was performed with relative ease and can be performed under mild conditions.

Carbodiimide coupling chemistry yielded a stable ZnPc-NHS derivative to allow conjugation of bovine serum albumin (BSA), insulin chain B and an oligonucleotide. Multiple products were observed in the chromatogram when Zn4CPc was labeled to insulin chain B due to multiple target molecules attached to Zn4CPc dye molecules that possesses several functional groups. The exact reason for the observed decreased amount of oligonucleotide conjugate formed when using a shorter aliphatic linker is unclear, however recent results showed an increase in labeling efficiency when the longer linker was used.[30] Furthermore, the data show that changes in the fluorescence lifetime of the dye might be used advantageously in developing fluorescence-based assays

3.5 References

(1) Doi, N.; Takashima, H.; Kinjo, M.; Sakata, K.; Kawahashi, Y.; Oishi, Y.; Oyama, R.; Miyamoto-Sato, E.; Sawasaki, T.; Endo, Y.; Yanagawa, H. *Genome Res.* **2002**, *12*, 487-492.

(2) Lefevre, C.; Kang, H. C.; Haugland, R. P.; Malekzadeh, N.; Arttamangkul, S.; Haugland, R. P. *Bioconjugate Chemistry* **1996**, *7*, 482-489.

(3) Kapanidis, A. N.; Weiss, S. *J. Chem. Phys.* **2002**, *117*, 10953-10964.

(4) Kelly, T. A.; Hunter, C. A.; Schindele, D. C.; Pepich, B. V. *Clinical Chemistry (Washington, DC, United States)* **1991**, *37*, 1283-6.

(5) Verdree, V. T., Su, G. Pakhomov, S., Allen, M.A., Countryman, A.C., Soper, S.A.., Hammer, R. P. *Journal of Fluorescence* **2007**, *In print*.

(6) Patonay, G.; Salon, J.; Sowell, J.; Strekowski, L. *Molecules* **2004**, *9*, 40-49.

(7) Williams, R. J.; Lipowska, M.; Patonay, G.; Strekowski, L. *Analytical Chemistry* **1993**, *65*, 601-605.

(8) de Jong, E. P.; Melanson, J. E.; Lucy, C. A. *Electrophoresis* **2004**, *25*, 3153-3162.

(9) Colyer, C. *Cell Biochemistry and Biophysics* **2000**, *33*, 323-337.

(10) Davidson, Y. Y.; Gunn, B. M.; Soper, S. A. *Applied Spectroscopy* **1996**, *50*, 211-21.

(11) Hammer, R. P.; Owens, C. V.; Hwang, S. H.; Sayes, C. M.; Soper, S. A. *Bioconjugate Chemistry* **2002**, *13*, 1244-1252.

(12) Legendre, B. L.; Soper, S. A. *Applied Spectroscopy* **1996**, *50*, 1196-1202.

(13) Peng, X.; Sternberg, E.; Dolphin, D. *Electrophoresis* **2005**, *26*, 3861-3868.

(14) Welder, F.; Paul, B.; Nakazumi, H.; Yagi, S.; Colyer, C. L. *Journal of Chromatography B-Analytical Technologies in the Biomedical and Life Sciences* **2003**, *793*, 93-105.

(15) Patonay, G.; Kim, J. S.; Kodagahally, R.; Strekowski, L. *Applied Spectroscopy* **2005**, *59*, 682-690.

(16) Nakazumi, H.; Colyer, C. L.; Kaihara, K.; Yagi, S.; Hyodo, Y. *Chem. Lett.* **2003**, *32*, 804-805.

(17) Berlier, J. E.; Rothe, A.; Buller, G.; Bradford, J.; Gray, D. R.; Filanoski, B. J.; Telford, W. G.; Yue, S.; Liu, J. X.; Cheung, C. Y.; Chang, W.; Hirsch, J. D.; Beechem, J. M.; Haugland, R. P.; Haugland, R. P. *Journal of Histochemistry & Cytochemistry* **2003**, *51*, 1699-1712.

(18) Hoare, D. G.; Koshland, D. E. *Journal of the American Chemical Society* **1966**, *88*, 2057-2061.

(19) Schaller, H.; Khorana, H. G. *Journal of the American Chemical Society* **1963**, *85*, 3828-3831.

(20) Weimann, G.; Khorana, H. G. *Journal of the American Chemical Society* **1962**, *84*, 4329-4333.

(21) Hermanson, G. T. *Bioconjugate techniques*; Academic Press: San Diego, 1996.

(22) Ibrahim, I. T.; Williams, A. *Journal of the Chemical Society-Perkin Transactions 2* **1982**, 1455-1458.

(23) Staros, J. V.; Wright, R. W.; Swingle, D. M. *Analytical Biochemistry* **1986**, *156*, 220-222.

(24) Liu, S.; Zhang, H. L.; Liu, T. C.; Liu, B.; Cao, Y. C.; Huang, Z. L.; Zhao, Y. D.; Luo, Q. M. *Journal of Biomedical Materials Research Part A* **2007**, *80A*, 752-757.

(25) Hua, X. F.; Liu, T. C.; Cao, Y. C.; Liu, B.; Wang, H. Q.; Wang, J. H.; Huang, Z. L.; Zhao, Y. D. *Analytical and Bioanalytical Chemistry* **2006**, *386*, 1665-1671.

(26) Williams, A.; Hill, S. V.; Ibrahim, I. T. *Analytical Biochemistry* **1981**, *114*, 173-176.

(27) Benson, S. C.; Zeng, Z. X.; Glazer, A. N. *Analytical Biochemistry* **1995**, *231*, 247-255.

(28) Zhu, Z. R.; Chao, J.; Yu, H.; Waggoner, A. S. *Nucleic Acids Research* **1994**, *22*, 3418-3422.

(29) Soini, A. E.; Yashunsky, D. V.; Meltola, N. J.; Ponomarev, G. V. *Luminescence* **2003**, *18*, 182-192.

(30) Nesterova, I. V., Verdree, Vera T., Pakhomov, Serhii, Hammer, Robert P., Soper, Steven A. *Submitted* **2007**.

Chapter 4
Fluorescence Microplate-Based Assays for High Throughput Optimization of Protein Labeling Using Functionalized Zinc Phthalocyanine

4.1 Introduction

In recent years, the number of organic and inorganic fluorescence compounds available for labeling proteins has increased and protein labeling has been well documented.[1-5] However, there remains a need for a versatile set of fluorescence dyes that can label proteins possessing diverse properties with high efficiency and selectivity. Challenges involved in labeling proteins include the production of a mixture of labeled products due to the presence of several amino groups on the protein that can react with the fluorescent moiety containing a reactive group for the primary amine; avoiding over-labeling of the protein causing self-quenching of the conjugate due to the close proximity of dye molecules; and modifying proteins without affecting its biological activity. Several authors have reported a decrease in fluorescence intensity when a protein is attached to a fluorescent dye because of one of the aforementioned challenges. For example, Ravdin and coworkers reported on the labeling of α-bungarotoxin with tetramethyl-rhodamine citing a decrease in fluorescence intensity due to the energy transfer between closely attached dye molecules and the formation of non-fluorescent derivatives.[6] Goussu and coworkers observed a 50% loss in the fluorescence intensity of protein conjugates with Cy3.[7] Previously, our group reported on the preparation of streptavidin conjugated with Zn4CPc and results indicated streptavidin molecules bearing two or more dye molecules (refer to Chapter 2 for details).

Experimental parameters for optimal labeling of proteins with fluorescein,[8] Alexa dyes,[9] as well as Bodipy dyes[10] have been reported, however, this information is not available for protein labeling with MPc fluorophores that represent promising candidates for bioanalytical applications requiring labeling fluorophores due to their photophysical characteristics and the

ability to alter the spectral properties of these dyes with minor structural changes. Therefore, it is desirable to develop a generalized protocol that can provide optimized conjugation conditions for labeling proteins with MPc and other dyes as well so that the targets retain their relatively high activity and the dyes show high fluorescence intensity even when heavily labeled.

In this report, we exploit the strength and specificity of streptavidin-biotin interactions for generating a procedure for optimizing the labeling conditions for the covalent attachment of fluorescent dyes to proteins using Zn4CPc as the model. This method involved the activation of all four carboxyl groups of Zn4CPc with N-hydroxysuccinimide (NHS) and 1-ethyl-3-[3-(dimethylamino) propyl] carbodiimide (EDC) and reacting the resulting Zn4CPc active ester (ZnPc-NHS) with streptavidin under different labeling conditions. Optimizing the labeling conditions were performed using a 96-well plate with biotin immobilized on the surface of each microwell for high throughput selection of proper reaction conditions to obtain a high yield of the conjugate and maintain protein activity. Parameters such as buffer pH, concentration ratio of Zn4CPc to streptavidin, and solvent composition were evaluated.

4.1.1 Challenges Using Metal Phthalocyanines as Labeling Reagents

Phthalocyanines (Pc's) are attractive fluorophores as a means of detecting biological molecules due to their unique spectroscopic characteristics. They have received much attention as reagents for photodynamic therapy [11-14] and are becoming increasingly popular in other biological application areas such as cell imaging, and thin films.[15-19] To date, only a few reports have appeared discussing the conjugation of phthalocyanines to biological targets, as this remains challenging due to the complex structure, hydrophobicity of the unsubstituted chromophore, and the tendency of the Pc's to form aggregates in aqueous solutions.[20, 21] La Jolla Blue, one of the first fluorescence probes produced from the phthalocyanine class of dyes containing axial ethylene glycol ligands, was conjugated to amine modified oligonucleotides for

nucleic acid hybridization assays monitored using transient-state polarized fluorescence measurements.[22] Chernonosov and coworkers reported on the conjugation of Co(II)tetracarboxyphthalocyanine with oligonucleotides for investigating the thermodynamic characteristics of DNA duplexes formed with the conjugates.[23] Li reported on the synthesis and spectroscopic properties of zinc(II)phthalocyanine conjugated to adenine concluding the conjugates possessed strong intermolecular interactions due the presence of the nucleobase substituent resulting in unusual spectral features attributed to aggregation.[24] Mikhaleno et al. reported on the preparation of phthalocyanine derivatives conjugated to amino acids.[25] Huang and coworkers studied the covalent interactions of silicon(IV) phthalocyanine with serum albumin for use in photodynamic therapy.[26] Nesterova and coworkers demonstrated the use of asymmetrical Zn(II) phthalocyanine (ZnPc) to label oligonucleotides reporting improved solubility of ZnPc in aqueous media when conjugated to an oligonucleotide due to the charge of the phosphate backbone, however, the formation of aggregates still occured.[8, 27, 28] We recently demonstrated the use of Zn4CPc to label peptides and proteins.[27, 29]

4.1.2 Streptavidin-Biotin Binding and Its Use in Bioassays

Biotin is a water-soluble vitamin that is an essential nutrient involved in important biological activities such as metabolism of amino acids.[30, 31] The chemical structure of biotin is shown in Figure 4.1.

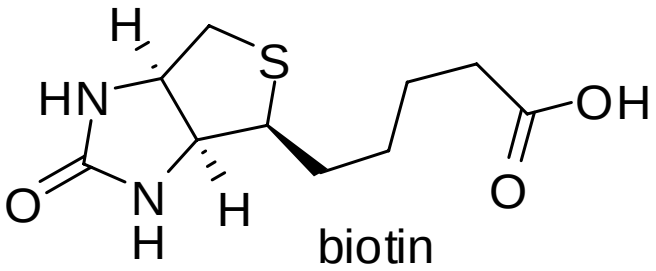

Figure 4.1 Chemical structure of biotin.

Streptavidin, a 60 kDa protein produced by Streptomyces, is a tetrameric protein consisting of four identical subunits with a molecular weight of 15,000 and binds to 4 mol of biotin per mol of protein. The tetrameric structure of streptavidin is shown in Figure 4.2.[31, 32]

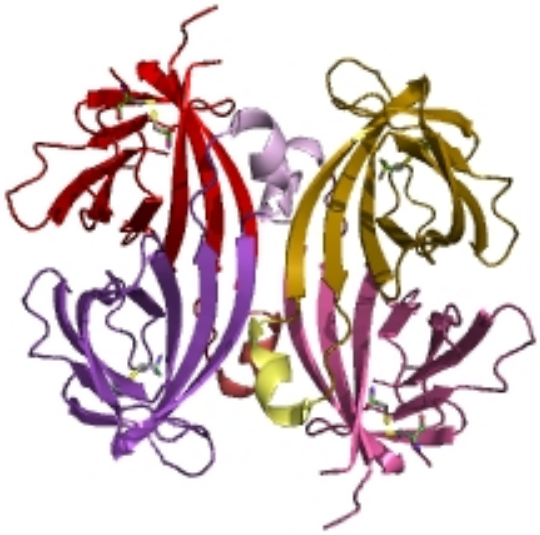

Figure 4.2 Tetrameric structure of streptavidin used as a model protein for optimization of the conjugation reaction with Zn4CPc. Each subunit has a molecular weight of 15 kDa.[31]

The binding affinity between biotin and streptavidin is > 10^{-15} M due to a number of hydrogen bonding and van der Walls interactions from each streptavidin subunit involved in the binding of biotin to streptavidin.[31] The specificity and strong binding feature of this system affords its use for many biological applications to include detection, and purification of nucleic acids and proteins.[30, 33-35] With the high availability of biotinylated materials, this classic model was useful for microplate-based binding assays to evaluate several labeling conditions.

4.2 Materials and Methods

4.2.1 Reagents and Samples

All reagents and materials were received and used without further purification. 1-ethyl-3-[3-(dimethylamino)propyl]carbodiimide (EDC) and N-Hydroxysuccinimide ester (NHS) were purchased from Sigma-Aldrich (St. Louis, MO, USA) Dimethylsulfoxide (DMSO), N-(2-

hydroxyethyl)piperazine-1-ethanesulfonic acid (HEPES) and carbonate buffer were purchased from Sigma-Aldrich (St. Louis, MO, USA). Sephadex LH-20 columns were purchased from GE Healthcare (Piscataway, NJ). Streptavidin from *Streptomyces avidinii* was also purchased from Sigma-Aldrich. Reacti-Bind biotin coated 96-well plates, purchased from Pierce Biotechnology (Rockford, IL, USA), were clear to minimize background fluorescence and light absorption. The activated ester form of Zn4CPc was synthesized in-house by Dr. Serhii Pakhomov using a method adapted from a procedure by Koval et al. with the structure of the fluorophore shown in Figure 4.3 (refer to Chapter 2 for synthesis details).[36] Dye solutions were first prepared by dissolving the dye in DMSO to ensure the dyes existed as monomers prior to the labeling reactions.

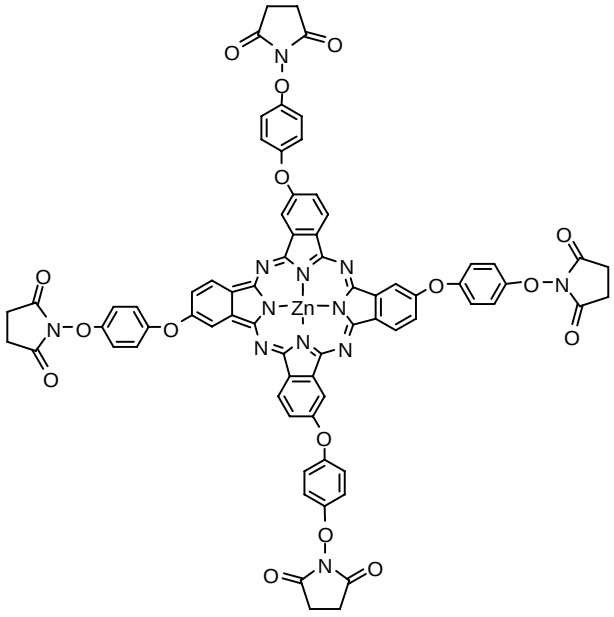

Figure 4.3 Molecular structure of the active N-hydroxysuccinimide (NHS) ester form of Zn4CPc. All four carboxyl groups are converted to NHS esters outlined by a procedure published by Koval et al.[36] Synthesis was performed in-house in collaboration with Dr. Hammer's laboratory.

4.2.2 Conjugation of Zn4CPc Activated Ester (ZnPc-NHS) to Protein

Streptavidin was conjugated to Zn4CPc-NHS as described previously in Chapter 2. Briefly, a 0.1 M stock solution of protein was freshly prepared by dissolving 5 mg of streptavidin

in HEPES. A stock solution of Zn4CPc-NHS in DMSO was also prepared to give a final concentration of 1 mM. Aliquots of Zn4CPc-NHS were slowly added to vials containing the protein diluted with 10 mM HEPES buffer to obtain the desired concentration ratio. The vials were then capped and covered with aluminum foil to avoid photodegradation of Zn4CPc-NHS. The labeling reactions were vortexed at room temperature for 24 h and then purified by size exclusion chromatography using a sephadex LH-20 columns. Sephadex LH-20 columns were chosen because they are designed for use solvent mixtures of organic and aqueous solvents. Fractions were collected and analyzed spectrophotometrically.

4.2.3 Reactivity Binding Assay

Four parameters of the conjugation reaction were investigated:

- The amount of Z4CnPc-NHS added to the reaction mixture varied from 1-to-1 molar ratio Zn4CPc-NHS to protein to a 15-fold excess of Zn4CPc-NHS
- The pH of the reaction was varied from pH 7 to 9.5
- The ZnPc-NHS concentration varied from 10 μM to 100 μM
- The amount of aqueous solvent added to the reaction was varied from 20% to 70% HEPES.

Figure 4.4 illustrates the assay format in which each well contained a reaction mixture under the different labeling conditions. The numbers above the microplate represent the concentration of Zn4CPc-NHS used for labeling and the numbers to the right represent the pH of HEPES in each well with the different dye-to-protein ratio. For example, in the well marked A1 is a reaction mixture with a dye-to-protein ratio of 1-to-1, Zn4CPc-NHS concentration of 10 μM in DMSO and HEPES at pH 7. The amount of aqueous solvent is shown as a percentage. Aliquots of the labeling reaction mixture were added to the biotin-coated wells and allowed to incubate for 30 min at room temperature. To determine the amount of non-specific adsorption of Zn4CPc to

streptavidin, the protein was allowed to incubate in a micro-well for 5 min in the absence of Zn4CPc that was subsequently added to the well and allowed to react for an additional 30 min. In addition, a control experiment of Zn4CPc-NHS in the absence of protein was carried out to determine the degree of nonspecific binding of Zn4CPc-NHS to the immobilized biotin. The plate was covered with aluminum foil to avoid photodegradation of the dye. After incubation, the plate was washed by adding 3 x 200 μL of 10 mM HEPES buffer. For assay measurements, the wells were filled with 200 μL of HEPES/DMSO and analyzed by fluorescence emission.

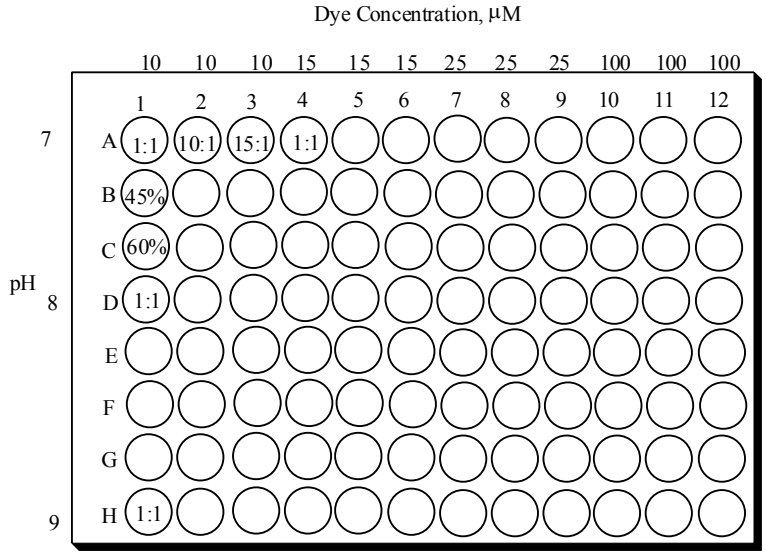

Figure 4.4 Schematic representing the microplate assay used for evaluating the optimal conditions. Parameters that were evaluated include pH, dye concentrations, dye-to-protein ratio, and amount of aqueous solvent (percentage).

4.3 Results and Discussion

4.3.1 Optimal Conditions for Labeling Streptavidin with ZnPc-NHS

MPc's represent a class of fluorophores in which only a few have reported on the conjugation of these dyes to proteins. Chen illustrated the use of a resonance light scattering (RLS) technique for quantitative measurements of proteins in human serum samples for clinical testing with tetra-substituted sulphonated aluminum phthalocyanine (AlS_4Pc).[37] Results from these studies showed that the RLS technique provided a convenient method for determining total

protein concentration in human serum with high sensitivity (detection limits of 16.1 ng ml^{-1}) and good selectivity. Ogunsipe reported on the conjugation of non-transition metal phthalocyanines to bovine serum albumin.[38] Here, we report on the optimal conditions for labeling streptavidin with Zn4CPc-NHS to provide a general optimized protocol that can easily be adapted for labeling proteins with MPc derivatives. Initially, an experiment was performed to evaluate the relative fluorescence units (RFU) for the Zn4CPc-streptavidin conjugate compared to unreacted Zn4CPc-NHS and unlabeled streptavidin when incubated in the microwell with biotin for 30 min and then washed repeatedly with buffer. The results from these studies are shown in Figure 4.5.

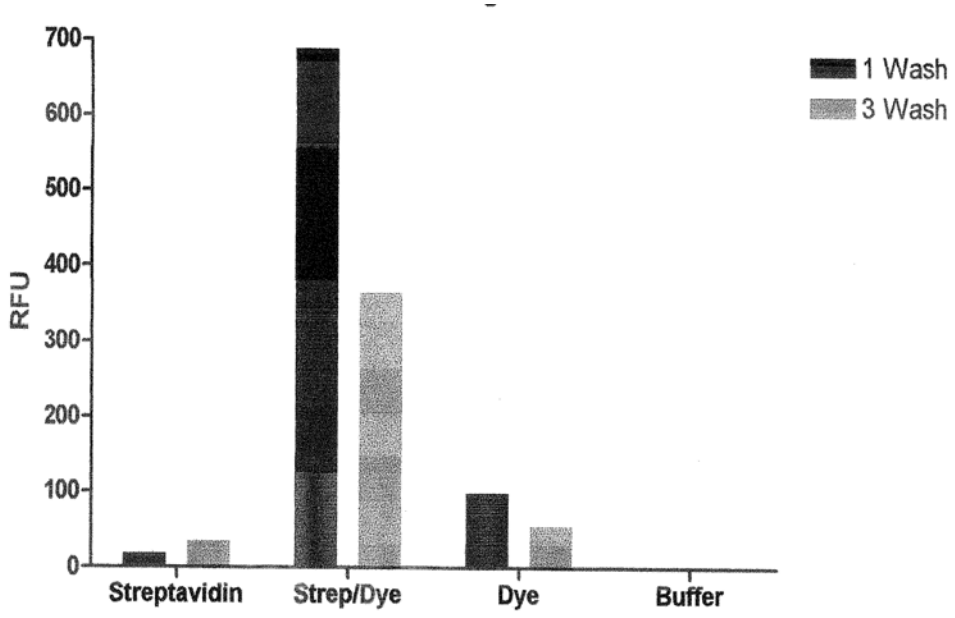

Figure 4.5 A comparison of the relative fluorescence intensity of unreacted streptavidin, free Zn4CPc, buffer, and streptavidin-dye conjugate. Results show minimal nonspecific adsorption of the free Zn4CPc-NHS. Excitation wavelength was 680 nm with an emission wavelength of 693 nm. The samples were incubated in the microwell for 30 minutes prior to rinsing.

The RFU was 7 times more intense for the Zn4CPc-streptavidin conjugate in comparison to the measured intensity of the unlabeled streptavidin. Background autofluorescence was observed with streptavidin alone; however, the intensity is relatively small. Originally, before the reaction mixture was incubated in the microwell, purification using gel-filtration was performed to isolate

the conjugate. When unconjugated Zn4CPc was incubated with no streptavidin present and low non-specific binding was observed without purification, labeling of streptavidin proceeded without any pre-purification of the reaction mixture (Figure 4.6).

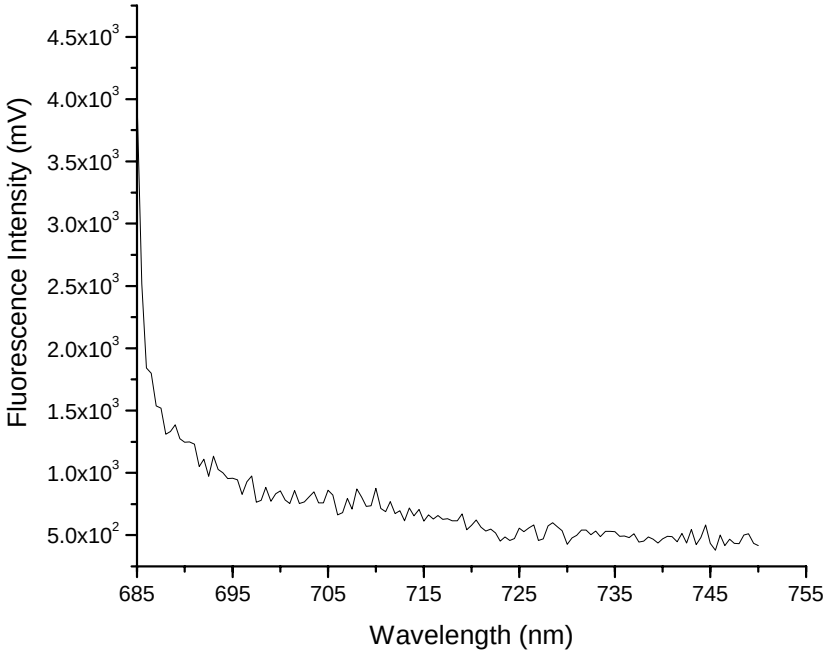

Figure 4.6 Fluorescence emission of Zn4CPc in the well with immobilized biotin in the absence of streptavidin. Results indicated minimal non-specific interaction of Zn4CPc with immobilized biotin.

The previously reported method for the conjugation of streptavidin with Zn4CPc was a simple procedure using conditions that resulted in over modification of the protein that can lead to a decrease in the reactivity of the protein. Thus, the use of a microplate assay allowed for the high throughput analysis of each condition in the labeling reaction in a single experiment. Optimization was determined by analyzing each conjugation reaction in a single well and the fluorescence intensity was measured at the maximum emission wavelength of 693 nm. Several modifications to the labeling procedure were made. The pH of the conjugation reaction was originally pH 5-6. However, carbodiimides are generally more stable at higher pH.[39] Thus, in the present work, the pH range was 7 to 9. The effect of pH on the fluorescence intensity is shown

in Figure 4.7. From these results, the optimal pH was observed at pH 8. At higher pH, the intensity significantly decreased.

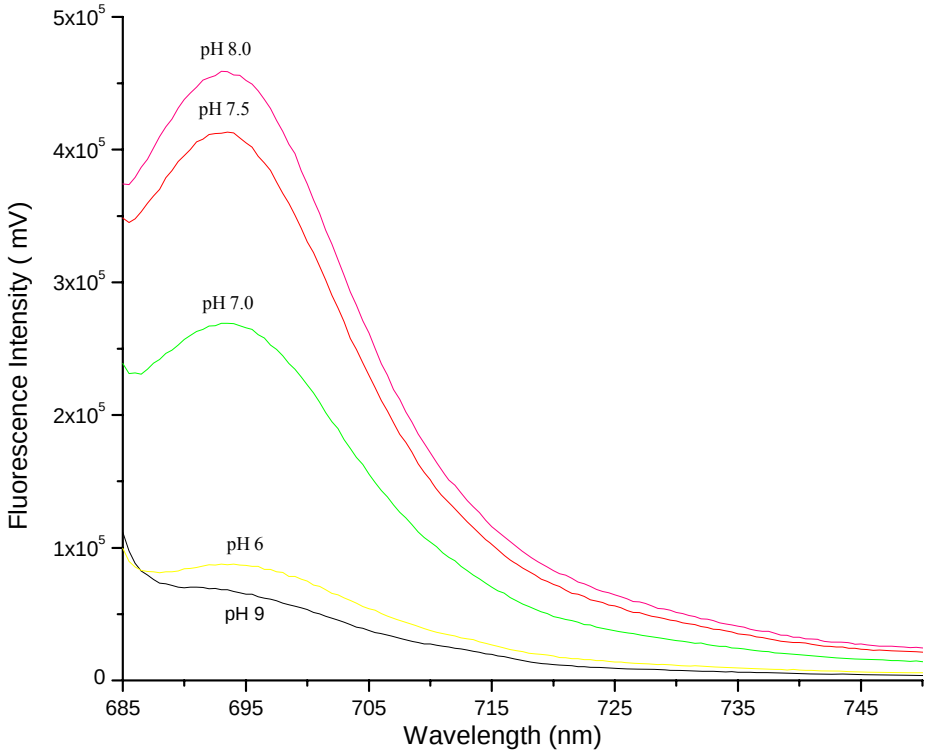

Figure 4.7 Fluorescence emission spectrum of Zn4CPc-streptavidin conjugate under varying pH conditions. The conjugate reaction mixture was allowed to incubate in the well with immobilized biotin for 30 min prior to rinsing 3 times with HEPES. Dye concentration used was 10 μM with a dye-to-protein ratio of 10-to-1.

This is expected since the rate of hydrolysis of the active ester converting back to the carboxylic acid is expected to increase at a higher pH resulting in a decreased yield of the conjugate due to hydrolysis (see Figure 4.8).[40,39] Second, buffer conditions of the conjugation reaction were evaluated. Several groups have reported optimum coupling with the use of carbonate buffer.[27] In the present work, HEPES buffer was found to be optimum due to its suitability at physiological pH and compatibility in mixed organic aqueous solvents.[41] The temperature remained constant for all reactions at 37°C due to previous studies showing an increase in the conjugate yield at this temperature.[42] Table 4.1 summarizes the conjugation reactions with Zn4CPc-NHS.

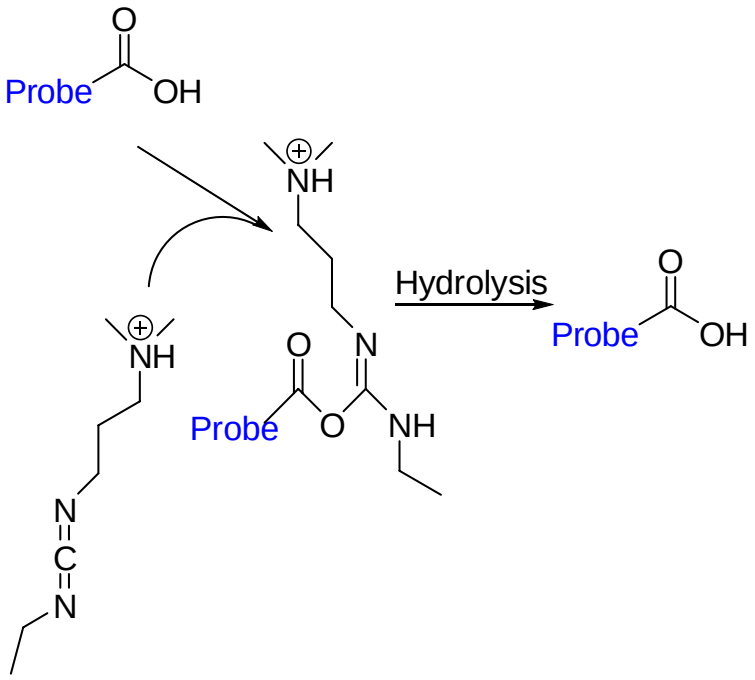

Figure 4.8 Schematic depicting hydrolysis of the N-hydroxysuccinimide active ester by which the ester converts back to the carboxyl group as a competing reaction. At high pH values, the rate of hydrolysis increases.

Table 4.1 Optimal method conditions for the general labeling of proteins. Parameters such as concentration, pH of buffer and amount of organic content were evaluated.

Method #	ZnPc-NHS (μM)	Dye:Protein ratio	%DMF	Buffer	Temp. °C
1	10	1:1	70	HEPES	37
2	10	10:1	70	HEPES	37
3	10	15:1	70	HEPES	37
4	15	1:1	70	HEPES	37
5	15	10:1	70	HEPES	37
6	15	15:1	70	HEPES	37
7	25	1:1	70	HEPES	37
8	25	10:1	70	HEPES	37
9	25	15:1	70	HEPES	37
10	50	1:1	70	HEPES	37
11	50	10:1	70	HEPES	37
12	100	15:1	70	HEPES	37

Figure 4.9 shows the comparison of Zn4CPc concentration on the fluorescence intensity. The increase in fluorescence intensity indicates an increase in the conjugate yield, which enhances the fluorescence creating an environment that favors emission of the Zn4CPc dye. A concentration of 15 μM was found to give the best results with a measured fluorescence intensity of 3.7×10^5. A high concentration of Zn4CPc-NHS (100 μM) resulted in a decrease in the fluorescence intensity possibly due to increased aggregation. It is well established in literature that the formation of dimers and higher order aggregates is prevalent in MPc dyes at high concentration (10^{-4}-10^{-3}).[43] For example, Reddi et al. showed that on increasing the concentration of aluminum tetrasulfonated phthalocyanine (AlPcS4), the fluorescence emission intensity appears to decrease.[44]

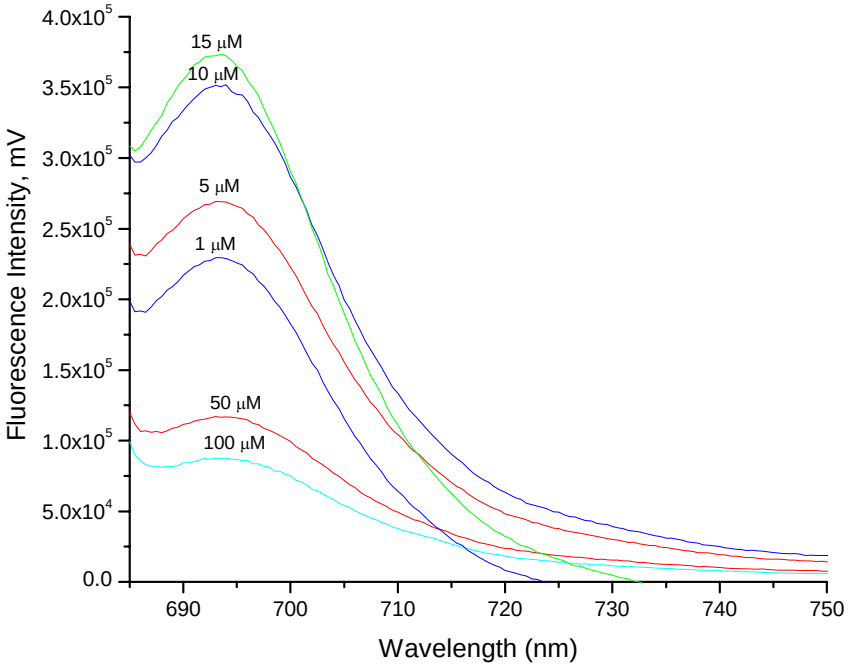

Figure 4.9 Fluorescence analysis of Zn4CPc-streptavidin conjugate as a function of (A) Zn4CPc concentration and (B) pH of HEPES buffer. Excitation, 680 nm; 5 nm slit width. Final volume of the labeling reaction incubated in the microwell was 200 μL at room temperature for 30 min and detected at an emission wavelength of 693. This pH range was chosen due to the solubility of Zn4CPc at this pH range.

Wagner and coworkers noted a decrease in the fluorescence intensity of gallium phthalocyanines due to aggregation effects resulting from high concentration of the dye.[45] Figure 4.10 compares the emission characteristics at different dye-to-protein ratios. A 10-to-1 ratio was found to give the highest fluorescence intensity, while a 15-to-1 ratio dramatically decreased the fluorescence intensity. This can be due to fluorescence energy transfer (FRET) between dye molecules in close contact because of the tertiary structure of streptavidin consisting of closely neighboring primary amine groups.[31,46] For example, the tertiary structure of streptavidin shows each subunit contains lysine groups closely positioned.[31]

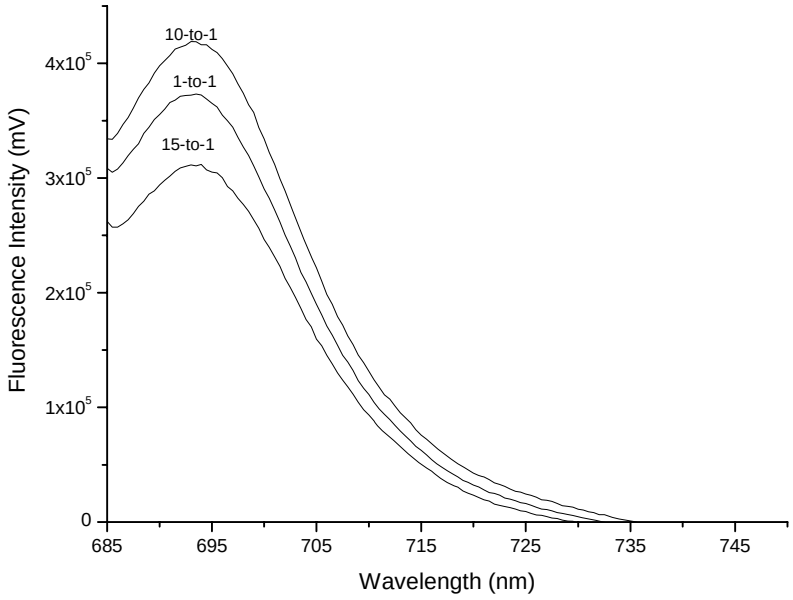

Figure 4.10 Fluorescence intensity of Zn4CPc-streptavidin conjugate with varying dye-to-protein ratio.

The amount of aqueous solvent was also varied to determine the minimum amount of organic solvent needed in the labeling reaction to solubilize Zn4CPc. Figure 4.11 shows the fluorescence intensity of labeled streptavidin in various amounts of HEPES buffer. Increasing the amount of aqueous content in the reaction mixture decreases the amount of conjugate that was produced. At >70% HEPES, precipitation of Zn4CPc was observed due to its insolubility in

aqueous solvents. In addition, upon examination of the absorption spectrum, the reaction mixture showed extensive ground-state aggregation (see Figure 4.12).

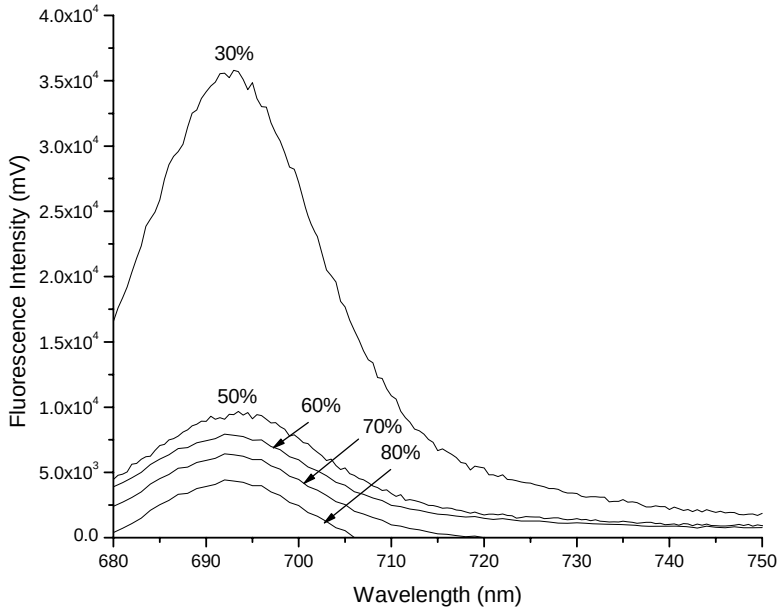

Figure 4.11 Fluorescence intensity of Zn4CPc-streptavidin conjugate as a function of the amount of HEPES in the reaction solution. The intensity continues to decrease as the amount of organic content lowers.

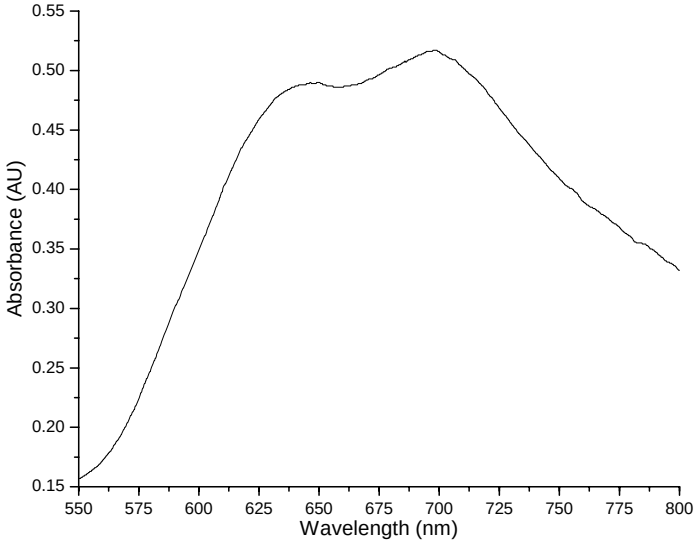

Figure 4.12 Absorption spectrum of Zn4CPc-streptavidin conjugate mixture in 80/20 HEPES/DMSO exhibiting extensive aggregation.

4.4 Conclusions

In conclusion, a simple and versatile protocol was developed for elucidating optimal labeling conditions of proteins using fluorescent dyes with Zn4CPc-NHS used as the model. By adjusting several experimental conditions such as buffer pH, concentration of the reactants and dye-to-protein molar ratio, a high amount of the conjugate was obtained as determined by the increase in fluorescence intensity. In these studies, it was found the optimal concentration of Zn4CPc used for labeling was approximately 10 μM. The effect of the dye-to-protein ratio demonstrated that the presence of a 15-fold excess of dye decreased the fluorescence intensity possibly due aggregation. A careful balance of aqueous to organic solvent is needed to minimize aggregation while maximizing the yield of the conjugate. The optimal amount of organic content was found to be 70%. Negative controls in the absence of protein resulted in low nonspecific binding of Zn4CPc to the immobilized biotin indicating the fluorescence intensity is due to conjugated streptavidin bound to the immobilized biotin.

4.5 References

(1) Doi, N.; Takashima, H.; Kinjo, M.; Sakata, K.; Kawahashi, Y.; Oishi, Y.; Oyama, R.; Miyamoto-Sato, E.; Sawasaki, T.; Endo, Y.; Yanagawa, H., *Genome Res.* 2002, 12, 487-492.

(2) Lipowska, M.; Patonay, G.; Strekowski, L., *Synth. Commun.* 1993, 23, 3087-3094.

(3) O'Riordan, T. C.; Soini, A. E.; Papkovsky, D. B., *Analytical Biochemistry* 2001, 290, 366-375.

(4) Thiele, C.; Ganzle, M. G.; Vogel, R. F., *J. Agric. Food Chem.* 2003, 51, 2745-2752.

(5) Wang, Z.-Q.; Diwu, Z.; Francisco-Reyes, J.; Yi, G. G., *Chem. Lett.* 2005, 34, 404-405.

(6) Ravdin, P.; Axelrod, D., *Analytical Biochemistry* 1977, 80, 585-592.

(7) Goussu, C.; Vasseur, J. J.; Bazin, H.; Trinquet, E.; Maurin, F.; Morvan, F.,*Bioconjugate Chemistry* 2005, 16, 465-470.

(8) Pitschke, M.; Fels, A.; Schmidt, B.; Heiliger, L.; Kuckert, E.; Riesner, D., *Colloid Polym. Sci.* 1995, 273, 740-52.

(9) Voloshina, N. P.; Haugland, R. P.; Bishop, J.; Bhalgat, M.; Millard, P.; Mao, F.; Leung, W. Y.; Haugland, R. P., *Mol. Biol. Cell* 1997, 8, 2017-2017.

(10) Tyagarajan, K.; Pretzer, E.; Wiktorowicz, J. E., *Electrophoresis* 2003, 24, 2348-2358.

(11) Lo, P. C.; Huang, J. D.; Cheng, D. Y. Y.; Chan, E. Y. M.; Fong, W. P.; Ko, W. H.; Ng, D. K. P., *Chemistry-a European Journal* 2004, 10, 4831-4838.

(12) Lukyanets, E. A., *Journal of Porphyrins and Phthalocyanines* 1999, 3, 424-432.

(13) Spikes, J. D., *Photochemistry and Photobiology* 1986, 43, 691-699.

(14) Vanlier, J. E.; Brasseur, N.; Ali, H.; Langlois, R.; Rousseau, J., *Lasers in Surgery and Medicine* 1986, 6, 230-231.

(15) Gundy, S.; Van der Putten, W.; Shearer, A.; Buckton, D.; Ryder, A. G.; Ball, M., *Phys. Med. Biol.* 2004, 49, 359-369.

(16) van Staveren, H. J.; Speelman, O. C.; Witjes, M. J. H.; Cincotta, L.; Star, W. M., *Photochem. Photobiol.* 2001, 73, 32-38.

(17) Gantchev, T. G.; Ouellet, R.; van Lier, J. E., *Arch. Biochem. Biophys.* 1999, 366, 21-30.

(18) Witjes, M. J. H.; Mank, A. J. G.; Speelman, O. C.; Posthumus, R.; Nooren, C.; Nauta, J. M.; Roodenburg, J. L. N.; Star, W. M.,*Photochem. Photobiol.* 1997, 65, 685-693.

(19) Caughey, W. S.; Raymond, L. D.; Horiuchi, M.; Caughey, B., *Proceedings of the National Academy of Sciences of the United States of America* 1998, 95, 12117-12122.

(20) Isago, H. *Chemical Communications* 2003, 1864-1865.

(21) Margaron, P.; Gregoire, M. J.; Scasnar, V.; Ali, H.; van Lier, J. E., *Photochem. Photobiol.* 1996, 63, 217-23.

(22) Devlin, R.; Studholme, R. M.; Dandliker, W. B.; Fahy, E.; Blumeyer, K.; Ghosh, S. S., *Clin. Chem.* 1993, 39, 1939-1943.

(23) Chernonosov, A. A.; Kuznetsov, N. A.; Koval, V. V.; Pyshnyi, D. V.; Derkacheva, N. M.; Lukyanets, E. A.; Fedorova, O. S., *Nucleosides Nucleotides & Nucleic Acids* 2004, 23, 983-987.

(24) Li, X. Y.; Ng, D. K. P., *Tetrahedron Lett.* 2001, 42, 305-309.

(25) Mikhalenko, S. A.; Solov'eva, L. I.; Luk'yanets, E. A., *Russian Journal of General Chemistry* 2004, 74, 451-459.

(26) Jiang, X. J.; Huang, J. D.; Zhu, Y. J.; Tang, F. X.; Ng, D. K. P.; Sun, J. C., *Bioorg. Med. Chem. Lett.* 2006, 16, 2450-2453.

(27) Nesterova, I. V., Verdree, Vera T., Pakhomov, Serhii, Hammer, Robert P., Soper, Steven A., *Submitted* 2007.

(28) Cooper, M.; Ebner, A.; Briggs, M.; Burrows, M.; Gardner, N.; Richardson, R.; West, R., *Journal of Fluorescence* 2004, 14, 145-150.

(29) Verdree, V., Pakhomov, S., Su, G., Allen, M. W., ; Soper, S. A. a. H., RP., *Journal of Fluorescence, Accepted*, Baton Rouge, LA 70803, 2006.

(30) Gruber, H. J.; Marek, M.; Schindler, H.; Kaiser, K., *Bioconjugate Chemistry* 1997, 8, 552-559.

(31) Weber, P. C.; Ohlendorf, D. H.; Wendoloski, J. J.; Salemme, F. R., *Science* 1989, 243, 85-88.

(32) Weber, P. C.; Cox, M. J.; Salemme, F. R.; Ohlendorf, D. H., *Journal of Biological Chemistry* 1987, 262, 12728-12729.

(33) Dorgan, L.; Magnotti, R.; Hou, J.; Engle, T.; Ruley, K.; Shull, B., *J. Magn. Magn. Mater.* 1999, 194, 69-75.

(34) Gao, X.; Mathieu, H. J.; Schawaller, M., *Surf. Interface Anal.* 2004, 36, 1507-1512.

(35) Wilbur, D. S.; Pathare, P. M.; Hamlin, D. K.; Frownfelter, M. B.; Kegley, B. B.; Leung, W.-Y.; Gee, K. R., *Bioconjugate Chemistry* 2000, 11, 584-598.

(36) Koval, V.V.; Chemonosov, A.A; Abramova, T.V.; Ivanova, T.M. *Biorganic Chemistry* 2000,26,118-125.

(37) Chen, X. L.; Li, D. H.; Zhu, Q. Z.; Yang, H. H.; Zheng, H.; Wang, Z. H.; Xu, J. G., *Talanta* 2001, 53, 1205-1210.

(38) Ogunsipe, A.; Nyokong, T., *Photochemical & Photobiological Sciences* 2005, 4, 510-516.

(39) Sehgal, D.; Vijay, I. K., *Analytical Biochemistry* 1994, 218, 87-91.

(40) Staros, J. V.; Wright, R. W.; Swingle, D. M., *Analytical Biochemistry* 1986, 156, 220-222.

(41) Hermanson, G. T., *Bioconjugate techniques*. Academic Press: San Diego, 1996; p xxv, 785 p.

(42) Somayaji, V. V.; Sykes, T. R.; Naicker, S. S.; Noujaim, A. A., *Appl. Radiat. Isot.* 1996, 47, 71-77.

(43) Reddi, E.; Jori, G. *Rev. Chem. Intermed*. 1988, 10, 241-268.

(44) Dhami, S.; De Mello, D.; Rumbles, G.; Bishop, S.M. *Photochem. Photobiol*. 1995, 61, 341-346.

(45) Wagner, J.R.; Ali, H.; Langlois, R. ; Brasseur, N. ; Van Lier, J.E. *Photochem. Photobiology*. 1987, 45, 587-594

Chapter 5
The Electrophoretic Behavior of Metal Phthalocyanines and Labeled Complexes Using Capillary Zone Electrophoresis

5.1 Theory of Electrophoresis

In the past few years, capillary electrophoresis (CE) has become a powerful tool among analytical methodologies for highly efficient separations of a variety of complex mixtures including peptides and proteins,[1-5] amino acids,[6-9] and nucleic acids.[10-13] Due to instrumentation simplicity, short separation times, and on-line detection, this technique has demonstrated its use in a wide range of applications such as drug discovery,[14] protein characterization,[15-17]and analysis of pharmaceuticals.[18-20] CE offers several advantages compared to traditional separation techniques including very high separating efficiency because there is no mass transfer between phases; minute sample requirements; and limited consumption of buffer reagents.[21-23] Thus, the benefits of CE make it an ideal system for the selective separation of MPc's and their bio-conjugates. Previously, we examined HPLC (Chapter 3) as the separation platform for analyzing MPc's and biomolecules tagged with Zn4CPc. In this chapter, the potential use of CE is evaluated to determine its suitability as a complementary technique for separating MPc's and MPc conjugates. Separation of the MPc conjugates was achieved with both conventional and microchip CE.

Electrophoresis is defined as the movement of charged analytes that are separated into individual species based on their mass-to-charge ratio as they migrate through a capillary filled with an electrolyte under the influence of an applied electric field. The bulk flow of the liquid electrolytes, referred to as the electroosmotic flow (EOF), drives charged and neutral analytes towards one end of the capillary. In the presence of electrolytes, negatively charged silanol groups attract positively charged counterions creating a layer of tightly bound cations on the

capillary surface due to electrostatic interactions.[24] A second layer, called the diffusional layer, contains cations in solution that move freely due to thermal motion, giving rise to a potential difference (zeta potential) near the capillary surface (Figure 5.1).[24] During separation, because of this "double layer" build-up, the EOF moves all species towards the negative electrode (cathode). Neutral analytes move at the same rate as the EOF, and cations move faster than anions, as depicted in Figure 5.2.

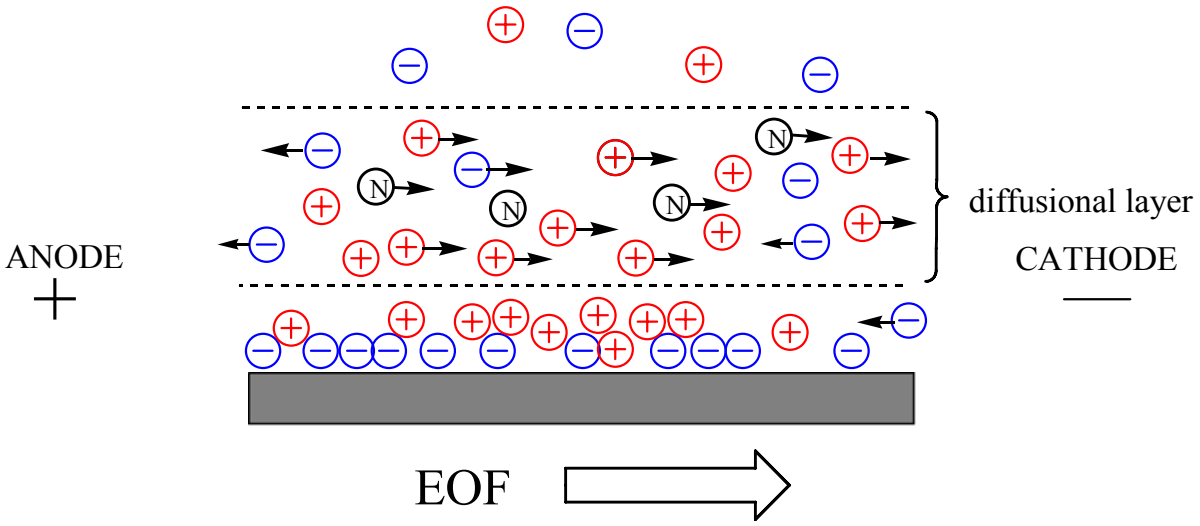

Figure 5.1 Depiction of the formation of a "double layer" near the capillary surface. The direction of the EOF moves all charged species toward the cathode. "N" represents neutral species.

The linear velocity of the EOF is dependent upon the zeta potential and can be calculated by the Helmholtz-von Smoluchowski equation:[23]

$$\nu_{eof} = (\varepsilon\zeta / \eta)E \qquad \textbf{(5.1)}$$

where ν_{eof} is the velocity, ε is the dielectric constant $(C^2 J^{-1} M^{-1})$, ζ is the zeta potential, η is the buffer viscosity $(N\ s\ m^{-1})$ and E is the electric field (Vm^{-1}).[23-25] The velocity of the EOF can be measured by observing the migration time of a neutral marker (i.e. methanol, DMSO), as the neutral analyte would have insignificant interaction with the capillary walls, does not possess an electrophoretic mobility and can be readily detected.[26] Although this approach is simple and the

most common, other approaches for measuring the EOF have been described.[26, 27] Huang et al. described a technique for measuring the EOF that does not require injection or detection of a neutral marker based on the time history of the electrical current during electrophoresis. Altria and coworkers measured the EOF by determining the mass of electrolyte transferred to the outlet over time.[28]

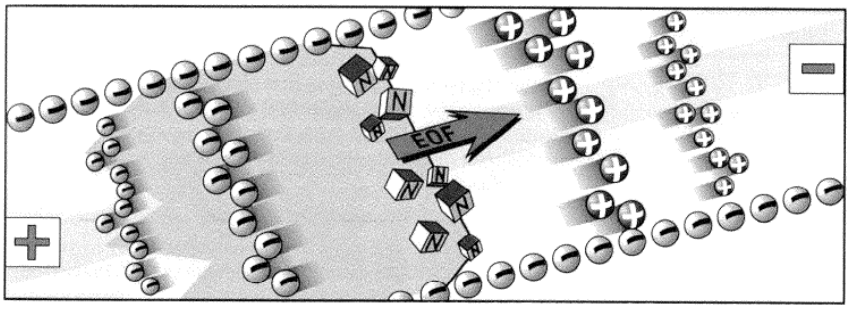

Figure 5.2 Schematic of capillary electrophoresis separation mechanism.[29]

The profile of the EOF is flat, giving a uniform flow through the capillary that contributes to the high separation efficiency and less band broadening due to low dispersion of analyte zones.[24] Figure 5.3 shows the flat profile in CE compared to the laminar flow profile commonly seen in pressure driven separation techniques such as HPLC.

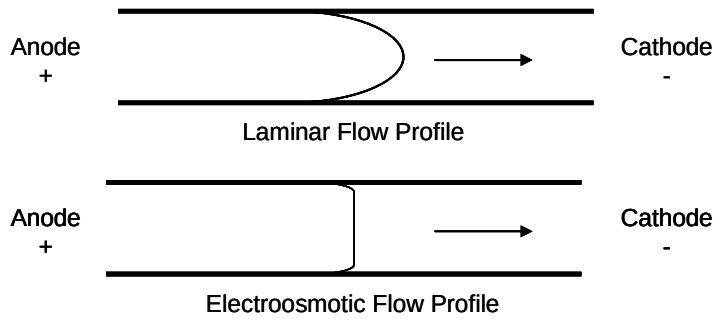

Figure 5.3 Depiction of electroosmotic flow profile compared to laminar flow profile typically seen for other analytical techniques such as HPLC.

Altering the surface charge on the capillary wall (zeta potential) by varying fundamental parameters such as buffer pH, ionic strength, and temperature can affect the direction or rate of the EOF. For example, at basic pH (>7), the silanol groups on the inner wall are ionized, giving

the wall a negative charge, whereas at acidic pH (<7), the capillary wall is uncharged making the dominating force of separation electrophoresis. The use of additives that adsorb to the capillary wall can also result in a decrease or a reverse flow of the EOF.[30-34]

As the EOF drags analytes through the capillary, an electrical force is exerted on the charged species and this force is represented by the equation;

$$F = qE \quad \textbf{(5.2)}$$

where q is the net charge of the molecule and E is the strength of the electric force.
In addition, it experiences a frictional force that pulls the analyte in the opposite direction of its movement. For a spherical ion, this frictional force is proportional to the velocity of the molecule given by;

$$F_f = 6\pi\eta R \quad \textbf{(5.3)}$$

where η is the viscosity of the solution, and R is the ion radius. During electrophoresis, the two forces offset each other and as a result, steady-state conditions are reached. The charged species travel through the capillary at a rate defined as:

$$\mu_e = \frac{q}{F_f} \quad \textbf{(5.4)}$$

where μ_e is the electrophoretic mobility. From the equation, differences in the electrophoretic mobility of molecules are based on properties such as size, shape and charge of the analyte.[21]

The apparent mobility of the ionic species, defined as the time it takes for the analyte to reach the detector, takes into account the influence of the EOF. The relationship between the apparent mobility, μ_{app}, and the actual mobility of the solute, μ, is given by,

$$\mu_{app} = \mu + \mu_{os} \quad \textbf{(5.5)}$$

where μ_{os} is defined as the electroosmotic flow. As a result, the analytes are separated into "zones" based on their different apparent mobility.

A measure of the separation (peak) efficiency is determined based on the number of theoretical plates, N, calculated by;

$$N = 16\frac{t_m}{w_{1/2}} \qquad \textbf{(5.6)}$$

where $w_{1/2}$ is the width at half peak height.

5.1.1 Instrumentation

Instrumentation for CE is simple and easily automated consisting of a capillary column immersed in two buffer vials; one at the cathode end where the sample is injected and the other placed at the anode end where the sample is detected, a high voltage supply, a detector, and data acquisition station. A schematic illustrating the components for a typical CE system is shown in Figure 5.4.

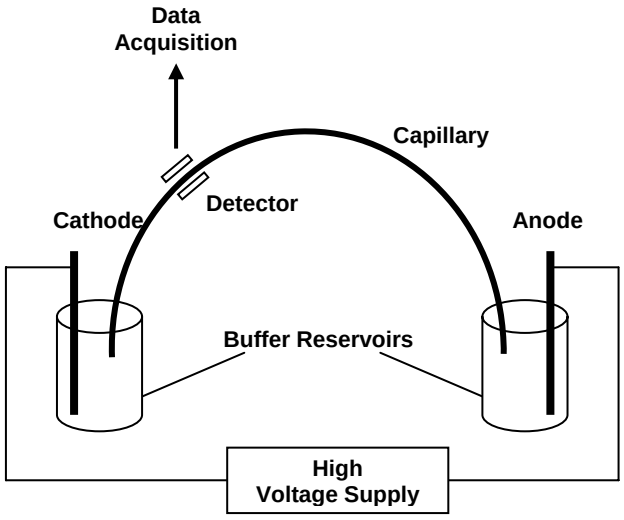

Figure 5.4 Basic components of a CE separation system. A capillary open on both ends are immersed in buffered solutions, across which a high voltage is applied. Detection is performed on-column.

Conventional separation is carried out in a narrow bore fused silica capillary available in a wide range of inner (10 to 200 μm) and outer diameters. Optimal conditions for separations are generally 25-75 μm I.D. and 350-400 μm O.D., however it is worthy to mention here, columns with smaller inner diameters are able to dissipate heat more efficiently due to higher surface-to-volume ratio preventing zone broadening, resulting in higher separation efficiencies.[35] The effective length of the capillary, defined as the length from the point of injection to the point of detection, is generally a large portion of the total length to be able to apply an electric field and decrease the time necessary for capillary conditioning and fraction collection. Reservoirs filled with the buffer also contain the electrodes used to provide electrical contact between the high voltage supply and the capillary. The high voltage is supplied with the use of a DC power supply used to apply up to 30 kV and current levels of 200-300 mA.

For highly efficient and reproducible separations, the sample volume injected must be small in reference to the size of the capillary.[36] Injection of the sample into the capillary is accomplished by hydrodynamic or electrokinetic injection. Hydrodynamic injection, applying a pressure for a certain amount of time driving a small plug of analyte into the capillary while immersed in sample solution, is the most widely used injection mode due to the absence of differences in the injection concentration for ionic species with different electrophoretic mobilities.[37] However, because the flow profile for hydrodynamic injection is parabolic, sample dispersion can occur causing significant band broadening.[21, 37] Generally, the amount of sample injected is less than 2% of the total capillary volume and can be calculated using the Hagen-Poiseuille equation,

$$V_{inj} = \frac{\Delta P d^4 \pi t}{128 \eta L} \qquad \textbf{(5.7)}$$

where ΔP is the change in pressure in the capillary, d is the capillary diameter, t is time, η denotes buffer viscosity, and L is the total capillary length. A sample introduced onto the column by electrokinetic injection is performed by placing the sample solution at the anodic end and applying voltage with a field strength 3 to 5 times lower than the field strength used for separation. Variations with electrokinetic injection may occur because of the different rates the analyte enters the capillary due to differences in mobilities.[36] The injection volume for electrokinetic injection is determined by

$$Q = \frac{(\mu_e + \mu_{eof})V\pi r^2 Ct}{L} \qquad \textbf{(5.8)}$$

where V is the voltage, r is the capillary radius, C is the analyte concentration, *t* represents time and L is the capillary length.[21, 36] For electrokinetic injection, the amount of sample injected is dependent on several parameters. A number of articles in the literature address the influence of the amount of material injected on the separation efficiency.[38-42]

Several detection modes are available for CE separation in which the analytes are detected as they move through the capillary (on-column) or after elution (post-column). For on-column detection, a detection window is created by removing a portion of the capillary coating making it optically transparent enabling detection with high resolution. The most commonly employed detection methods include UV-Vis, fluorescence , and conductivity with UV-V being the most universal detection scheme.

5.1.2 Modes of Separation

Capillary electrophoresis encompasses several separation modes offering versatility and specificity for the relevant application including capillary zone electrophoresis (CZE), micellular electrokinetic chromatography (MEKC), and capillary gel electrophoresis (CGE).[21, 36] In CZE, also referred to as free solution capillary electrophoresis, separation of ionic species are due to the analytes migrating at different velocities creating "zones" (see equations 5.2-5.4). MEKC

separations are based on the hydrophobic/ionic interactions with the micelle.[43] At concentrations above the critical micelle concentration (CMC), micelles are essentially spherical aggregates of surfactants with hydrophobic tails and charged head groups that migrate with or against the EOF.[44, 45] In capillary gel electrophoresis, a cross-linked polymer acts as a "molecular sieve" separating solutes based on size. As molecules move through the polymeric network, migration is reduced for larger molecules compared to smaller species.[36, 46]

5.1.3 Separation of Metal Phthalocyanines (MPc's)

The separation and analysis of Pc's and their metal derivatives has long been a challenge for many researchers due to the isomeric structures that form during ring synthesis.[47-49] The complexity of the mixture along with their notorious insolubility in aqueous solvents makes separation difficult using conventional chromatographic techniques. Reverse-phase liquid chromatography (RP-HPLC) is routinely used for the separation and purification of Pc's and metal complexes.[48, 50, 51] The usefulness of RP-HPLC can be limited, however, due to the similar properties of the structural isomers, aggregation, solubility and the strong tendency to adsorb to the columns' stationary phase.[52] For example, the formation of structural isomers of tetra-butylphthalocyanine posed a problem for Hanack and coworkers in their attempt to completely separate the isomeric mixture using HPLC. They were able to isolate only two of the isomers formed during synthesis.[53] Görlach was able to achieve separation of the structural isomers of 2(3)-tetraalkyloxysubstituted Pc by employing a nitrophenyl stationary phase linked to the silica surface requiring tedious chromatographic procedures.[54]

Recently, CE has proven to be a useful technique for the separation of porphyrin derivatives, which are structurally similar to Pc's and this work has been well documented in the literature.[55-59] Chan reported on the electrophoretic separation of an oligomeric mixture of haematoporphyrin, a photosensitizer used in photodynamic therapy, using free solution capillary

electrophoresis (FSCE). In their studies, complete separation of the mixture was obtained when sodium dodecyl sulfate (SDS) was added to the background electrolyte (BGE). Wu et al demonstrated the selective separation of porphyrin isomers with a differing number of carboxylic side chains using ionic surfactants combined with bovin serum albumin (BSA) reporting better separation was achieved with SDS in the run buffer compared to sodium taurodeoxycholate.[60] A nonaqueous CE system was developed by Bowser for the separation of a complex mixture of porphyrin derivatives found in photofrin.[55] Zhang reported on the complete separation of the free acid forms of porphyrins by FSCE using a variable wavelength epifluorescence microscope as on-column detection.[61]

While a number of studies have been reported on the electrophoretic analysis of porphyrin derivatives, only a few studies have been documented describing the CE analysis of MPc's and no attempts have been made to examine MPc labeled conjugates. Barbosa and coworkers investigated the efficiency of capillary electrophoresis to monitor the purity of sulphonated cobalt (II) phthalocyanine after several purification treatments concluding CE was an adequate analytical method for use in determining the degree of purity.[62] Dixon studied the extent of sulphonation for several MPc's by capillary electrophoresis in conjunction with mass spectrometry at pH 6 and 9 with better separation achieved at higher pH.[63] Peng and coworkers reported on the optimization of several experimental conditions such as buffer pH, additives, and organic solvents for the separation of porphyrin and phthalocyanine regioisomers with laser-induced fluorescence detection.[52] Despite these reports, the affect of critical factors on the electrophoretic mobility of MPc's such as the central metal, degree of peripheral substitution, and solubility in aqueous media have not been extensively investigated. These factors become very important when using MPc's as fluorescent probes for applications such as DNA sequencing or genotyping.

In this report, FSCE was used to examine the electrophoretic behavior of several MPc's (M = Zn, Al, and Ga) bearing 4 to 16 carboxylic acid groups and the separation efficiency with the use of a binary solvent system with organic media. Physical parameters that can affect separation efficiency such as molecular structure and electronegativity of the metal ion will be considered. The migration behavior of insulin chain B, used here as a model peptide conjugated to Zn4CPc, was also determined. In addition, the separation of native peptides generated from trypsin digested with β-casein and then covalently labeled with Zn4CPc was also examined.

5.1.4 Electrophoresis Considerations of MPc's

5.1.4.1 Role of Metal

Several modeling approaches have been developed in an attempt to understand the relationship between the structure and mobility of a metal complex. So far, these approaches are mathematical interpretations using multivariate regression techniques. Timerbaev suggested that for any metal complex, the identity of the metal does not play a significant role in the electrophoretic mobility. For our studies, the metal ion does not significantly alter the overall charge of the complex. The nature of the axial ligand complexed to the metal atom will also change the migration rate as a result of the electron charge density distribution of the complex.[64]

5.1.4.2 Role of peripheral groups

A varying number of ionizable groups substituted on the periphery of MPc's can alter the electrophoretic mobility based on differences in the net charge as well as the degree of water solubility. Generally, under normal polarity and alkaline conditions, complexes carrying an increasing number of anionic substituents will migrate to the detector slower resulting in a higher electrophoretic mobility, whereas for cationic moieties, the observed migration rate is reversed.[58] Reports have been published comparing the electrophoretic mobility of several complexes with a varying number of charged substituents. For example, Schofield and coworkers reported on the

use of CZE to separate a mixture of sulphonated zinc phthalocyanine according to the degree of substitution.[65] An increasing number of sulphonate groups resulted in multiple peaks partially resolved. The authors suggested that with direct sulphonation, there are four positions on the benzene ring substituents can reside and sulphonate groups in the 3 position on the benzene ring resulted in increased hydrophobic interaction with the nitrogen groups located on the chromophore producing a variation in the charge distribution accounting for the multiple peaks observed in the electropherogram.[65] Weinberger illustrated the separation of urinary porphyrins possessing two to eight carboxylic acid groups exploring the effect of biological fluids on the separation efficiency using FSCE and MEKC. The authors concluded the use of MEKC with the presence of an anionic surfactant was found to provide better separation by controlling the adsorption of the porphyrins on the capillary wall.[66]

5.1.4.3 Aggregation Effects of MPc's (buffer issues)

Peripheral substitution with ionizable groups such as carboxyl groups improves the solubility of MPc's, in aqueous solvents, however the propensity to form ground state aggregates remains an issue in CZE causing decrease in separation efficiency, distorted peak shapes, and reduced plate counts due to band broadening.[55, 67 68] Several parameters such as ionic strength and buffer pH can contribute to the degree of aggregation.[62] One experimental approach that has proven to minimize aggregation is the addition of organic modifiers to the carrier electrolyte increasing the solubility of hydrophobic molecules.[68-73] Other advantages to using organic modifiers in the carrier electrolyte include increases in separation selectivity and efficiency due to differences in dielectric constants and solvent viscosity; the use of high separation voltages due to lower dielectric constants producing higher field strengths for rapid analysis times, and less Joule heating.[68] A fundamental understanding of these changes was published in recent reviews presented by Huie and coworkers,[72] Fillet,[74]and Steiner.[75] Our group recently reported

that an increase in pH plays an effective role in minimizing the mechanism for aggregation of MPc's in aqueous solvents (see Chapter 2).

5.2 Experimental

5.2.1 Materials and Methods

Carboxylate substituted MPc dyes (Zn*x*CPc, where *x* = 4, 8, and 16; Al4CPc, and Ga4CPc) were synthesized in-house by Serhii Pakhomov in collaboration with Dr. Hammer's laboratory. Detailed information on the synthesis is provided elsewhere.[76] Alexa Fluor 680 was purchased from Molecular Probes (Carlsbad, CA). Dimethyl sulfoxide (DMSO), 4-(2-Hydroxyethyl) piperazine 1-ethanesulfonic acid (HEPES), and streptavidin were purchased from Sigma-Aldrich (St. Louis, MO). HPLC grade methanol, insulin chain B, β-casein, iodoacetamide, and ammonium bicarbonate were also purchased from Sigma-Aldrich (St. Louis, MO). Dithiothreitol (DTT), boric acid, and 3-cyclohexylamino-1 propanesulfonic acid (CAPS) were purchased from Fluka (St. Louis, MO). Modified trypsin solution was purchased from Promega (Madison, WI). Deionized water (18 MΩ) was provided in house (Nanopure filtration system, Barnstead, Chicago, IL). Sephadex LH-20 was purchased for GE Healthcare (Piscataway, NJ). The buffer solutions were 40 mM borate, pH 9, and 10 mM CAPS, pH 11. Buffer solutions were prepared by dissolving the acid in deionized water and adjusting the pH with 1 M NaOH measured with a pH meter model 410 (Thermo, Waltham, MA). The buffer was then filtered with a 0.22 μm pore size filter prior to use. BGE were prepared by increasing the amount of methanol (20% to 80%) added to the buffer solutions. MPc's were dissolved in the running buffer at concentrations in the range of 1μM to 10 μM. Zn4CPc labeled insulin chain B was prepared by dissolving the peptide in HEPES buffer, pH 8 (1×10^{-5} M) and adding enough dye solution to produce a 10-fold molar excess of Zn4CPc. The reaction was incubated overnight at room temperature in the dark. Zn4CPc and Alexa Fluor dyes were covalently

labeled with streptavidin at a dye/protein ratio of 15:1 at room temperature in 500 μL reaction solutions as follows: 1 μM protein (dissolved in 0.1 M HEPES) was reacted with 150 μM dye dissolved in DMSO. After the reaction was incubated overnight, the mixture was purified using Sephadex LH-20 and dissolved in HEPES buffer.

The digestion of β-casein was performed using a procedure modified from Pierce.[55] Briefly, β-casein (1.0 μg – 10 μg, 10 μL) was incubated with 15 μL of ammonium bicarbonate (50 mM) and DTT (100 mM) for 5 min at 95°C. Iodoacetamide (3 μL) was added to the β-casein solution and incubated in the dark for 20 min. Modified trypsin was added (5 μL) and incubated at 37°C for 10 h. A molar excess of Zn4CPc-NHS (15:1) was added to the peptides and the reaction mixture was incubated overnight at room temperature.

5.2.2 Instrumentation

5.2.2.1 Capillary Electrophoresis

CZE was performed on an Agilent 3D capillary electrophoresis system (Agilent, Foster City, CA). The system was equipped with UV-Vis photodiode array detection. Analysis of the separations was performed using ChemStation software provided by Agilent Technologies. A polyimide coated silica capillary column, 75 μm i.d., 375 μm o.d. (Polymicro, Phoenix, AZ) was cut to a length of 50 cm and a detection window was created by burning a small portion of the polyimide coating using a flame. The capillary column was rinsed with 1.0 M NaOH for 1 h followed by a 2 h wash with deionized water. The column was then equilibrated with the BGE for 30 min, consisting of methanol/borate buffer at pH 9.0. The sample was introduced by electrokinetic injection at 15 kV for 5 s. The separations were performed at a voltage set at 30 kV and a column temperature of 24°C. Normal polarity was used for the separation of the MPc's. Between each run, the capillary was equilibrated with the BGE for 20 min. Because

MPc's have strong absorption in the UV region of the spectrum, the diode array detector was set to 260 nm and 345 nm.

Microchip electrophoresis of streptavidin labeled with Alexa Fluor 680 and Zn4CPc was carried out with a laser-induced fluorescence (LIF) system that was constructed in-house. Briefly, a helium-neon laser source (NT 54-151, Edmund Industrial Optics, Barrington, NJ) provided an excitation wavelength of 633 nm, which was filtered using a line filter (XF-1026, Omega, Brattleboro, VT) before it was reflected off a dichroic mirror (XF-2022, Omega) into a 40X objective (Melles Griot, Zevenaar, the Netherlands). The objective focused the laser beam into the microchannel positioned on an x-y-z translational stage. Emission from dye-labeled streptavidin was collected by the same objective, passed through the dichroic mirror and an emission band pass filter (XF-3030, Omega) before it impinged onto a photomultiplier tube (RT-1508, Hamamatsu, San Jose, CA), which transduced the photon events. A pulse converter (TB-01, HORIBA Jobin Yvon Inc., Edison, NJ) was used to shape the output prior to the data being processed by an I/O card (CB-68 LP) and a PCI board (PCI-6601) both from National Instruments (Austin, TX).

Voltage was applied using a high voltage power supply (EMCO, Sutter Creek, CA) via 0.3 mm diameter platinum wires (Scientific Instrument Services, Ringoes, NJ), which was used to make electrical contact with the fluid reservoirs of the microchip. The power supply and associated relays were controlled by an analog output (D/A) card (PCI-DDA04/12, National Instruments) of the computer. Voltages and data acquisition were controlled by in-house written LabView software (National Instruments). During separation, the buffer was pre-electrophoresed for 5 min at 250 V/cm through the separation channel. The separation channel was 11 cm in length with channel dimensions of 20 μm in width and 120 μm in depth. The samples were loaded by applying 250 V/cm across the injection channel for 50 s and the separations were run

at 150 V/cm. Pull Back voltages were applied to prevent sample leakage in to the injection cross. Laser-inducted fluorescence detection was measured at an excitation wavelength of 633 nm.

5.3 Results and Discussion

5.3.1 Electrophoretic Separation of MPc's

5.3.1.1 Effect of Metal Center of Mobility

Figure 5.5 illustrates the structure of the MPc's studied in this report, having 4, 8, or 16 carboxylic acids as substituents around the periphery.

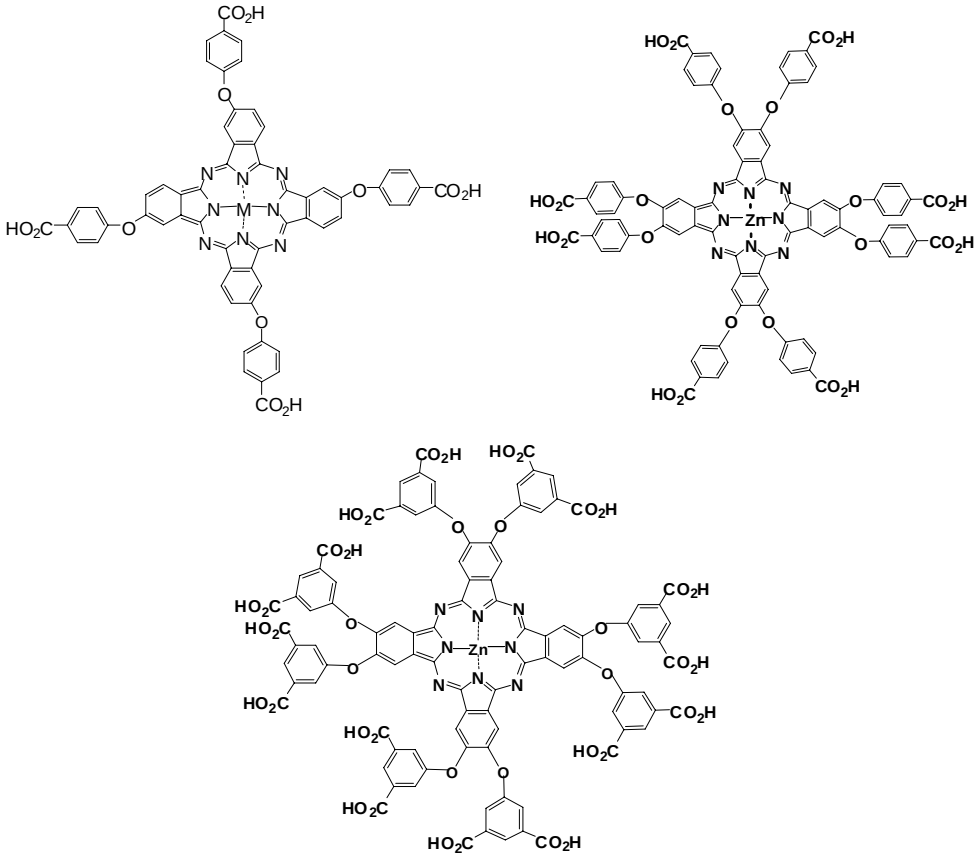

Figure 5.5 Structure of MPc with carboxylic acid functional groups substituted on the periphery of the macrocycle. M = Zn, Al, and Ga.

To examine the influence of the metal ion on the electrophoretic mobility, conventional free solution CE was performed on Al4CPc, Ga4CPc, and Zn4CPc. Figure 5.6 shows the

electropherograms of Zn4CPc, Ga4CPc, and Al4CPc, which possessed migration times of 10.1 min, 10.3 min, and 10.6 min, respectively. The electrophoretic analysis was performed with 80% methanol in the BGE to reduce aggregation and increase the solubility of the MPc's. Figure 5.6 shows a single peak indicating the MPc dyes exist in the monomeric state. The electrophoretic mobilities for Zn4CPc, Al4CPc, and Ga4CPc were calculated using DMSO as a neutral marker to determine the μ_{os} and are presented in Table 5.1. Zn4CPc and Ga4CPc have an electrophoretic mobility of -1.01×10^{-4} $cm^2V^{-1}s^{-1}$ and -1.03×10^{-4} $cm^2V^{-1}s^{-1}$, while the electrophoretic mobility for Al4CPc was slightly increased at -1.07×10^{-4} $cm^2V^{-1}s^{-1}$.

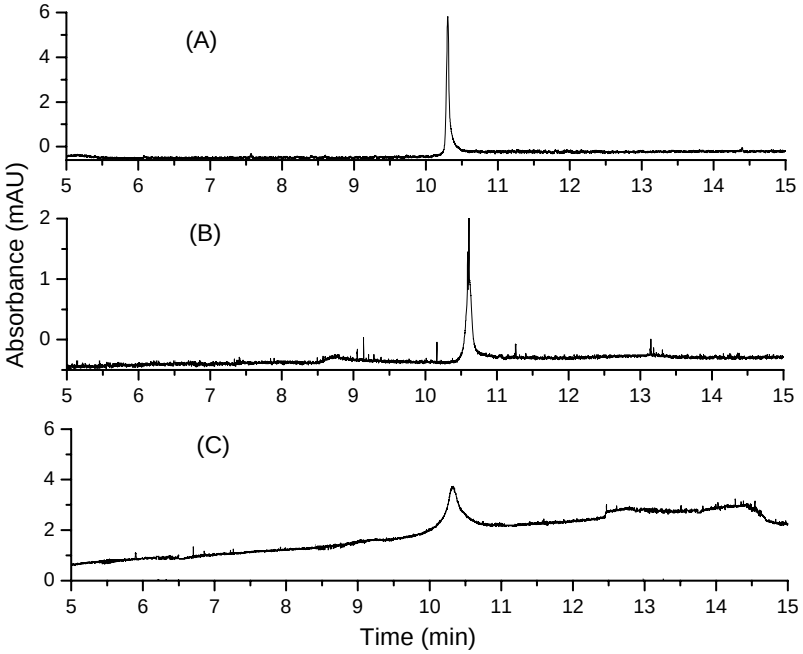

Figure 5.6 CZE separation of (A) Zn4CPc, (B) Al4CPc, and (C) Ga4CPc in 80/20 methanol/borate buffer, pH 9. Separation was performed in a bare silica capillary column, 75 μm i.d., 375 μm o.d. with a total effective length of 40 cm, field strength = 300 V/cm. Samples were introduced using electrokinetic injection at 10 kV for 5 s. UV-Vis detection was monitored at 260 nm. Dye concentrations: Zn4CPc: 1×10^{-5} M, Al4CPc: 1×10^{-6} M, Ga4CPc: 1×10^{-6} M

Results from a previous study suggested Al4CPc possessed an –OH axial ligand, which may account for the slight decrease in the electrophoretic mobility of Al4CPc attributed to the deprotonation of the –OH ligand at high pH. A second factor is the valence of the central metal

ion. While Zn has a valence of +2, Ga and Al are trivalent. The charge of this macrocycle is -2 and thus the Zn complex will have a net charge of neutral with Al4CPc and Ga4CPc having a net charge of +1. However, it seems that the central metal ion has a negligible effect on the electrophoretic mobility, except in cases where an axial ligand may be present.[64, 77, 78]

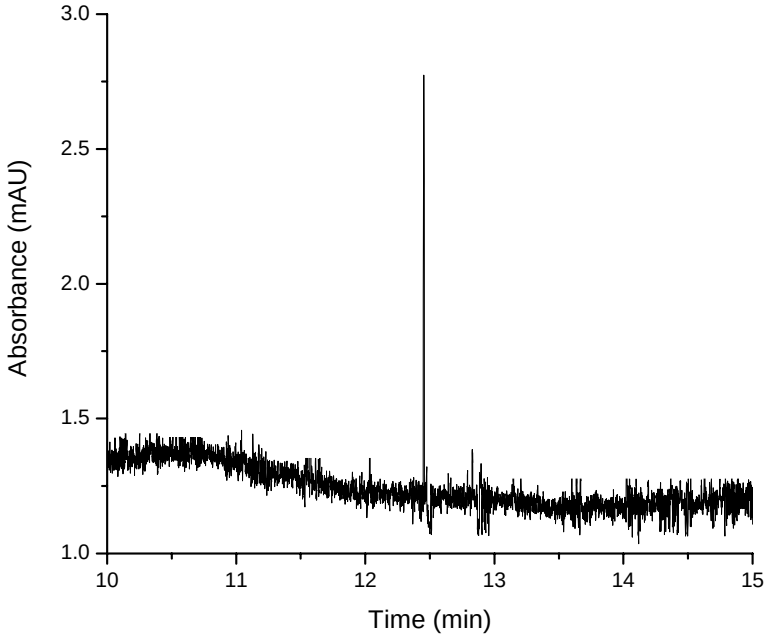

Figure 5.7 CZE separation of Zn8CPc dye with a migration time of 12.47 min. Separation conditions were the same as those used in Figure 5.6. The dye concentration was 2.0 x 10^{-6} M with detection at 345 nm.

5.3.1.2 Effect of Peripheral Groups on Mobility

We have incorporated carboxylic acid groups around the MPc ring to increase water solubility and at pH 9, MPc's exist predominately as negative ions resulting from the deprotonation of the acid groups. Under normal polarity, MPc's with a greater number of carboxylic acid groups should migrate to the detector later and possess a higher electrophoretic mobility due to the increase in negative charge.[79] This trend was observed for the ZnxCPc series with varying degrees of carboxylation. Figure 5.7 shows the electropherogram for Zn8CPc dye, with a migration time of 12.47 min. Shown in Figure 5.8 is the electropherogram

for Zn16Pc with a migration time of 16.39 min. The electrophoretic mobilities for Zn8CPc and Zn16CPc were calculated to be 1.33×10^{-4} and 1.45×10^{-4}, respectively (see Table 1). With Zn16CPc bearing twice the number of carboxylic acid groups, we would expect to see a larger difference in the mobility of Zn8CPc and Zn16CPc. The close similarity in the electrophoretic mobility for Zn8CPc and Zn16CPc can be due to the presence of protonated carboxylic acid groups (pKa range from 3.5 to 8.5) accompanied with an increase in size decreasing the mobility.[79] Studies reporting the electrophoretic analysis of porphyrins with a different number of carboxylic side chains at high pH obtained similar results.[79] The authors found that porphyrins with eight carboxylic acid side chains migrated last and porphyrins substituted with only four carboxylic acid groups had the highest mobility.

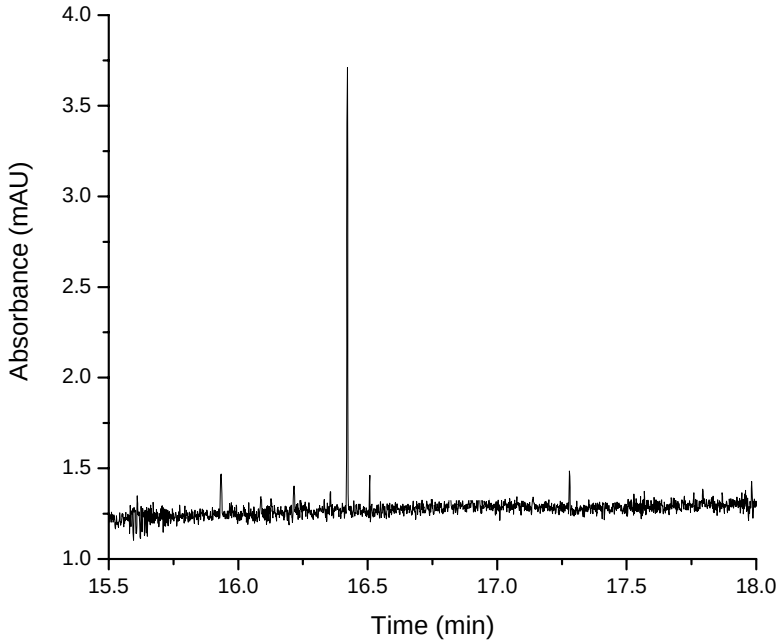

Figure 5.8 Electropherogram of Zn16CPc with a migration time of 16.39 min. Detection was accomplished with UV detection at 340 nm. Dye concentration: 10^{-6} M.

Separation efficiency of the MPc's was determined by calculating the number of theoretical plates using the following equation;

$$N = 5.5(\frac{t_r}{w_{1/2}})^2 \qquad \textbf{5.8}$$

where, t_r is the migration time and $w_{1/2}$ is the peak width at half height. The electrophoretic mobility of the MPc's, along with the theoretical plates and relative standard deviations (RSD) were calculated and the results are summarized in Table 1. The plate count generated was over 100,000 for Zn16CPc having the highest number of theoretical plates. The plate numbers were found to increase as the number of carboxylic acids increase for the ZnPc series and the plate numbers for Ga4CPc and Al4CPc calculated to be much lower resulting from poorer solubility in the CZE buffer.

Table 5.1 Electrophoretic mobility, theoretical plates, and standard deviation for the native MPc's studied. All dyes were dissolved in the running buffer at concentration of 10^{-6} M.

Dye (MPc)	Migration Time (min)	Theoretical Plates	μ_e (cm^2/VS)	%RSD n = 5
Zn4CPc	10.3	495,883	1.01×10^{-4}	4.4
Zn8CPc	12.47	528,325	1.33×10^{-4}	4.4
Zn16CPc	16.39	648,327	1.49×10^{-4}	4.3
Ga4CPc	10.3	119,867	1.01×10^{-4}	4.5
Al4CPc	10.6	126,118	1.07×10^{-4}	4.6

5.3.1.3 Effect of Aggregation on Mobility (carrier electrolyte selection)

The aggregation behavior of Pc's in aqueous solution is well-known and the degree of aggregation is largely dependent on the electrolyte concentration.[80, 81] In an attempt to evaluate the effect of electrolyte on the aggregation of MPc's, we examined the absorption properties and the electrophoretic analysis of Zn4CPc in the presence of NaCl, added at increased molar concentrations to the dye solution. The concentration of Zn4CPc was kept constant (1 μM) to ensure the dye exists in the monomeric form before the addition of NaCl. Figure 5.9 shows the absorption spectra of Zn4CPc dissolved in 80/20 methanol/borate solvent mixture with the

addition of NaCl. Zn4CPc has an absorption maxima of 677 nm in this solvent mixture with no NaCl added. Introducing NaCl to the solution resulted in a decrease of the monomer peak at 677 nm and an increase in a new peak blue-shifted to 640 nm due to J-aggregate formation.[82] The enhancement of aggregation is due to an increase in the solvent dielectric constant reducing the π-electron repulsion between two dye molecules known as the "salt effect". [80, 83]

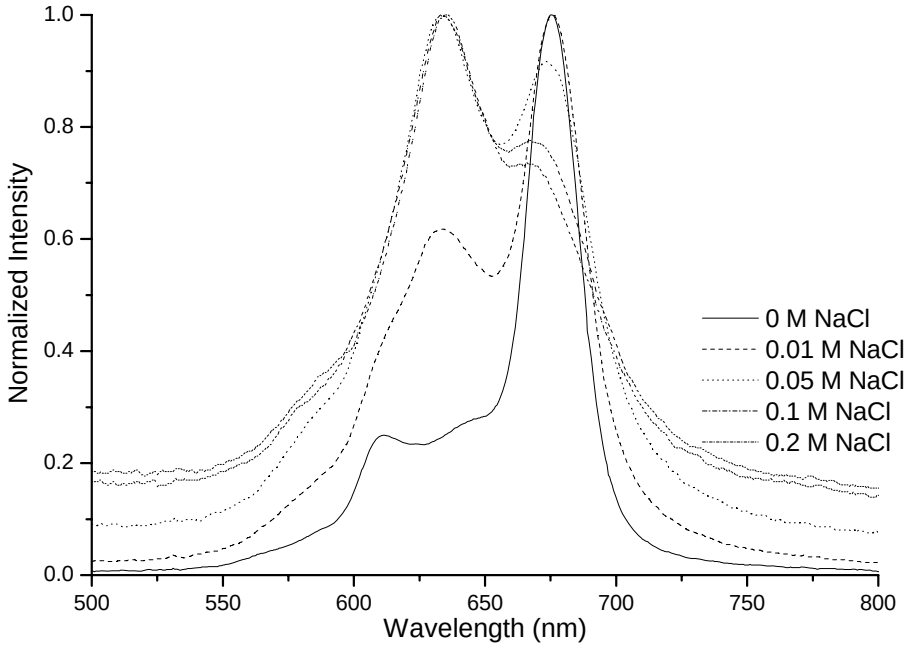

Figure 5.9 Effect of NaCl on the absorption spectra of Zn4CPc in 80/20 methanol/borate mixture. An increase in electrolyte concentration increases aggregation by the increase appearance of an aggregate peak at 640 nm.

Figure 5.10 shows the effect of increased salt concentration on the electrophoretic performance of Zn4CPc. The electropherogram exhibited two sharp peaks with migration times of 4.1 and 10.3 min, respectively, and a broad peak at 7.2 min. At 0.05 M NaCl, monomeric dye peak previously identified as peak **3** is still present in solution also seen in the absorption profile (Figure 5.10 A). As the amount of salt increases, the monomer peak disappears and peaks **1** and **2** increase in absorbance intensity. At 0.2 M NaCl, band broadening of peak **2** worsens due to significant aggregation at this moderately high concentration of salt present in solution.[84]

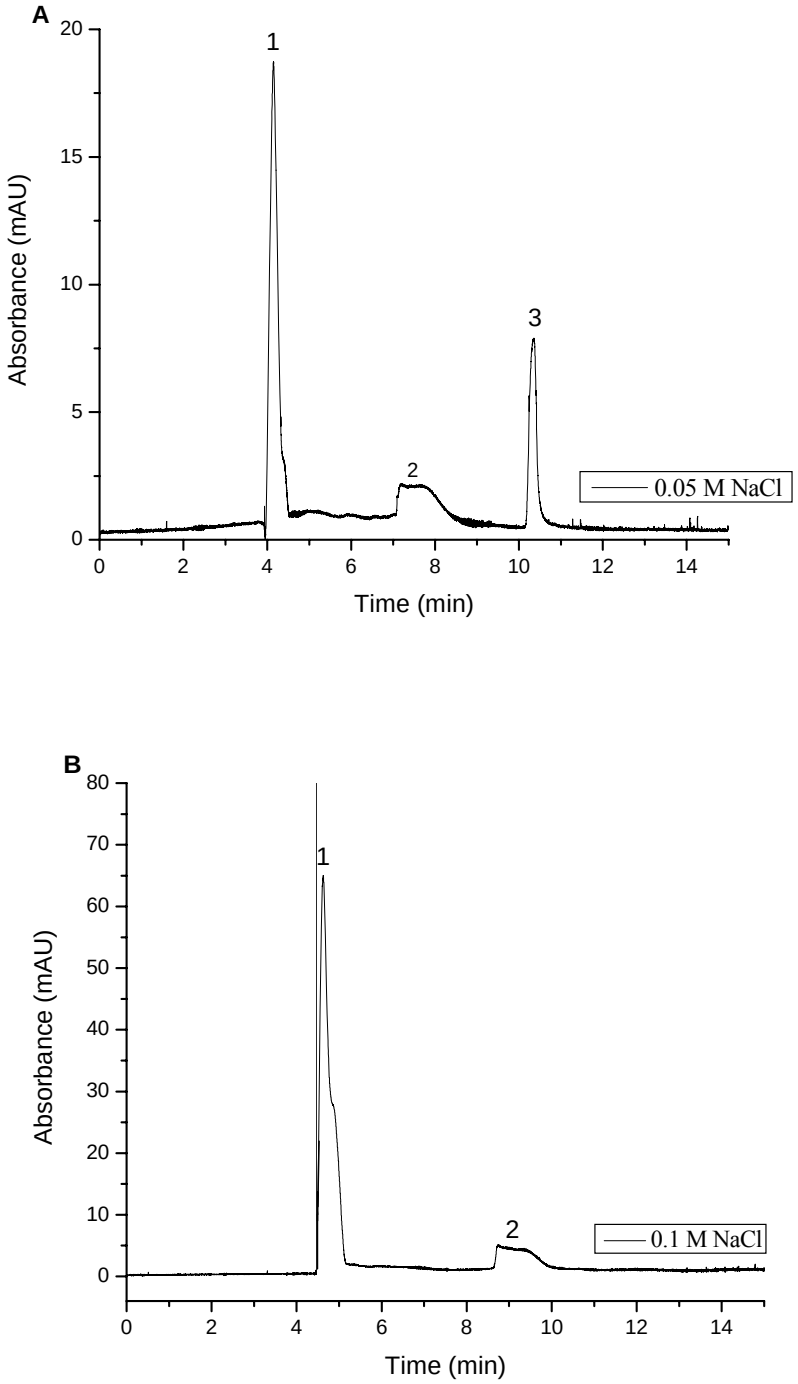

Figure 5.10 Effect of the presence of salt on the CE separation of Zn4CPc. Carrier electrolyte: 40 mM borate buffer, pH 9. Salt concentration: 0.05 M NaCl (A), 0.1 M NaCl (B), and 0.2 M NaCl (C).

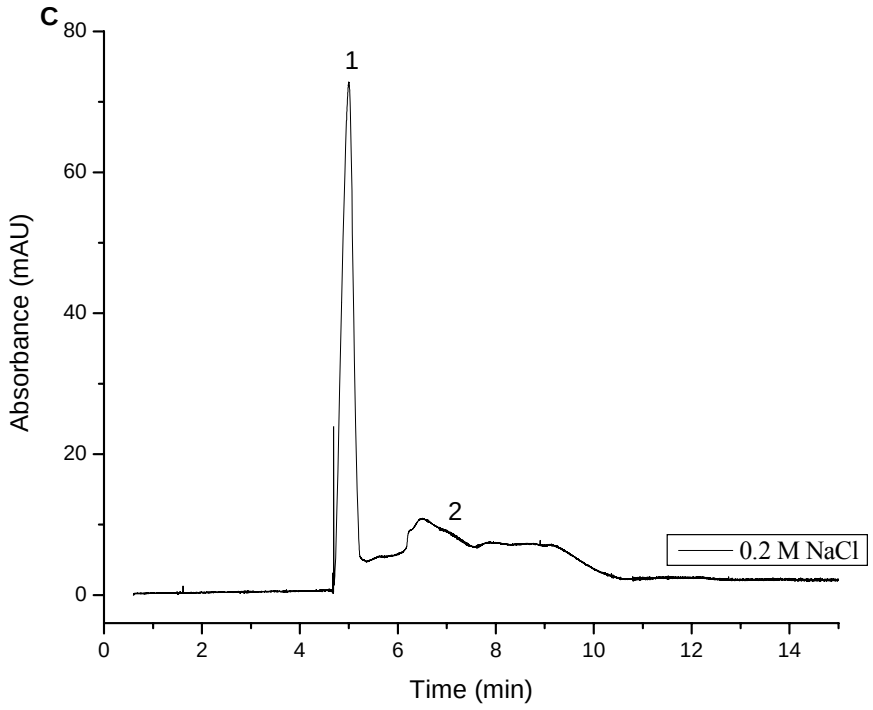

Figure 5.10 continued

It is worth noting that as you increase the salt content, the migration times for the monomer increased from 4.1 min to 5.0 min for peak **1** and 7.1 to 9 min for peak **2.** At higher salt concentrations, the migration times increase resulting from a decrease in the effective charge of the analyte due to increase shielding effect.[84, 85] In addition, a higher salt content compresses the double layer and decreases the EOF, which will increase the apparent mobility of Zn4CPc. Ding and coworkers studied the electrophoretic mobility of inorganic and organic anions containing various salts at high concentrations. Sufficient separation of the analyte was possible if the buffer electrolyte contained three times the amount of salt than the analyte solution. [84]

5.3.1.4 Effect of Methanol Concentration

It has previously been shown the use of pure aqueous running buffers for the separation of cationic tricarbocyanine dyes resulted in poor separation efficiency due to extensive aggregation in water.[68] The use of organic modifiers in the BGE enhances separation selectivity

of hydrophobic complexes by changing the magnitude of the EOF, reducing current in the capillary resulting in less joule heating and increasing the resolution.[68, 86 71] The influence of methanol in a mixed organic/aqueous buffer system on the electrophoresis of Zn4CPc was evaluated. Methanol was chosen as the organic modifier to enhance the solubility of MPc's by decreasing aggregation. In Figure 5.11, the electropherogram of Zn4CPc electrophoresed with 60/40 methanol/borate solvent mixture is shown.

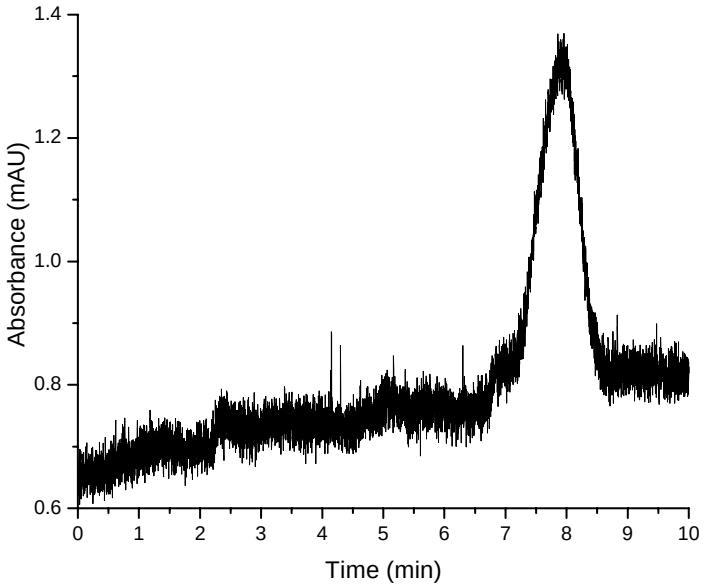

Figure 5.11 Electrophoretic analysis of Zn4CPc separation in 60/40 methanol/borate running buffer at pH 9. Sample concentration: 1×10^{-5} M. Detection was monitored at wavelength of 260 nm. Other separation conditions are given in Figure 5.6.

As can be seen, the migration time decreased to 7.8 min compared to 10.3 min in 80% methanol. The mobility of Zn4CPc continued to decrease to a migration time of 4.6 min as the water content increased as shown in Figure 5.12. At lower percentages of methanol, the results were poor due to the insolubility of Zn4CPc. Figure 5.13 shows the apparent mobility of Zn4CPc as a function of methanol content in the carrier buffer. The decrease in migration time for Zn4CPc with increasing water content is likely due to the changes in the solvent viscosity and solvation

properties of Zn4CPc.[68, 87] The EOF, which contributes to the migration time of the analyte, is also increased as the amount of water content increases, generating a shorter separation path for the analyte.

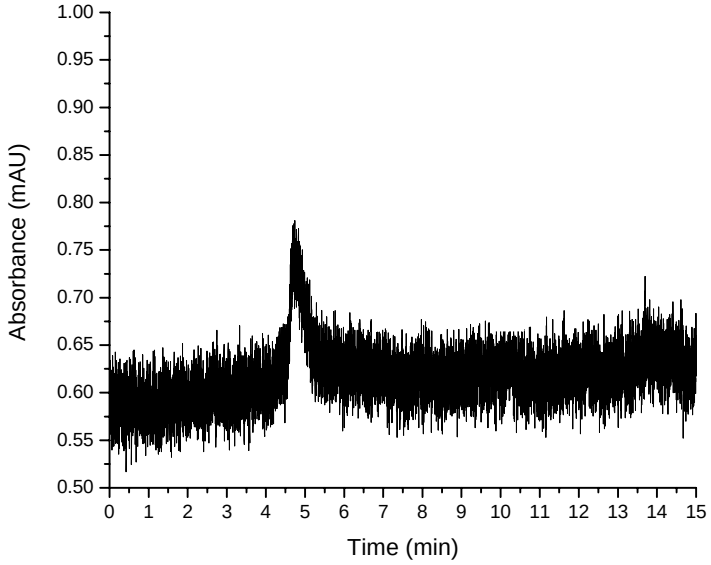

Figure 5.12 Electropherogram of Zn4CPc obtained in 20/80 methanol/borate running buffer. Conditions: 50 cm capillary; 40 mM borate buffer (pH 9).

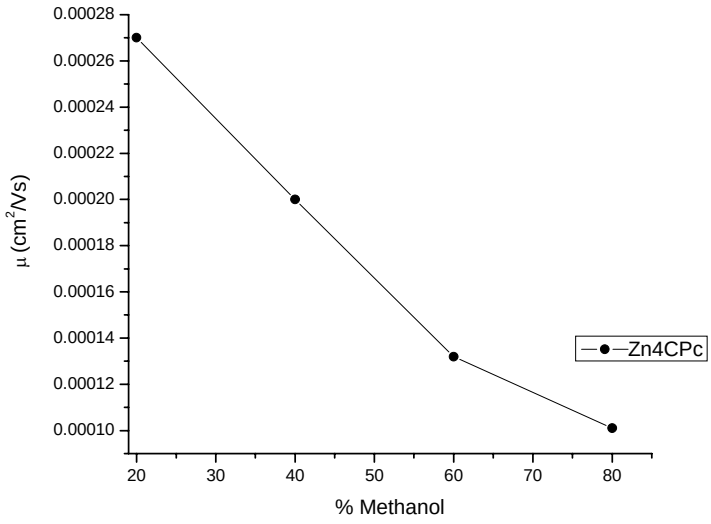

Figure 5.13 Apparent mobilities of Zn4CPc as a function of the methanol content in the BGE. The CZE conditions are described in the experimental section.

At higher percentages of methanol, separation was not obtained resulting from much longer migration times due to the increase in methanol in the running buffer.

5.3.1.5 Effect of pH

The effect of pH on the electrophoretic mobility of Zn4CPc was briefly examined. Shown in Figure 5.14 is the electrophoretic analysis of Zn4CPc separated in CAPS at pH 11. The migration time remained unchanged at pH 11 compared to pH 9. At pH 11, both the silanol groups on the capillary wall and the carboxylic acid groups are deprotonated, therefore, little change of the EOF should occur. However, peak fronting is observed likely as a result of poor solubility of Zn4CPc

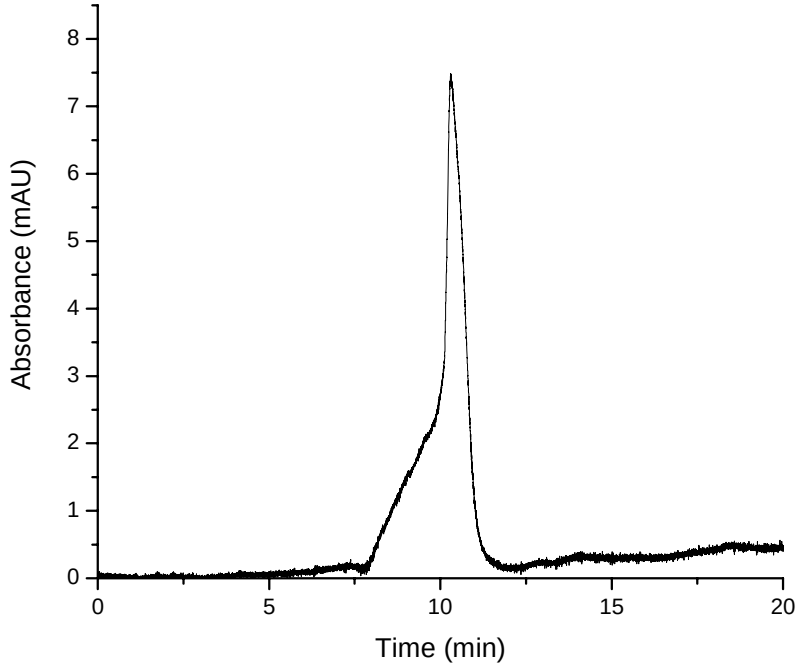

Figure 5.14 Effect of pH on the CZE of Zn4CPc. The running buffer consisted of 80/20 methanol/CAPS at pH 11. Dye concentration: 3×10^{-5} M. Other experimental separation conditions are described in Figure 5.6.

5.3.2 Electrophoretic Separation of Labeled Insulin Chain B and Digested β-casein

To investigate the use of CZE for the analysis of MPc-labeled peptides, the electrophoretic behavior of insulin chain B and tryptic-digested β-casein previously labeled with Zn4CPc was evaluated. While Zn8CPc and Zn16CPc could be viewed as better fluorophores due to increased solubility in buffered media, Zn4CPc was used for labeling in these studies due to ease of purification and quantification of the conjugate (see chapter 2). Insulin is a small globular protein comprised of two chains, A and B.[89] Insulin chain B is a peptide made up of 30 amino acids consisting of a hydrophobic core due to the presence of carbon rich amino acids. It has two primary amine groups, phenylalanine at the η-terminus and lysine at the C-terminus, that are available sites for fluorescent labeling.[89, 90] The amino acid sequence of insulin chain B is given in Figure 5.16.

α-Phe-Val-Asn-Gln-His-Leu-Cys-Gly-Ser-His-Leu-Val-Glu-Ala-
Leu-Tyr-Leu-Val-Cys-Gly-Arg-Gly-Phe-Phe- Tyr-Thr-Pro-Lys-ε

Figure 5.15 Amino acid residue sequence of insulin chain B with one N-terminal primary amine and one ε primary amine on the lysine residue available for labeling.

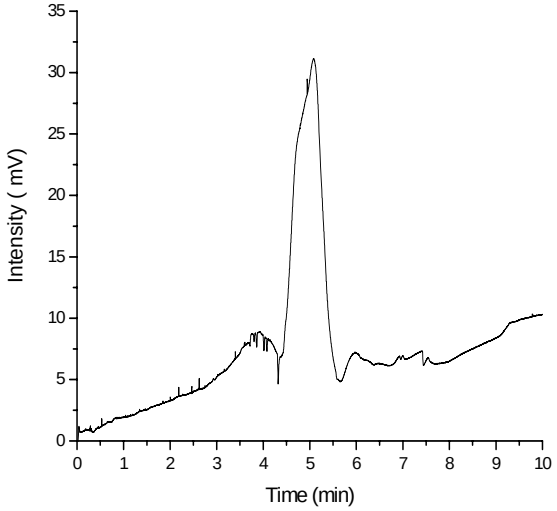

Figure 5.16 Electropherogram of insulin chain B dissolved in HEPES pH 8 at a sample concentration of 1 mM. Detection was monitored at a wavelength of 260 nm using a photodiode array (PDA).

The electropherogram for insulin chain B showed a single peak with a migration time of 5.2 min (Figure 5.16). The electropherogram of labeled insulin chain B is represented in Figure 5.17. Modification of insulin chain B with Zn4CPc-NHS afforded a reaction mixture containing a number of possible conjugation products due to labeling of two primary amine groups with several of the four binding sites on Zn4CPc-NHS. Electrophoresis of the reaction showed several peaks with migration times between 20 and 25 min and a minor peak **1** previously identified as unreacted Zn4CPc. Peaks **2-4** and **5-7** can be identified as multi-substituted insulin chain B of both amine groups. Specifically, the reaction may contain a mixture of monosubstituted, di- and trisubstituted insulin chain B possessing different migration times because of the difference in charge of the Zn4CPc conjugate.

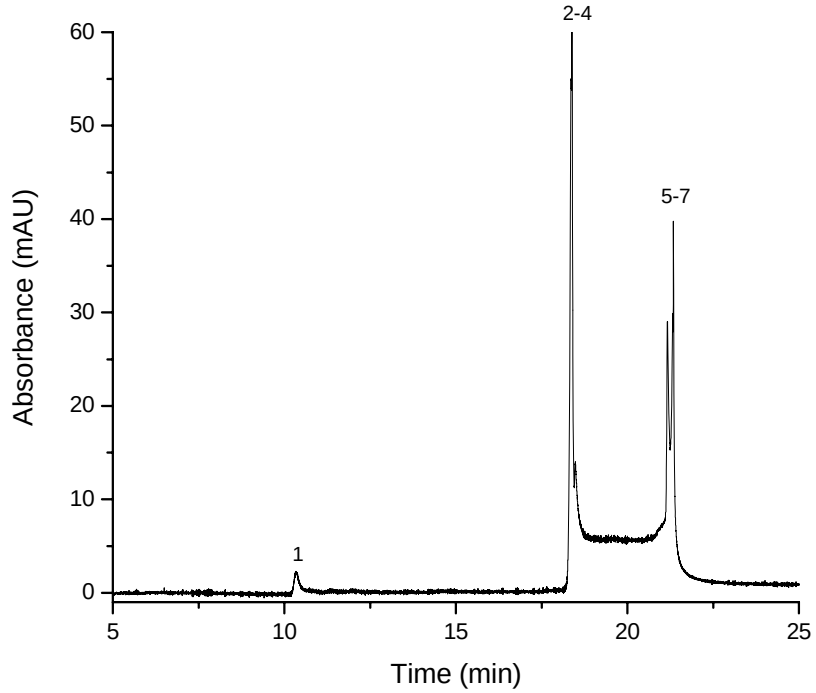

Figure 5.17 Free solution electropherogram of insulin chain B conjugated to Zn4CPc. The amount of dye used was a 10-fold molar excess over the peptide. Sample was injected using electrokinetic injection for 5 sec. UV detection was monitored at 340 nm. The conjugate reaction mixture was purified using sephadex LH-20 prior to electrophoresis.

Zn4CPc modified with several insulin chain B molecules is expected to migrate last due to the increase in negative charge and size of the conjugate.

CZE separation of the peptide fragments produced from tryptic-digested β-casein labeled with Zn4CPc was also evaluated. β-casein, a phosphoprotein (23 kDa), was used here as a model protein because its peptide map has been well identified when digested with trypsin.[91] Trypsin is a proteolytic enzyme, which cleaves proteins at arginine and lysine residues generating peptide fragments of different molecular weights.[91] The sequence of peptide fragments are listed in Table 5.2.

Table 5.2 Sequence of theoretical tryptic peptides for β-casein.

Fragment no.	Sequence of Tryptic Peptide Fragment
1	R
2	K
3	VK
4	INK
5	SVLSLSQSK
6	AVPYPQR
7	IEK
8	HK
9	VLPVPQK
10	GPFPIIV
11	IHPFAQTQSLVXPFPGPIPNSLPQNIPPLTQTPVVVPPFLQPEVMGVSK
12	EAMAPK
13	EMPFPK
14	DMPIQAFLLYQEPVLGPVR
15	YPVEPFTESQSLTLTDVENLHLPLPLLQSWMHQPHQPLPPTVMFPPQ
16	FQSEEQQQTEDELQDK
17	ELEELNVPGEIVESLSSESSITR

Tryptic digestion of β-casein and peptide mapping using CZE has been previously reported.[91, 92] The electrophoresis of Zn4CPc labeled β-casein prior to digestion is shown in Figure 5.17. The CZE analysis of the tryptic digest of β-casein before and after labeling with Zn4CPc is represented in Figure 5.18 with a blow-up representation of several regions shown in

Figure 5.19. The migration of the peptide fragments was directly related to the net charge of the analyte. At pH 9, positive and negative charged peptides exist in the mixture. Based on the calculated charges at this pH, the migration of the peptide fragments can be predicted. The numbered peaks in the electropherogram refer to the fragment number listed in Table 5.2. All peaks can be identified in the electropherogram corresponding to the expected tryptic fragments. Several peaks exhibited shifts to a longer migration time for the labeled peptide fragments due to the negatively charge dye moiety attached, altering the structure and net charge of the peptides. The peak identified as β-casein is evident in both electropherograms (see Figure 5.19 C). The peak observed at 22 min is of the undigested β-casein, which is in agreement with previous findings.[91] Incomplete digestion of β-casein is frequently observed due to the dilute nature of the protein/trypsin mixture.[91] When a higher concentration of trypsin was used to ensure complete digestion, extra peaks appeared in the electropherogram due to autolysis of trypsin (data not shown).

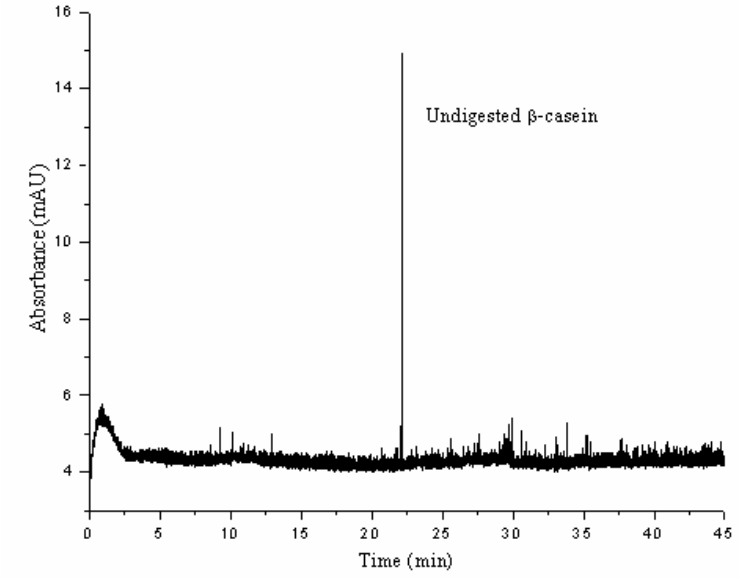

Figure 5.18 Electropherogram showing the separation of Zn4CPc labeled β-casein in a 40 mM borate buffer at pH 9**.** Sample was injected onto a bare silica capillary using electrokinetic injection for 5 sec and detected using a PDA monitored at 340 nm.

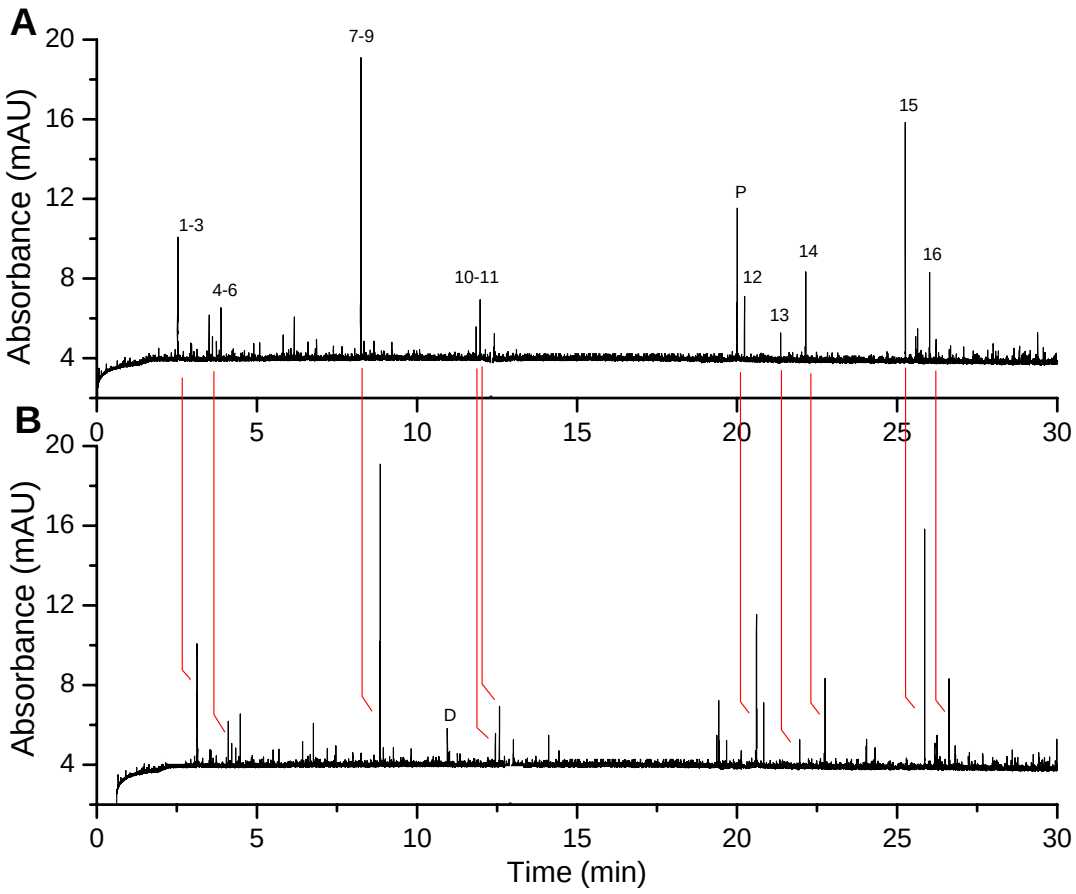

Figure 5.19 Capillary electropherogram of unlabeled peptides (A) and Zn4CPc labeled peptides (B) generated from trypsin digestion of β-casein. Capillary electrophoresis was performed at pH 9.1 in 40 mM borate buffer. The sample was electrokinetically injected onto the column at 15 KV for 5 s and separated using a carrier buffer at V = 30 KV. Separation was monitored at 345 nm. Peak labeled "P" represents undigested β-casein.

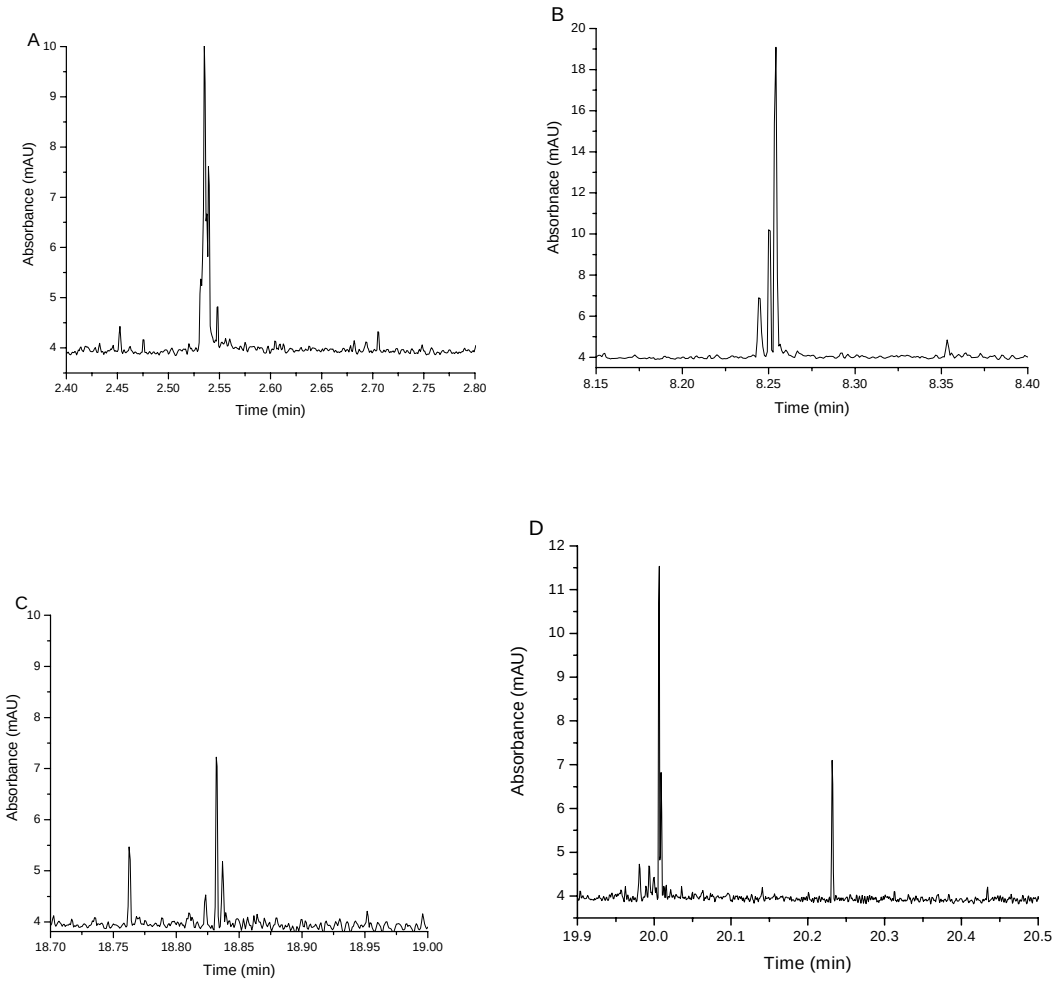

Figure 5.20 A blow up of several regions representing the electropherogram of Zn4CPc labeled β-casein digested with the enzyme trypsin.

It has been demonstrated that attaching a biomolecule moiety to Zn4CPc-NHS greatly increases the water solubility of the complex.[93] Thus, separation of the labeled peptides was achieved with no organic modifier added to the running buffer. Legendre reported on the use of laser-induced fluorescence (LIF) detection for the analysis of labeled tryptic digested β-casein and β-lactoglobulin A with commercially available near-IR tricarbocyanine dyes.[94] However, the authors were unable to assign peaks observed in the electropherogram.

To evaluate Zn4CPc and Alexa Fluor dyes for use in LIF microchip separations, studies were performed to compare their fluorescence intensities when covalently attached to

streptavidin. Zn4CPc and Alexa Fluor dyes have been used for pre-column labeling of amino acids, peptides, and proteins in conventional capillary electrophoresis.[95-98] Zn4CPc has an absorption maximum of 677 nm with a molar extinction coefficient of 250,000 cm-1M-1, while the molar extinction coefficient for Alexa Fluor is 250,000 $cm^{-1}M^{-1}$ with an absorption maximum of 680 nm. The quantum efficiency for Zn4CPc and Alexa Fluor is 0.4 and 0.6, respectively. Streptavidin contains four lysine residues and an N-terminal amine that can potentially react with Zn4CPc and Alexa Fluor dyes. Figure 5.21 shows the electropherogram of Zn4CPc in the absence of streptavidin. The results indicate two well-resolved peaks migrating at 100 and 127 s. These peaks are most likely a result of Zn4CPc-NHS and the product of hydrolysis of the activated Zn4CPc ester. Figure 5.22 shows the microchip separation of Zn4CPc-streptavidin conjugate in HEPES buffer at pH 8. Results showed several peaks separated with a peak eluting at 150 s, and several peaks eluting between 500 and 580 s.

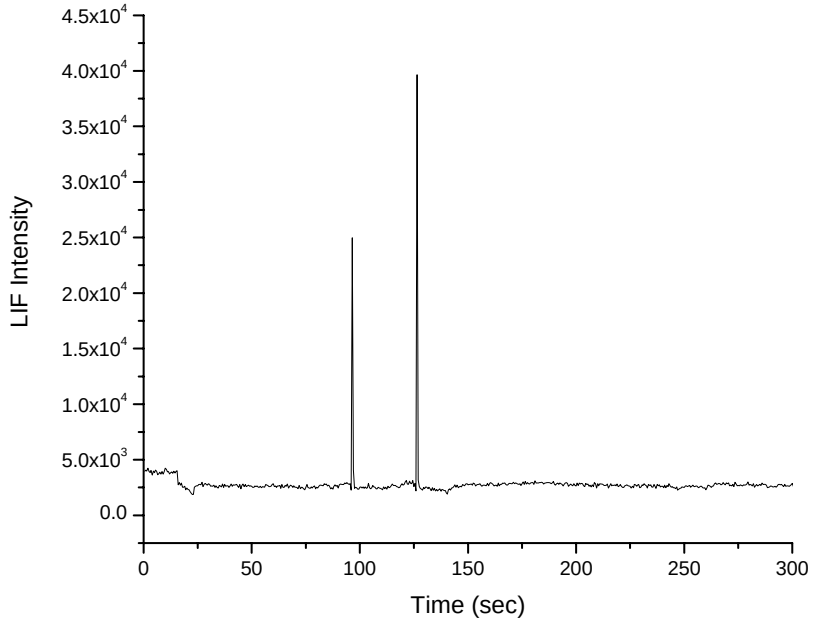

Figure 5.21 Microchip (PMMA) electrophoresis of Zn4CPc active ester without the presence of streptavidin. Dye concentration: 150 μM, injection time: 50 s. Separation was performed in HEPES, pH 8. Detection monitored using laser-induced fluorescence detector at an excitation wavelength of 633 nm.

The peak observed early in the separation is mostly likely due to unreacted Zn4CPc present in solution. The peaks eluting later in the separation are due to a mixture of multiply labeled streptavidin. The extra peak observed in the control reaction of Zn4CPc is absent in the electropherogram of the Zn4CPc-streptavidin conjugate because the reaction mixture was subjected to size-exclusion purification prior to analysis eliminating the lower molecular weight impurities.

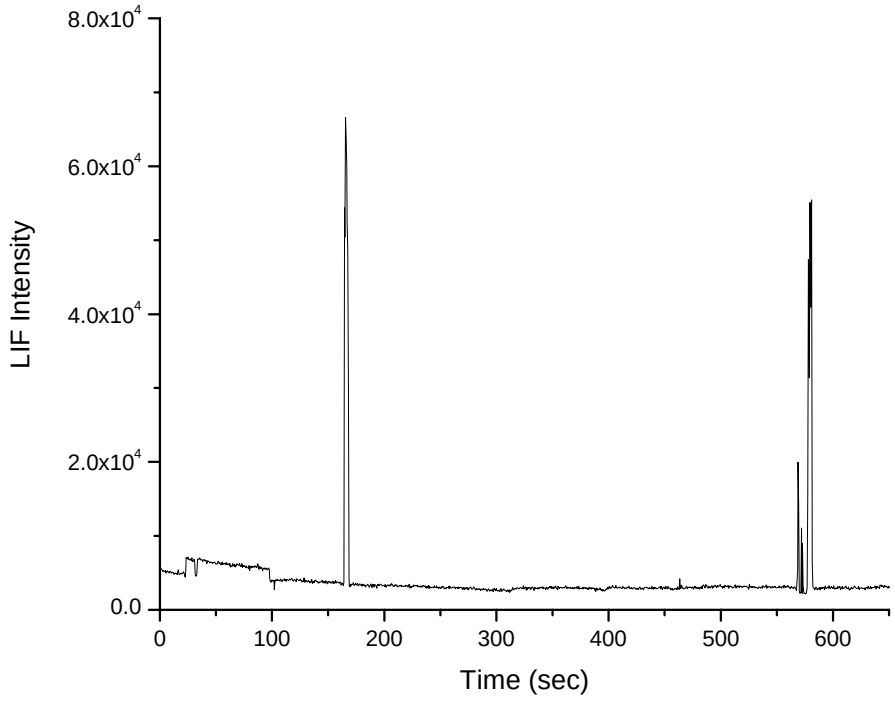

Figure 5.22 Electropherogram of ZnPc-streptavidin conjugate separated on PMMA microchip. Protein concentration: 1 μM, dye-to-protein ratio: 15-to-1, injection time: 50 sec. Separation was performed in HEPES at pH 8 and detection was monitored using a laser-induced fluorescence detector at an excitation wavelength of 633 nm.

These results are compared to streptavidin modified with a commercially available dye, Alexa Fluor 680. Results are shown in Figure 5.23 exhibiting several peaks eluting around 200 s. Labeling with Zn4CPc gave slightly lower fluorescence intensities with increased migration time for the conjugate compared to the Alexa Fluor-streptavidin conjugate due to the excitation source

wavelength (633 nm) not optimized at the excitation wavelength of Zn4CPc. In addition, the fluorescence quantum yield of Zn4CPc was found to decrease upon conjugation to streptavidin.[76] One possibility for the slower migration time for the ZnPc-streptavidin conjugate is because of the increased negative charge of the ZnPc dye compared to Alexa Fluor.[97] In addition, the difference in labeling yield will also contribute to the migration differences.

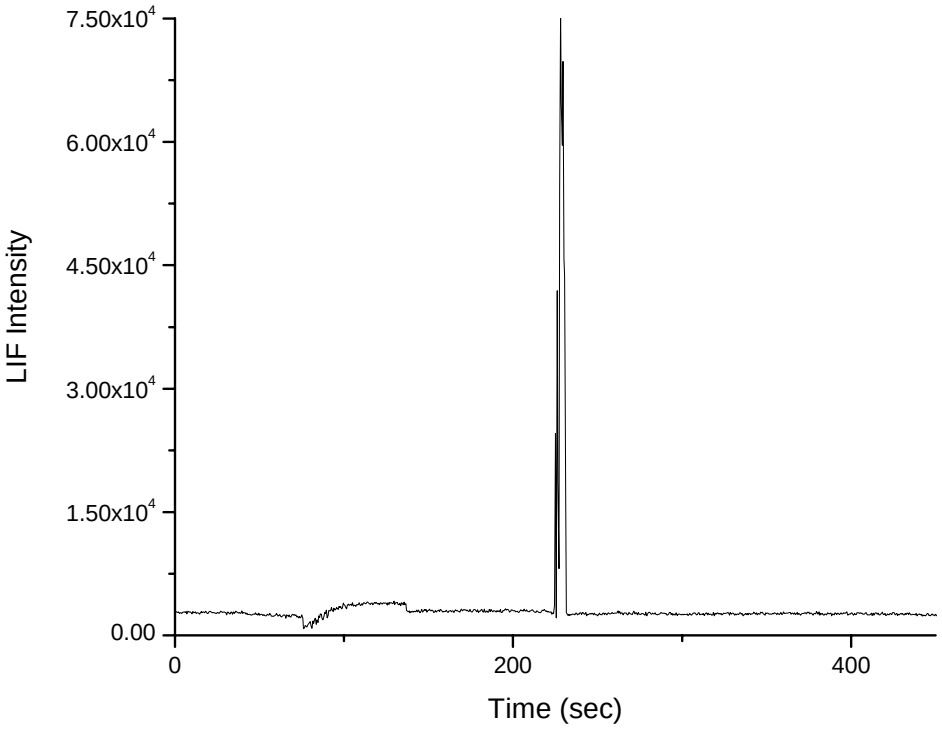

Figure 5.23 Electropherogram of Alexa Fluor-streptavidin conjugate obtained on an uncoated microchip. Sample injection time: 50 s. Dye concentration: 150 μM. Dye-to-protein ratio for labeling: 15-to-1.

5.3.2.1 Effect of pH

The separation of proteins and peptides in capillary zone electrophoresis without the use of additives or organic modifiers is based on differences in their electrophoretic mobility, which is related to the charge density of the protein/peptide.[92] Manipulating the selectivity of the separation can be achieved by altering the buffer pH, modifying the charge density of the

peptide. Buffers at low pH are often used to ensure homogeneity of the solution and to give reproducible separations.[99] Disadvantages with working at low pH however, include decrease in separation efficiency of similarly charged species, and denaturation of the protein resulting in irreversible adsorption of the protein to the capillary walls.[100] For the studies reported here, the buffer was maintained at pH 9.0 in which the complex mixture of labeled digested protein contains both positively and negatively charged peptide fragments. Hence, separation of the peptide fragments was possible in a single electrophoretic run with high resolution. The pK_a for the primary amines of β-casein tryptic fragments have been reported.[90] Selecting a buffer pH above the pK_a, the amine groups were protonated. The effect of pH on the separation of Zn4CPc labeled tryptic peptide fragments was studied using phosphate buffer at pH 2. The results are shown in Figure 5.24. As can be seen, the use of phosphate buffer at lower pH resulted in a loss of separation of the peptide fragments possibly due to capillary adsorption.

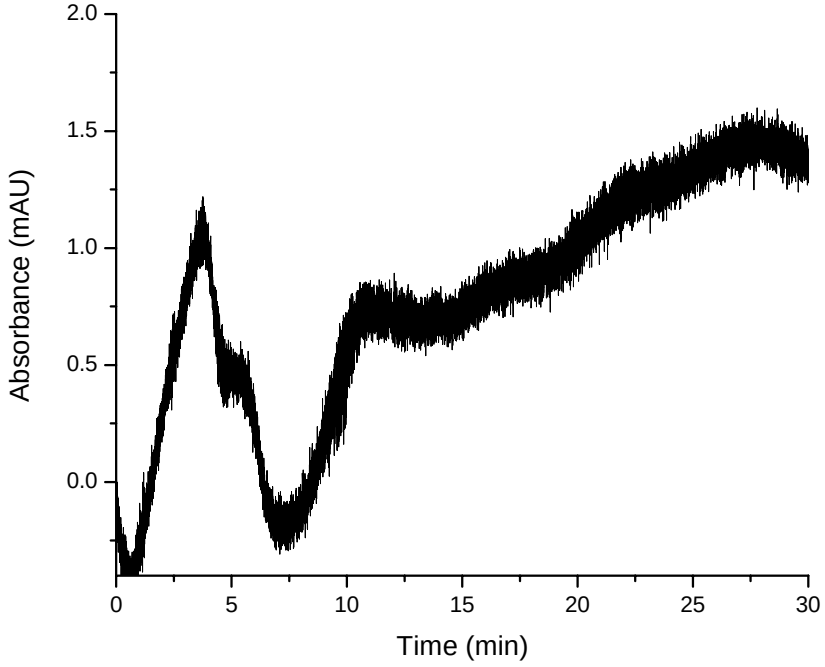

Figure 5.24 CZE electropherogram of tryptic peptide fragments produced from β-casein digestion. Separation was performed using 40 mM phosphate buffer at pH 2.

5.4 Conclusions

In conclusion, we have demonstrated CZE as a useful technique for determining the migration behavior of MPc complexes and biomolecules labeled with Zn4CPc-NHS. The identity of the metal center was found to play no significant role in the electrophoretic mobility of MPc's and the axial ligand had a greater influence. We have shown that the use of a mixed organic/aqueous running buffer with high organic content enhances the separation efficiency of Zn*x*CPc's due to improved solubility and decreased propensity to form ground state aggregates. An increase in the number of carboxylic acid groups on the periphery of the chromophore increased the migration time for each of the dyes due to the increase in size and negative charge of Zn8CPc and Zn16CPc. Electrophoretic analysis of insulin chain B labeled with ZnPc-NHS via primary amine groups was demonstrated. In addition, β-casein digested with trypsin is an excellent peptide to study the effect of the Pc moiety on the mobility of the peptide fragments. No significant adsorption of the peptide fragments to the capillary wall was evident due the absence of peak broadening and tailing in the electropherogram. Due to increased water solubility of the labeled conjugates, the optimal conditions were found to be different compared to the conditions for the native dyes requiring the addition of organic solvent in the background electrolyte.

5.5 References

(1) Swedberg, S. A., *Anal. Biochem.* **1990,** 185, 51-56.

(2) Benavente, F.; Balaguer, E.; Barbosa, J.; Sanz-Nebot, V., *Journal of Chromatography A* **2006,** 1117, 94-102.

(3) Liu, S. R.; Gao, L.; Pu, Q. S.; Lu, J. J.; Wang, X. J., *Journal of Proteome Research* **2006,** 5, 323-329.

(4) Catai, J. R.; Tervahauta, H. A.; de Jong, G. J.; Somsen, G. W., *Journal of Chromatography A* **2005,** 1083, 185-192.

(5) Jalali-Heravi, M.; Shen, Y.; Hassanisadi, M.; Khaledi, M. G., *Electrophoresis* **2005,** 26, 1874-1885.

(6) Chang, P. L.; Chiu, T. C.; Chang, H. T., *Electrophoresis* **2006,** 27, 1922-1931.

(7) Poinsot, W.; Lacroix, M.; Maury, D.; Chataigne, G.; Feurer, B.; Couderc, F., *Electrophoresis* **2006,** 27, 176-194.

(8) Zhao, S. L.; Shen, J. S., *Chemical Journal of Chinese Universities-Chinese* **2005,** 26, 1613-1617.

(9) Veledo, M. T.; de Frutos, M.; Diez-Masa, J. C., *Journal of Chromatography A* **2005,** 1079, 335-343.

(10) Meagher, R. J.; Won, J. I.; McCormick, L. C.; Nedelcu, S.; Bertrand, M. M.; Bertram, J. L.; Drouin, G.; Barron, A. E.; Slater, G. W., *Electrophoresis* **2005,** 26, 331-350.

(11) Hsieh, M. M.; Chiu, T. C.; Tseng, W. L.; Chang, H. T., *Current Analytical Chemistry* **2006,** 2, 17-33.

(12) Sang, F. M.; Ren, J. C., *Journal of Separation Science* **2006,** 29, 1275-1280.

(13) Owens, C. V.; Davidson, Y. Y.; Kar, S.; Soper, S. A., *Analytical Chemistry* **1997,** 69, 1256-1261.

(14) Holzgrabe, U.; Brinz, D.; Kopec, S.; Weber, C.; Bitar, Y., *Electrophoresis* **2006,** 27, 2283-2292.

(15) Kasicka, V., *Electrophoresis* **2006,** 27, 142-175.

(16) Jalali-Heravi, M.; Shen, Y.; Hassanisadi, M.; Khaledi, M. G., *Journal of Chromatography A* **2005,** 1096, 58-68.

(17) Miksik, I.; Charvatova, J.; Eckhardt, A.; Deyl, Z., *Journal of Chromatography B-Analytical Technologies in the Biomedical and Life Sciences* **2004,** 800, 155-160.

(18) Samanidou, V. F.; Christodoulou, E. A.; Papadoyannis, I. N., *Current Pharmaceutical Analysis* **2005,** 1, 155-193.

(19) Hamoudova, R.; Pospisilova, M., D *Journal of Pharmaceutical and Biomedical Analysis* **2006,** 41, 1463-1467.

(20) Kamoda, S.; Kakehi, K., *Electrophoresis* **2006,** 27, 2495-2504.

(21) Grossman, P. D.; Colburn, J. C., *Capillary electrophoresis : theory & practice*. Academic Press: San Diego, 1992; p xvi, 352 p.

(22) Camilleri, P., *Capillary electrophoresis : theory and practice*. CRC Press: Boca Raton, 1993; p 495 p.

(23) Foret, F.; K*rivánková, L.; Bo*cek, P., *Capillary zone electrophoresis*. VCH: Weinheim ; New York, 1993; p xiv, 346 p.

(24) Stevens, T. S.; Cortes, H. J., *Anal. Chem.* **1983,** 55, 1365-1370.

(25) Tallarek, U.; Rapp, E.; Scheenen, T.; Bayer, E.; Van As, H., *Anal. Chem.* **2000,** 72, 2292-2301.

(26) Huang, X. H.; Gordon, M. J.; Zare, R. N., *Anal. Chem.* **1988,** 60, 1837-1838.

(27) Ermakov, S. V.; Capelli, L.; Righetti, P. G., *Journal of Chromatography A* **1996,** 744, 55-61.

(28) Altria, K. D.; Simpson, C. F., *Anal. Proc. (London)* **1986,** 23, 453-4.

(29) Hieger, D., *High Performance Capillary Electrophoresis*. 3rd ed.; Hewlett Packard: 1997; p 136.

(30) Maichel, B.; Kenndler, E., *Electrophoresis* **2000,** 21, 3160-3173.

(31) Jorgenson, J. W.; Lukacs, K. D., Capillary Zone Electrophoresis. *Science* **1983,** 222, 266-272.

(32) MacDonald, A. M.; Sheppard, M. A. W.; Lucy, C. A., *Electrophoresis* **2005,** 26, 4421-4428.

(33) Grob, M.; Steiner, F., *Electrophoresis* **2002,** 23, 1853-1861.

(34) Beckers, J. L.; Bocek, P., *Electrophoresis* **2002,** 23, 1947-1952.

(35) Lukacs, K. D.; Jorgenson, J. W., *Journal of High Resolution Chromatography & Chromatography Communications* **1985,** 8, 407-411.

(36) Gordon, M. J.; Huang, X. H.; Pentoney, S. L.; Zare, R. N., *Science* **1988,** 242, 224-228.

(37) Dose, E. V.; Guiochon, G., *Anal. Chem.* **1992,** 64, 123-128.

(38) Terabe, S.; Otsuka, K.; Ando, T., *Anal. Chem.* **1989,** 61, 251-260.

(39) Huang, X. H.; Coleman, W. F.; Zare, R. N., *Journal of Chromatography* **1989,** 480, 95-110.

(40) Burton, D. E.; Sepaniak, M. J.; Maskarinec, M. P., *Chromatographia* **1986,** 21, 583-586.

(41) Rose, D. J.; Jorgenson, J. W., *Anal. Chem.* **1988,** 60, 642-648.

(42) Delinger, S. L.; Davis, J. M., *Anal. Chem.* **1992,** 64, 1947-1959.

(43) Ozaki, H.; Terabe, S., *Kuromatogurafi* **1994,** 15, 116-18.

(44) Palmer, C. P., *J. Chromatogr. A* **1997,** 780, 75-92.

(45) Palmer, C. P.; Terabe, S.,. *Analytical Chemistry* **1997,** 69, 1852-1860.

(46) Guttman, A., *Electrokinetic Phenomena* **2004**, 69-108.

(47) Sastre, A.; delRey, B.; Torres, T., *J. Org. Chem.* **1996,** 61, 8591-8597.

(48) Gorlach, B.; Dachtler, M.; Glaser, T.; Albert, K.; Hanack, M., *Chemistry-a European Journal* **2001,** 7, 2459-2465.

(49) Uchida, H.; Tanaka, H.; Yoshiyama, H.; Reddy, P. Y.; Nakamura, S.; Toru, T., *Synlett* **2002**, 1649-1652.

(50) Hanack, M.; Meng, D. Y.; Beck, A.; Sommerauer, M.; Subramanian, L. R., *Journal of the Chemical Society-Chemical Communications* **1993**, 58-60.

(51) Ma, C.; Tian, D.; Hou, X.; Chang, Y.; Cong, F.; Yu, H.; Du, X.; Du, G., *Synthesis* **2005**, 741-748.

(52) Peng, X.; Sternberg, E.; Dolphin, D., *Electrophoresis* **2005,** 26, 3861-3868.

(53) Hanack, M.; Lang, M., *Advanced Materials* **1994,** 6, 819-833.

(54) Sommerauer, M.; Rager, C.; Hanack, M., S., *Journal of the American Chemical Society* **1996,** 118, 10085-10093.

(55) Bowser, M. T.; Sternberg, E. D.; Chen, D. D. Y., *Analytical Biochemistry* **1996,** 241, 143-150.

(56) Dixon, D. W.; Pu, G.; Wojtowicz, H., *Journal of Chromatography, A* **1998,** 802, 367-380.

(57) Naqvi, N. A.; Rede, T.; Bonifacio, M.; Ma, D. D. F., *Analytical Biochemistry* **1999,** 269, 426-427.

(58) Charvatova, J.; Kasicka, V.; Kral, V.; Deyl, Z., *Journal of Chromatography, B: Analytical Technologies in the Biomedical and Life Sciences* **2002,** 770, 165-175.

(59) Gunaratne, T. C.; Gusev, A. V.; Peng, X. Z.; Rosa, A.; Ricciardi, G.; Baerends, E. J.; Rizzoli, C.; Kenney, M. E.; Rodgers, M. A. J., *Journal of Physical Chemistry A* **2005,** 109, 2078-2089.

(60) Wu, N.; Barker, G. E.; Huie, C. W., *J. Chromatogr.* **1994,** 659, 435-42.

(61) Zhang, Y.; Lee, H. K.; Li, S. F. Y., *Talanta* **1998,** 45, 613-618.

(62) Barbosa, C. A. S.; Constantino, V. R. L.; Tavares, M. F. M., *J. Capillary Electrophor.* **1997,** 4, 157-166.

(63) Dixon, D. W.; Gill, A. F.; Sook, B. R., *Journal of Porphyrins and Phthalocyanines* **2004,** 8, 1300-1310.

(64) Timerbaev, A. R.; Semenova, O. P.; Petrukhin, O. M., *Journal of Chromatography, A* **2002,** 943, 263-274.

(65) Schofield, J.; Asaf, M.,. *Journal of Chromatography, A* **1997,** 770, 345-348.

(66) Weinberger, R.; Sapp, E.; Moring, S., *J. Chromatogr. A* **1990,** 516, 271-285.

(67) Andrighetto, P.; Carofiglio, T.; Fornasier, R.; Tonellato, U., *Electrophoresis* **2000,** 21, 619-626.

(68) Flanagan, J. H.; Legendre, B. L.; Hammer, R. P.; Soper, S. A., *Analytical Chemistry* **1995,** 67, 341-347.

(69) Porras, S. P.; Kenndler, E., *Electrophoresis* **2005,** 26, 3203-3220.

(70) Vaher, M.; Koel, M., *Journal of Chromatography, A* **2005,** 1068, 83-88.

(71) Fritz, J. S., *Electrophoresis* **2003,** 24, 1530-1536.

(72) Huie, C. W., *Electrophoresis* **2003,** 24, 1508-1529.

(73) Roy, K. I.; Lucy, C. A., *Journal of Chromatography, A* **2002,** 964, 213-225.

(74) Fillet, M.; Servais, A. C.; Crommen, J., *Electrophoresis* **2003,** 24, 1499-1507.

(75) Steiner, F.; Hassel, M., *Electrophoresis* **2000,** 21, 3994-4016.

(76) Verdree, V. T., Su, G. Pakhomov, S., Allen, M.A., Countryman, A.C., Soper, S.A.., Hammer, R. P., *Journal of Fluorescence* **2006,** Submitted.

(77) Timerbaev, A. R.; Semenova, O. P., *J. Chromatogr. A* **1995,** 690, 141-148.

(78) Timerbaev, A. R., *J. Capillary Electrophor.* **1995,** 2, 165-174.

(79) Melanson, J. E.; Lucy, C. A., *Electrophoresis* **2002,** 23, 1689-1694.

(80) Arun, K. T.; Epe, B.; Ramaiah, D., *Journal of Physical Chemistry B* **2002,** 106, 11622-11627.

(81) Chen, H. J.; Farahat, M. S.; Law, K. Y.; Whitten, D. G., *Journal of the American Chemical Society* **1996,** 118, 2584-2594.

(82) Szymczyk, I.; Abramczyk, H., *Pure Appl. Chem.* **2004,** 76, 183-187.

(83) Valdesaguilera, O.; Neckers, D. C., *Acc. Chem. Res.* **1989,** 22, 171-177.

(84) Ding, W. L.; Thornton, M. J.; Fritz, J. S., *Electrophoresis* **1998,** 19, 2133-2139.

(85) Leone, A. M.; Francis, P. L.; Rhodes, P.; Moncada, S., *Biochem. Biophys. Res. Commun.* **1994,** 200, 951-957.

(86) Kanitsar, K.; Chen, Z.; Owens, G.; Naidu, R., *Journal of Liquid Chromatography & Related Technologies* **2003,** 26, 455-468.

(87) Li, Q.; Chang, C. K.; Huie, C. W., *Electrophoresis* **2005,** 26, 3349-3359.

(88) Kasicka, V.,

(89) Gao, J. M.; Mrksich, M.; Gomez, F. A.; Whitesides, G. M., *Analytical Chemistry* **1995,** 67, 3093-3100.

(90) Yang, Z. R.; Beale, S. C., *Journal of Liquid Chromatography & Related Technologies* **1998,** 21, 1591-1611.

(91) Amankwa, L. N.; Kuhr, W. G., Trypsin-Modified Fused-Silica Capillary Microreactor for Peptide-Mapping by Capillary Zone Electrophoresis. *Analytical Chemistry* **1992,** 64, 1610-1613.

(92) Cobb, K. A.; Novotny, M., *Anal. Chem.* **1989,** 61, 2226-2231.

(93) Nesterova, I. V., Verdree, Vera T., Pakhomov, Serhii, Hammer, Robert P., Soper, Steven A., *Submitted* **2007**.

(94) Legendre, B. L., Flanagan, J.H., Soper, S.A., *SPIE* **1994,** 2136, 244-254.

(95) Voloshina, N. P.; Haugland, R. P.; Bishop, J.; Bhalgat, M.; Millard, P.; Mao, F.; Leung, W. Y.; Haugland, R. P., *Mol. Biol. Cell* **1997,** 8, 2017-2017.

(96) Wilbur, D. S.; Pathare, P. M.; Hamlin, D. K.; Frownfelter, M. B.; Kegley, B. B.; Leung, W.-Y.; Gee, K. R., *Bioconjugate Chemistry* **2000,** 11, 584-598.

(97) Berlier, J. E.; Rothe, A.; Buller, G.; Bradford, J.; Gray, D. R.; Filanoski, B. J.; Telford, W. G.; Yue, S.; Liu, J. X.; Cheung, C. Y.; Chang, W.; Hirsch, J. D.; Beechem, J. M.; Haugland, R. P.; Haugland, R. P., *Journal of Histochemistry & Cytochemistry* **2003,** 51, 1699-1712.

(98) Verdree, V. T., Su, G. Pakhomov, S., Allen, M.A., Countryman, A.C., Soper, S.A.., Hammer, R. P., *Journal of Fluorescence* **2007,** In print.

(99) McCormick, R. M., *Analytical Chemistry* **1988,** 60, 2322-2328.

(100) Grossman, P. D.; Colburn, J. C.; Lauer, H. H.; Nielsen, R. G.; Riggin, R. M.; Sittampalam, G. S.; Rickard, E. C., *Analytical Chemistry* **1989,** 61, 1186-1194.

Chapter 6
Unsuccessful Approaches, Summary and Future Experiments

6.1 Unsuccessful Labeling Approaches

Initially, a two-step route was used to label biomolecules with symmetrical zinc tetracarboxylate phthalocyanine (Zn4CPc) by adding EDC/NHS to active N, hydroxysuccinimide functional groups on symmetrical zinc tetracarboxylate phthalocyanine (Zn4CPc) and conjugating biomolecules in sequence (Figure 6.1). This approach was not preferred because tt was found that the method produced low yields of the conjugate because

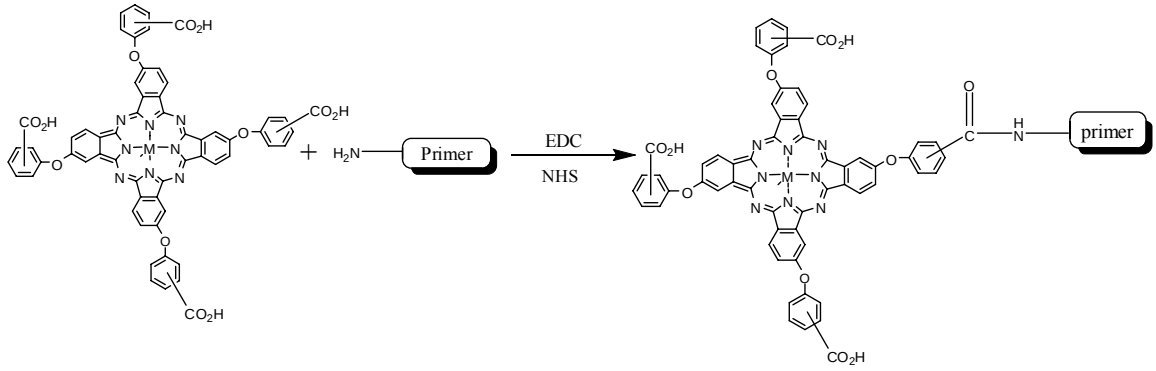

Figure 6.1 Schematic illustrating the reaction to convert carboxylic acid groups to active functional esters while reacting with amino modified primer simultaneously.

converting the carboxylic acid groups competed with the conjugation reaction and a large amount of Zn4CP precipitated out of solution due to its insolubility in aqueous solvents. Figure 6.2 is an example of a chromatogram showing the separation of the reaction mixture. The results showing only the dye peak eluting early and the primer peak eluting around 12.2 minutes was expected due to the precipitation of Zn4CPc. Thus, it was determined the conjugation procedure needed to be optimized; therefore several methods were tried in an attempt to achieve the desired yield of the conjugate. For example, the cationic detergent cetyltrimethylammonium bromide was used to precipitate the oligonucleotide increasing the hydrophobicity of the oligonucleotide making it more soluble in non-aqueous solvents due to the MPc dye soluble in organic solvents.

The reaction mixture was analyzed by ion-exchange chromatography and the result is shown in Figure 6.3. Here, a chromatogram representing a control reaction in the absence of Zn4CPc was overlaid to identify changes in the retention time of the oligonucleotide that may indicate the presence of a different species. Results only show what appears to be unreacted Zn4CPc and unlabeled oligonucleotide. Recently, a method published by Koval and coworkers was adapted in which the carboxylic acid groups on Zn4CPc are converted to functional succinimidyl esters and this compound is isolated and purified prior to labeling.[1] The chromatographic separation of this reaction mixture is shown in Figure 6.4. In comparison with previous results, the conjugate yield increased. From the results, the presence of a peak with retention time of around 14 min. that is absent in control reactions indicated the formation of the conjugate.

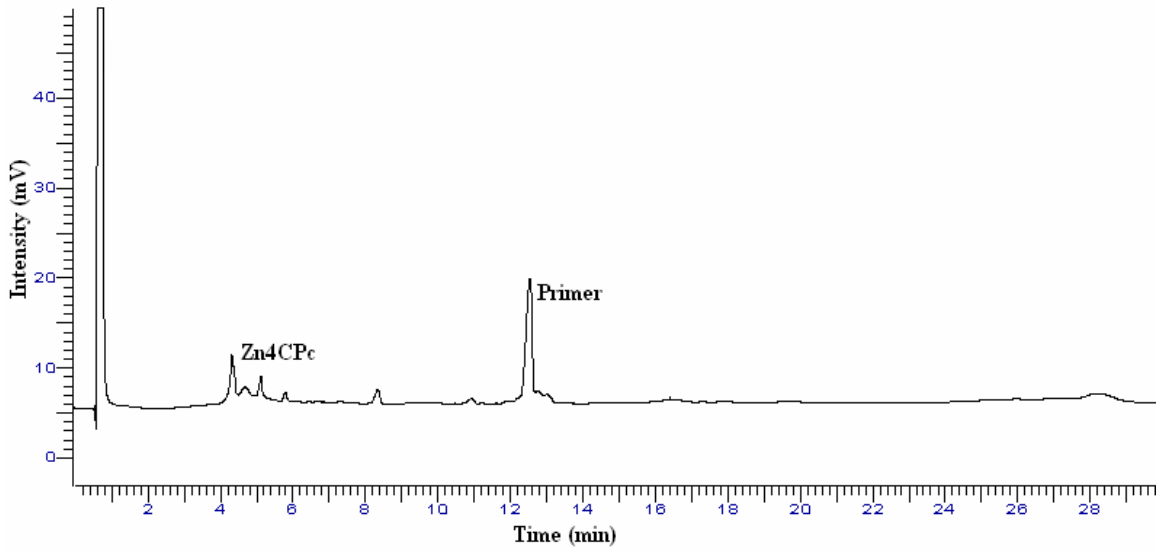

Figure 6.2 Anion-exchange chromatogram of a labeling reaction mixture consisting of Zn4CPc, EDC/NHS, and oligonucleotide present in solution. Precipitates formed when carbonate buffer was added. Concentration: 10^{-5} M Dye:10^{-6} M DNA.

The purification of labeled oligonucleotides was found to be challenging due to the aggregation tendency of MPc dyes and the complicated pattern of multiply labeled biomolecules making identification of the desired product difficult. In addition, little was known about the retention mechanism of Zn4CPc-labeled oligonucleotide. The initial experimental conditions

were the use of an anion exchange column and sodium perchlorate as the elution buffer in which separation is driven by the negative charge of the oligonucleotide. The results shown in Figure 6.3 were acquired using anion-exchange chromatography.

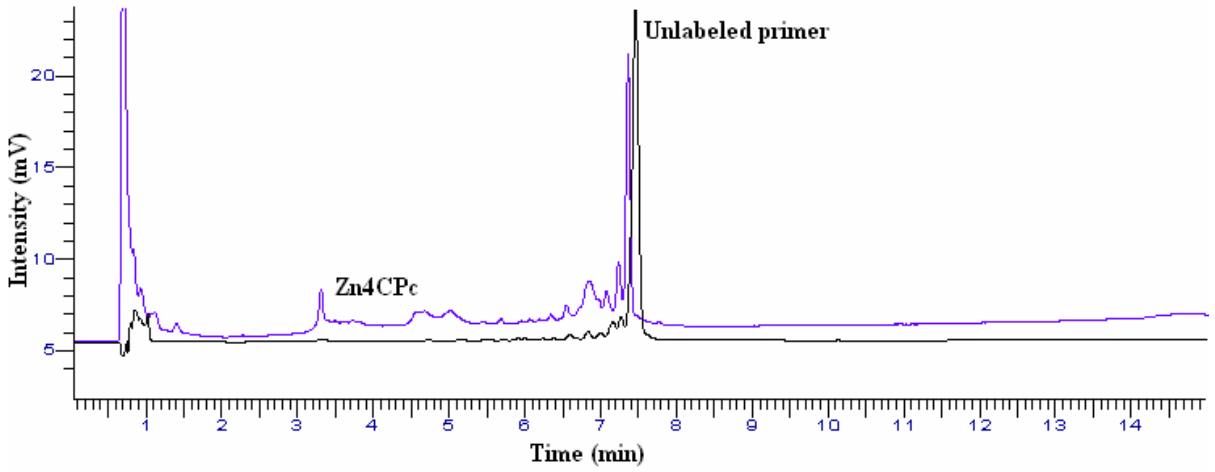

Figure 6.3 HPLC chromatogram of labeling reaction mixture. Reaction quenched using NaOH. Concentration ratio: 15:1 Dye:DNA (10^{-3} M:10^{-5} M) Analysis method - 0-90 % $NaClO_4$ in 30 minutes using anion exchange column. Detection was monitored at 260 nm. Black line represents DNA only.

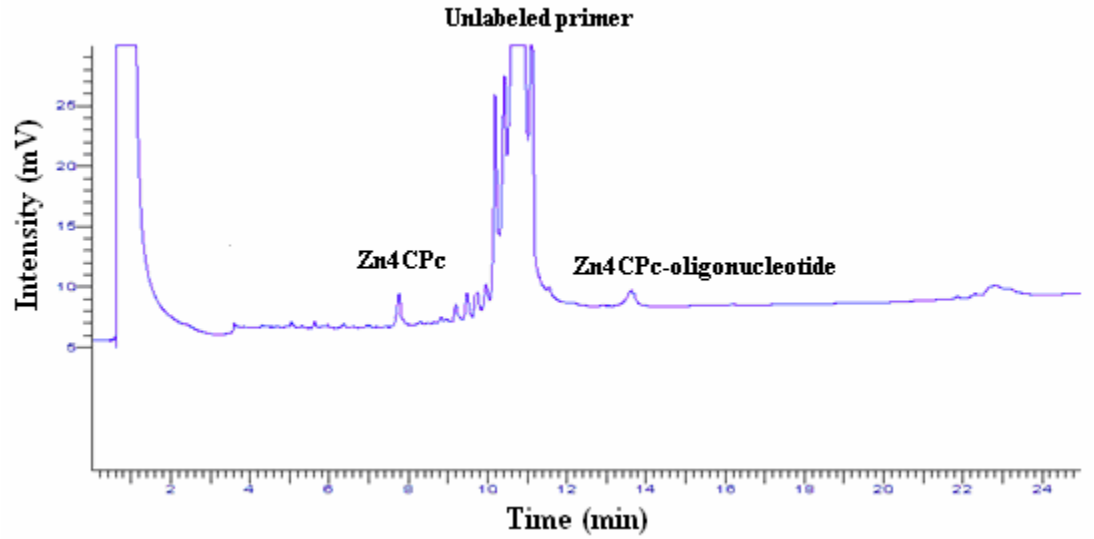

Figure 6.4 Anion-exchange chromatography of a 1 mM Zn4CPc-oligonucleotide reaction mixture. Fractions were collected and monitored at 260 nm. Dionex DNAPac anion-exchange (4 × 250 mm analytical column), 13 µm column. Gradient from 0% to 75% 0.375 M $NaClO_4$ in 45 minutes, room temperature.

The separation was monitored at 260 nm due to both Zn4CPc and the oligonucleotide absorbing in this region. It was suggested the fluorescent dye significantly affects the retention of the oligonucleotide due to the hydrophobicity of the label. This was found to be the case and our group recently demonstrated the use of reverse-phase chromatography using triethylammonium acetate (TEAA) as an ion-pairing reagent as an optimal separation technique for the isolation and purification of the MPc-oligonucleotide conjugate.[2]

HPLC analyses was not sufficient to identify the eluting peaks as the conjugates. Therefore, we employed LC-MS and MALDI-MS to identify the components of the reaction mixture. Previous reports have been made employing MALDI-MS in an attempt to obtain structural information on MPc's, however, there are no reports to our knowledge of MPc bioconjugates characterized by MALDI-MS.[3]

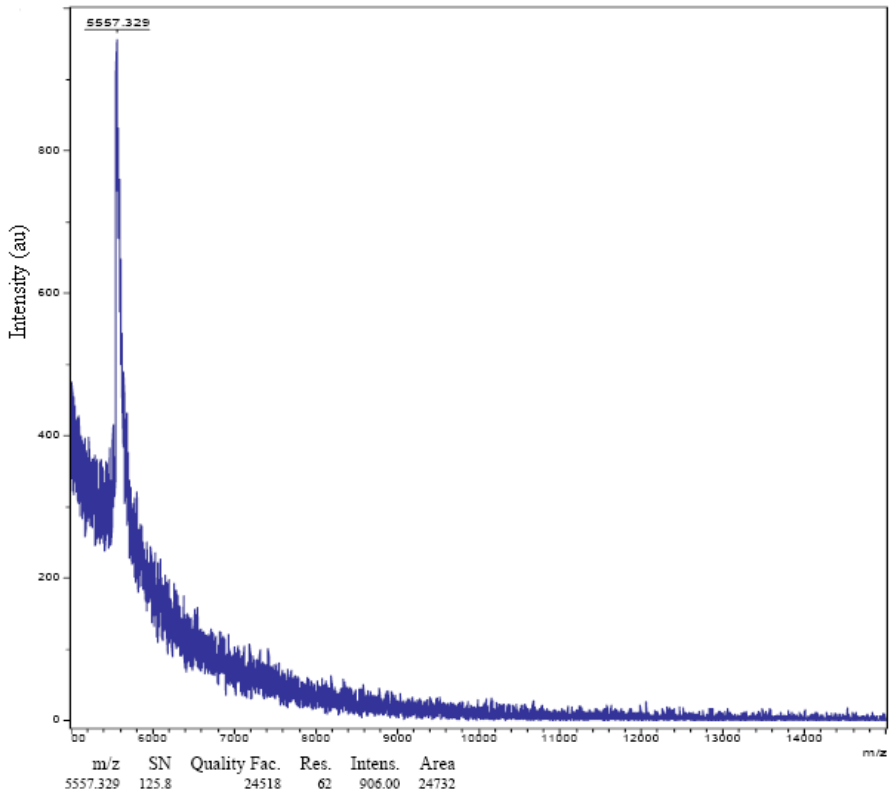

Figure 6.5 Mass spectra of Zn4CPc-oligonucleotide conjugate. MALDI-TOF was acquired on a Bruker Pro-Flex equipped with a 337 N_2 laser.

Therefore, fractions from chromatographic separations were collected and submitted for MALDI analysis. An example of the results obtained from MALDI-TOF analysis of Zn4CPc-oligonucleotide conjugate is shown in Figure 6.5. The expected mass for the conjugate is approximately 7100 Da or higher depending on the number of dye molecules attached to the oligonucleotide.

6.2 Summary

Fluorescence-based technologies have played an increasing role in the development of high sensitivity assays making the detection and analysis of complex biological systems possible. The research presented in this manuscript focused on the characterization of the photophysical and photochemical properties of a set of fluorophores with unique characteristics that have been synthesized for applications involving near-IR detection. The major drive in developing near-IR fluorophores was the increased sensitivity within this spectral region due to less matrix interferences. The cardinal of this research lies in the ability to label a variety of biological entities with these fluorophores producing conjugates with reasonably high yields that are suitable for ultra sensitive fluorescence detection in applications such as bio-imaging or DNA sequencing.[5-8]

Chapter 1 reviews the theory of fluorescence spectroscopy. This chapter focused on the process of emission and the recent development of detection in the near-IR region of the electromagnetic spectrum which has shown to be advantageous over visible. fluorescence detection systems.[8, 9] These advantages include simplified instrumentation, and less background interference due to the low number of molecules that fluoresce in this region. The major bottleneck of near-IR fluorescence-based detection is finding an appropriate set of fluorophores with desirable spectroscopic properties.

Much of the work performed in near-IR fluorescence labeling focuses on the use of carbocyanine dyes, but the photochemical instability of these fluorophores prompted the development of alternative dyes. Chapter 2 introduced dye sets that were suitable for near-IR detection. Within this chapter, the preparation of metal phthalocyanine derivatives, porphyrin analogs, synthesized in collaboration with Dr. Hammer's laboratory was described, detailing the spectral and photophysical characterization of several metal phthalocyanine compounds. The photophysical properties are of crucial importance in determining the suitability of the chromophore in NIR fluorescence based detection systems. Pc's have been of interest in the application of photodynamic therapy because they are photochemically reactive resulting in high yields of singlet oxygen formation [10-12]. The MPc's have high extinction coefficients, high quantum yields, and absorption and emission maxima in the NIR (λ_{abs} = 680 nm, λ_{em} = 686 nm). Several spectral changes can occur because of aggregation depending on solvent properties such as ionic concentration and pH. This chapter also highlighted an additional property that is unique with phthalocyanines to possess a different fluorescence lifetime when a different metal ion was inserted into the central cavity of the macrocycle with lifetimes varying from 2.9 for Zn4CPc to 5.0 for Al4CPc. These differences allow for sufficient discrimination of these dyes when used in applications such as DNA sequencing in a two-color, four-lifetime arrangement. These dyes also exhibited superior photostabilities compared to commercially available dyes. Disadvantages include aggregate formation and solubility in aqueous media.

Chapter 3 presented a general route for modifying biomolecules with MPc's. A popular approach employed carbodiimide coupling converting carboxylic acid groups to N, succinimidyl esters that are highly reactive towards the target molecule containing available primary amines. This type of derivatization was chosen due to the ease of preparation and it was found to be straightforward producing high yields of the conjugate.[13-15] We presented work in which an

oligonucleotide, streptavidin and insulin chain B were covalently attached to Zn4CPc using excess dye. The analysis of the conjugate mixture was performed using reverse-phase HPLC (RP-HPLC) and results indicated multiple dye molecules attached to one streptavidin molecule due to several functionalized carboxylic acids available for labeling. The functionality of streptavidin to bind to its natural target, biotin, was also examined by fluorescence measurements of ZnPc-streptavidin conjugate attached to biotinylated microspheres.

Chapter 4, which was a continuation of chapter 3, was dedicated to the optimization of the carbodiimide coupling approach for labeling Zn4CPc to proteins with streptavidin used as a model for a microplate assay. In essence, biotin was immobilized on the surface of microplate wells and the Zn4CPc-streptavidin conjugate was added. After incubation, the bound conjugates were detected using fluorescence detection at the wavelength 686 nm. This assay was ideally suited for investigating the optimal labeling conditions in a high-throughput format. Results were in agreement with recent studies citing the optimal conditions for labeling ZnEPc with oligonucleotides, which provided an optimal are pH 8, and a minimal amount of organic content.[2]

For the analysis of sequencing reactions in a single electrophoretic lane, the use of dyes that have similar dye structure prevents mobility shifts due to structural differences.[16] Chapter 5 concentrates on the use of capillary zone electrophoresis (CZE) in determining the effect of the metal ion and peripheral substitution on the electrophoretic mobility of the MPc's. Chapter 5 also presented the CZE of Zn4CPc conjugates determining the electrophoretic behavior of Zn4CPc-insulin chain B conjugate. In addition, this chapter demonstrated the usefulness of CZE in applications such as peptide mapping with the fragments labeled with Zn4CPc. These results were acquired using UV-Vis detection. Lastly, near-IR laser induced fluorescence (LIF) detection coupled to microchip electrophoresis was applied to compare the fluorescence intensity

of covalently labeled streptavidin with Zn4CPc and commercially available Alexa Fluor 680. It was concluded the instrumentation setup was not optimized for detecting at the maximum wavelength of the Zn4CPc and resulted in low fluorescence intensity for the conjugates.

6.3 Current and Future Work

Much of the work presented here describes the use of symmetrical zinc phthalocyanine for the covalent attachment to biomolecules for DNA sequencing. Several labeling sites that are available on the biomolecule along with four active esters located on the periphery of the phthalocyanine dye results in multiple labeling. Future works may include the use of Pc derivatives containing a different metal center for the covalent attachment to peptides, proteins, and single stranded DNA. The significance of this work is that a different metal center changes the fluorescence lifetime, which would allow increased multiplexing capabilities due to lifetime discrimination in conjunction with color discrimination between dye labeled nucleotide bases for applications such as DNA sequencing. Future studies could also include developing asymmetrical phthalocyanines containing an axial ligand to decrease aggregate formation. Asymmetrical phthalocyanines are of growing interest for labeling procedures due to the lack of multiple labels that could potentially interfere with the analysis in applications such as DNA sequencing. Applications involving fluorescence resonance energy transfer (FRET) -based detection for sample analysis are currently under investigation in our laboratory using asymmetrical MPc's. Figure 6.6 shows a schematic of the asymmetrical MPc's with a single primary amine group or carboxylic acid group. The presence of ethylene glycol groups helps to increase their solubility in both organic and aqueous media. These studies are based on FRET between Ni4CPc and Zn4CPc with Ni4CPc as an acceptor because Ni4CPc shows very weak fluorescence and Zn4CPc as a donor. Lastly, studies to determine the potential use of MPc's as photosensitizers for photodynamic therapy will also be investigated.

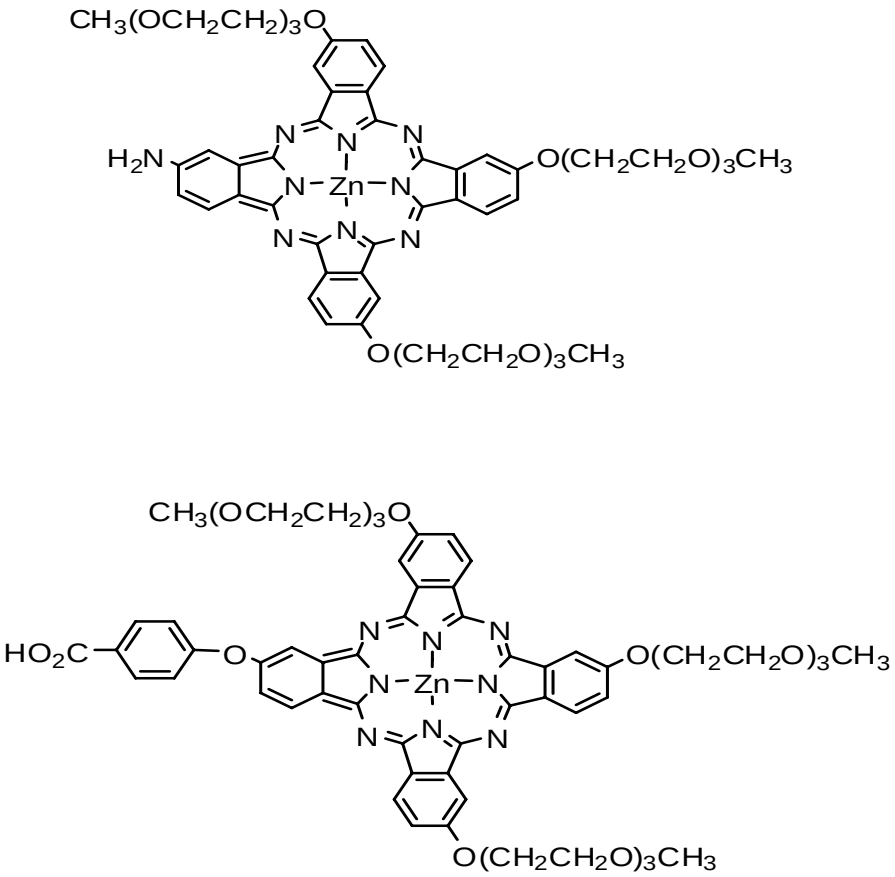

Figure 6.6 Structure of asymmetrical Pc dyes for labeling biomolecules.

6.4 References

(1) Koval, V. V.; Chernonosov, A. A.; Abramova, T. V.; Ivanova, T. M.; Fedorova, O. S.; Knorre, D. G., *Bioorg. Khim.* **2000,** 26, 118-125.

(2) Nesterova, I. V., Verdree, Vera T., Pakhomov, Serhii, Hammer, Robert P., Soper, Steven A., *Submitted for publication,* **2007**.

(3) Dixon, D. W.; Gill, A. F.; Sook, B. R., *Journal of Porphyrins and Phthalocyanines* **2004,** 8, 1300-1310.

(4) Conneely, A.; McClean, S.; Smyth, W. F.; McMullan, G., *Rapid Communications in Mass Spectrometry* **2001,** 15, 2076-2084.

(5) Giusti, W. G.; Adriano, T., *PCR Methods Appl.* **1993,** 2, 223-7.

(6) Griffin, H. G., Griffin, A.M., *Appl. Biochem. Biotechnol.* **1993,** 38, 147-159.

(7) Iizuka, M.; Sugiyama, Y.; Iida, S.; Sekiya, T., *Analytical Biochemistry* **1996,** 241, 136-139.

(8) Soper, S. A., Williams, D., *Analytical Chemistry* **1995,** 67, 3427-3432.

(9) Flanagan, J. H.; Legendre, B. L.; Hammer, R. P.; Soper, S. A., *Analytical Chemistry* **1995,** 67, 341-347.

(10) Liu, W.; Jensen, T. J.; Fronczek, F. R.; Hammer, R. P.; Smith, K. M.; Vicente, M. G. H., *J. Med. Chem.* **2005,** 48, 1033-1041.

(11) Lukyanets, E. A., *Journal of Porphyrins and Phthalocyanines* **1999,** 3, 424-432.

(12) Phillips, D., *Pure Appl. Chem.* **1995,** 67, 117-26.

(13) Sehgal, D.; Vijay, I. K., *Analytical Biochemistry* **1994,** 218, 87-91.

(14) Staros, J. V.; Wright, R. W.; Swingle, D. M., *Analytical Biochemistry* **1986,** 156, 220-222.

(15) Williams, A.; Hill, S. V.; Ibrahim, I. T., *Analytical Biochemistry* **1981,** 114, 173-176.

(16) Lassiter, S. J.; Stryjewski, W.; Owens, C. V.; Flanagan, J. H.; Hammer, R. P.; Khan, S.; Soper, S. A., *Electrophoresis* **2002,** 23, 1480-1489.

Vita

Vera Verdree was born on January 2, 1977 in Savannah, Georgia to the proud parents of Marilyn and Fernando Verdree. She attended Reese Road Elementary School where her passion for music began becoming a gifted violinist. In 1992, she attended Governors Honors Program for talented musicians. She attended Shaw High School where she was a member of the student council, and the Shaw Orchestra before graduating in 1995 with honors.

In 1995, she enrolled in Columbus State University majoring in chemistry after receiving the HOPE Scholarship. She participated in Research Experience for Undergraduates (REU) summer internship program for undergraduates at Toledo University where here project involved computer stimulation of sputter deposition. In 2000, she received her Bachelors degree in chemistry.

In August 2000, she was accepted into the graduate program in chemistry at Louisiana State University and joined Dr. Steven A. Soper research group. Her work focuses on the characterization of metal phthalocyanines for tagging biomolecules for highly sensitive detection. During her graduate career, she became a member of the American Chemical Society (ACS), and the National Organization for the Professional Advancement of Black Chemist and Chemical Engineers (NOBCChE) where she served as the regional student representative in 2005, and chair of the education committee. She presented her research at several national conferences to include ACS and PITTCON. She has received several awards including outstanding teaching award in 2001 and in 2005 she was awarded a dissertation writing fellowship from the Graduate Alliance for Education in Louisiana (GAELA). At the August 2007 commencement, she will receive the degree of Doctor of Philosophy in chemistry.